

UCLA

UCLA Electronic Theses and Dissertations

Title

Redox-Responsive Nanocapsules for Intracellular Protein Delivery

Permalink

<https://escholarship.org/uc/item/6d4337c9>

Author

Zhao, Muxun

Publication Date

2014

Peer reviewed|Thesis/dissertation

UNIVERSITY OF CALIFORNIA

Los Angeles

Redox-Responsive Nanocapsules for Intracellular Protein Delivery

A dissertation submitted in partial satisfaction
of the requirements for the degree Doctor of Philosophy
in Chemical Engineering

by

Muxun Zhao

2014

© Copyright by

Muxun Zhao

2014

ABSTRACT OF THE DISSERTATION

Redox-Responsive Nanocapsules for Intracellular Protein Delivery

by

Muxun Zhao

Doctor of Philosophy in Chemical Engineering

University of California, Los Angeles, 2014

Professor Yi Tang, Chair

Proteins play a crucial role in life, taking part in all vital processes in the body. Intracellular protein delivery holds enormous promise for biological and medical applications, including cancer therapy, vaccination, regenerative medicine, treatment for loss-of-function genetic diseases and imaging. Engineering vehicles for escorting therapeutic proteins into specific cells in a controlled release fashion has thus generated considerable interest. The development of such therapeutics to selectively target tumor has also been a major research focus in cancer nanotechnology. A novel strategy using polymeric redox-responsive nanocapsules for intracellular protein delivery is described, in which through in situ interfacial polymerization, the target therapeutic protein is noncovalently encapsulated into a biocompatible polymeric shell interconnected by disulfide-containing crosslinkers. The dissociation of the polymeric shell under reducing conditions and the subsequent release of protein were confirmed using cell-free assays in the presence of glutathione. Several therapeutic proteins with different properties, both cytosolic and nuclear, were successfully delivered using the platform. The nanocapsules were demonstrated to be efficiently internalized into mammalian cells through interactions between charge or targeting ligand,

and to release the protein in the reducing cytosol in active forms. Using such redox-responsive nanocapsule as a vehicle, pro-apoptotic protein caspase 3 was delivered to induce apoptosis in a variety of human cancer cell lines, including HeLa, MCF-7 and U-87 MG. Tumor-selective killer apoptin was delivered into different breast cancer cell lines as well, which led to rapid resurrection of apoptosis in breast cancer cell lines and shrinkage of xenograft mice models. Tumor suppressor p53 protein, the most commonly mutated protein, was also delivered selectively into tumor cells for apoptosis induction, through targeted redox-responsive nanocapsules. The delivery methodology is general, effective and nontoxic towards healthy cells. This work facilitate the development of new tools for tumorigenesis and drug resistance studies, as well as expanding current therapeutic target pool to many other tumor suppressor proteins for cancer treatment.

The Dissertation of Muxun Zhao is approved.

Tatiana Segura

Daniel T. Kamei

Yi Tang, Committee Chair

University of California, Los Angeles

2014

Table of Contents

Chapter 1 Background and Significance	1
1.1 Introduction	1
1.2 Lipid-based nanocarriers	4
1.2.1 Liposomes	4
1.2.2 Solid lipid nanoparticles	7
1.3 Polymeric nanocarriers.....	7
1.3.1 Direct attachment	7
1.3.2 Physical adsorption and interaction	10
1.3.3 Emulsion-based encapsulation.....	14
1.3.4 In situ polymerization	16
1.3.5 Polymeric micelles.....	20
1.3.6 Layer-by-layer encapsulation.....	22
1.4. Inorganic nanocarriers	27
1.4.1 Carbon nanotubes.....	27
1.4.2 Quantum dots	28
1.4.3 Gold nanoparticles	30
1.4.4 Silica nanoparticles	31
1.4.5 Magnetic nanoparticles	32
1.5. Protein-mediated carriers	33

1.6. Summary and outlook	36
Chapter 2 Redox-Responsive Nanocapsules for Intracellular Protein Delivery.....	41
2.1. Introduction	41
2.2 Materials and Methods	43
2.2.1 Materials	43
2.2.2 Instruments.....	43
2.2.3 Methods.....	44
2.3. Results and Discussion.....	48
2.3.1 Formation and characterization of protein NCs.....	48
2.3.2 Cellular uptake, Internalization Pathway and Trafficking of S-S NCs.....	53
2.3.3 Apoptosis is observed following delivery of CP-3 S-S NCs	55
2.4 Conclusion.....	59
Chapter 3 Degradable Polymeric Nanocapsule for Efficient Intracellular Delivery of a High Molecular Weight Tumor-Selective Protein Complex.....	61
3.1. Introduction	61
3.2. Materials and Methods	63
3.2.1. Materials	63
3.2.2 Instruments.....	64
3.2.3. Protein Expression and Purification method.....	64
3.2.4. Protein nanocapsule preparation	65

3.2.5. Characterization of protein nanocapsules	66
3.2.6. Cellular uptake and localization of nanocapsules	66
3.2.7. Cytotoxicity Assays	67
3.2.8. In vivo studies with MCF-7 xenograft model.....	68
3.3. Results and Discussion.....	69
3.3.1. Synthesis and characterization of apoptin nanocapsules	69
3.3.2. Cellular uptake and localization of nanocapsules	73
3.3.3. Tumor-selective cytotoxicity of apoptin nanocapsules	76
3.3.4. In vivo evaluation of apoptin nanocapsules.....	81
3.4. CONCLUSIONS	82
Chapter 4 Clickable Protein Nanocapsules for Targeted Delivery of Recombinant p53.....	83
4.1 Introduction	83
4.2. Material and methods	85
4.2.1. Construction, expression and purification of proteins	85
4.2.2. Synthesis of N-(azidoethyl-decaethylene glycol)-acrylamide	87
4.2.3. Protein nanocapsule preparation	88
4.2.4 Characterization of protein nanocapsules	89
4.2.5 Internalization and trafficking of nanocapsules	90
4.2.6. Localization of protein delivered by nanocapsules	91
4.2.7. Cytotoxicity Assays and Apoptosis detection.....	91

4.3 Results and Discussion	93
4.3.1 Synthesis of nanocapsules with clickable monomer.....	93
4.3.2. Conjugation of nanoparticles with ligands	96
4.3.3. Synthesis of clickable p53 nanocapsules	103
4.3.4. Internalization and Release of p53 in cancer cells.....	105
4.3.5. Cytotoxicity of p53 Nanocapsules	107
4.4 Conclusions	110
Chapter 5 Summary	112
References.....	113

Acknowledgements

Chapter 1 contains reproduced material by permission of The Royal Society of Chemistry from Z. Gu, A. Biswas, M. Zhao, Y. Tang, Chem. Soc. Rev. 40 (2011) 3638. © The Royal Society of Chemistry.

Chapter 2 contains reproduced material by permission of Elsevier from M. Zhao, A. Biswas, B. L. Hu, K. I. Joo, P. Wang, Z. Gu, Y. Tang, Biomaterials 32 (2011) 5223. © Elsevier.

Chapter 3 contains reproduced material by permission of Elsevier from M. Zhao, B. Hu, Z. Gu, K. Joo, P Wang, Y. Tang, Nano Today 8 (2013) 11. © Elsevier.

The work in this dissertation was supported by from the Defense Treat Reduction Agency, the David and Lucile Packard Foundation, and CDMRP BCRP Idea Award BC101380 to Dr. Yi Tang. We thank Dr. A. Clay Clark (NC State University), Dr. C. Backendorf and Dr. M. Noteborn (Universiteit Leiden) for the providing expression plasmids of for this dissertation work.

There are many people that I would like to thank for their support and guidance through my education. First, I would like to thank my advisor, Dr. Yi Tang, for providing me the opportunity to work on this frontier bio-nanotechnology project. Dr Yi Tang's innovative insights and strong passion about research have always been the inspiration and fuel in experimenting new directions and progressing forward in my project. He provided me invaluable technical training and research experience that have well-prepared me for my future career.

I would also like to thank Dr. Harold G. Monbouquette, Dr. Tatiana Segura, and Dr. Daniel T. Kamei for being my committee member and providing valuable insights for my project. I would like to thank my collaborators, Dr. Pin Wang from University of Southern California and his lab members Dr. Kye-Il Joo, Dr. Biliang Hu, and Yarong Liu, for their training on new techniques and assistance for experiments.

I am also grateful to have Dr. Zhen Gu, who was my senior graduate student mentor when I joined the lab. He showed me not only useful experimental techniques but also his dedication for research work as a scientist, from which I benefit very much throughout my Ph.D. education. I would like to thank my past and present group members, Dr. Hui Zhou, Dr. Yanran Li, Dr. Kangjian Qiao, Dr. Lauren Pickens, Dr. Yit-Heng Chooi, Dr. Wei Xu, Dr. Hsiao-Ching Lin, Dr. Youcai Hu, Dr. Jaclyn Winter, Ralph Cacho, Anthony DeNicola, and Carly Bond for their help and support both professionally and personally. Several undergraduate students, Renee Hsieh, Mariel Lising, John Mac, Nova Wang, Laura Hua and Thet Pyone, have helped with my project. I appreciate the opportunity to developing my mentoring skills and greatly appreciate their work and effort.

My ultimate gratitude goes to my parents, whose unconditional love, support and encouragement keep me going and moving forward. Also to my boyfriend, thank you for all the encouragement along the way.

VITA

- 2009 B.S. Biochemistry,
Biology and Biotechnology
with concentration in Cell and Molecular Biology and
Genetics
Worcester Polytechnic Institute, Worcester, MA.
- 2011-2012 Teaching Assistant
Department of Chemical and Biomolecular Engineering
University of California, Los Angeles
- 2009-2014 Graduate Student Researcher
Department of Chemical and Biomolecular Engineering
University of California, Los Angeles

Publications and Presentations

Zhao, M., Liu, Y., Hsieh, R., Wang, N., Wang, P., Gu, Z., Tang, Y., “Clickable Protein Nanocapsules for Targeted Delivery of Recombinant p53”. Submitted.

Zhao, M., Hu, B., Joo, K., Wang, P., Tang, Y. “Degradable Polymeric Nanocapsule for Efficient Intracellular Delivery of a High Molecular Weight Tumor-Selective Protein Complex.” **2013**, *Nano Today*, DOI 10.1016/j.nantod.2012.12.003. Featured by *SciTechDaily*, *ScienceDaily*, *UCLA Newsroom*, etc.

Gu, Z., Biswas, A., Zhao, M., Tang, Y. “Tailoring Nanocarriers for Intracellular Protein Delivery.” **2011**, *Chem. Soc. Rev.* 40, 3638-3655.

Gu, Z., Zhao, M., Sheng, Y., Bentolila, L. A. Tang, Y. “Detection of Mercury Ion by Infrared-Fluorescent Protein and Its Hydrogel-Based Paper Assay.” **2011**, *Analytical Chemistry*, 83, 2324-2329.

Zhao, M., Gu, Z., G., Biswas, A., Tang, Y. “Redox-Responsive Single Protein Encapsulation for Intracellular Protein Delivery.” **2010**, *Biomaterials*, 32, 5223-5230.

Biswas, A., Joo, K., Zhao, M., Fan, G., Wang, P., Zhen, G., Tang, Y. “Endoprotease-Mediated Intracellular Protein Delivery using Nanocapsules.” **2010**, *ACS Nano*, 5, 1385-1394.

Dai, Q., Wang, Y., Li, X., Zhang, Y., Pellegrino, D. J., Zhao, M., Zou, B., Seo, J., Wang, Y., Yu, W. W. “Size-dependent composition and molar extinction coefficient of PbSe semiconductor nanocrystals.” **2009**, *ACS Nano*, 3, 1518-1524.

American Institute of Chemical Engineers Annual Meeting (**2013**) San Francisco, Oral Presentation: *Redox-Adaptive Protein Intracellular Delivery For Targeted p53 Therapy*.

Society of Biomaterials Annual Meeting (**2013**) Boston, Poster presentation: *Redox-Responsive Polymeric Nanocapsules for Protein Delivery*.

American Institute of Chemical Engineers Annual Meeting (**2012**) Pittsburgh, Oral Presentation: *Redox-Responsive Polymeric Nanocapsules for Protein Delivery*.

American Association for Cancer Research Molecular Targets and Cancer Therapeutics (**2011**) San Francisco, Poster presentation: *Delivery of Tumor-Killing Protein to Cancer Cells*.

American Association for Cancer Nano In Cancer: Linking Chemistry, Biology, and Clinical Applications In Vivo (**2011**) Miami, Poster presentation: *Delivery of Nanocapsules with Apoptotic Proteins to Cancer Cells*.

Chapter 1 Background and Significance

1.1 Introduction

Proteins are the engines of life that perform essential functions inside cells, such as enzyme catalysis, signal transduction, gene regulation and maintaining a fine balance between cell survival and programmed death. Many diseases arise from the alterations in the functions of intracellular proteins.^{1,2} Therefore, a general method of delivering active forms of proteins to specific cells and organs in living organisms is an important goal in many medical applications, including cancer therapy, vaccination, regenerative medicine, treating loss-of-function genetic diseases and imaging. From a therapeutic perspective, protein-based approaches may be safer than gene therapy because no random or permanent genetic changes are involved, but only transient actions of proteins are needed.

The main barriers of delivering target proteins to the intracellular space result from intrinsic properties of most proteins, including the large sizes, varying surface charges and the fragile tertiary structures.² When administered into serum, native proteins can suffer from serum instability and can be rapidly degraded or inactivated. Most native proteins are also membrane impermeable due to electrostatic repulsions. Therefore like drug, DNA or siRNA delivery systems³⁻⁶, appropriate delivery vehicles for escorting proteins to the cytosol are highly important. In addition to the obstacles mentioned above, the vehicle often needs to help the protein cargo in endolysosomal escape. Fig. 1 displays a schematic process of typical endocytic pathway for protein delivery vehicles. Importantly, to successfully reach the various desired subcellular compartments, such as the cytosol, the mitochondria or the nucleus, the delivery vehicle must be able to escape the endosomal pathway to avoid being trafficked through

endomembrane compartments and being subject to clearance and degradation under harsh lysosomal conditions.⁷ To date, the most commonly used approach for intracellular protein delivery is the genetic fusion of the target protein to protein transduction domains (PTDs) or cell-penetrating peptides (CPPs), such as the HIV-1 transactivator of transcription (TAT) peptide, oligoarginines, and the *Drosophila* Antennapedia-derived penetratin peptide.⁸ Despite many practical advantages of the protein transduction technology, the main drawback of this method is the inefficient escape of protein from the endosome to the cytosol, leading to CPP-tagged proteins sequestered in intracellular vesicles.^{9, 10}

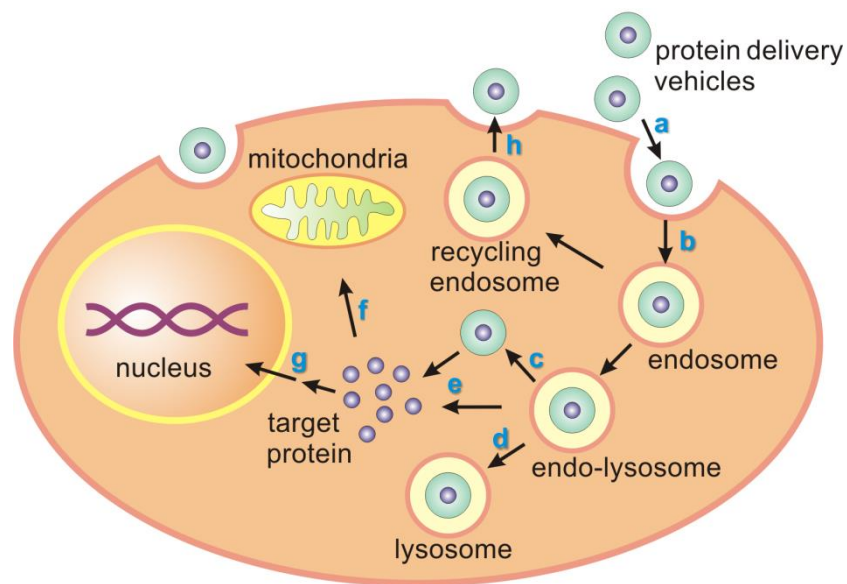


Figure 1. Schematic process of a typical endocytic pathway for nanocarriers of protein cargoes. (a) cell-surface attachment of protein delivery vehicles; (b) internalization of delivery vehicles via endocytosis; (c) endosomal escape of delivery vehicles or (d) lysosomal degradation; (e) target protein diffuses into cytoplasm; (f) transport of target proteins to specific organelle; (g) participate in cellular functions such as signal transduction; (h) exocytosis of delivery vehicles.

In the past decade, nanocarrier-based^{3, 11} intracellular protein delivery approaches have generated considerable interest and have been shown to be promising strategies. As summarized in Fig. 2, these nanosized carriers include lipid-containing colloidal systems such as liposomes and solid lipid nanoparticles, polymeric nanocarriers, inorganic nanoparticles/nanotubes and protein-based carriers. Target protein cargos can be loaded into various nanocarriers using different strategies, including direct conjugation via either chemical or genetic modifications, physical adsorption and covalent/noncovalent encapsulation. One of the key functions of the nanocarriers is to serve as shields to protect proteins from premature degradation and various denaturing interactions with the biological environment^{3, 12, 13}. They can increase the stealth of the delivered protein by concealing antigenic and immunogenic epitopes and attenuating receptor-mediated uptake by the reticuloendothelial system (RES)¹⁴. Furthermore, nanocarriers can prevent protein proteolysis and can increase the size of the delivered cargo *in vivo*, thus reducing renal filtration. The high surface area to volume ratio of nanocarriers also leads to improved pharmacokinetics and biodistribution of payload^{3, 15, 16}. Another crucial feature of nanocarrier-based delivery system is the increased flexibility of tailoring the chemical and physical properties of the vehicle through controlled synthesis, assembly, and facile biocompatible chemical modifications.^{17, 18} Key particle properties such as size, surface charge and displayed ligands¹⁹ can be customized to facilitate cell penetration and endolysosomal escape, as well as to optimize stability, targeting specificity and cargo release kinetics.

In the following sessions, recent methodologies developed for intracellular protein delivery using nanocarriers are summarized. Advantages and limitations of current approaches, as well as future opportunities and challenges are also discussed.

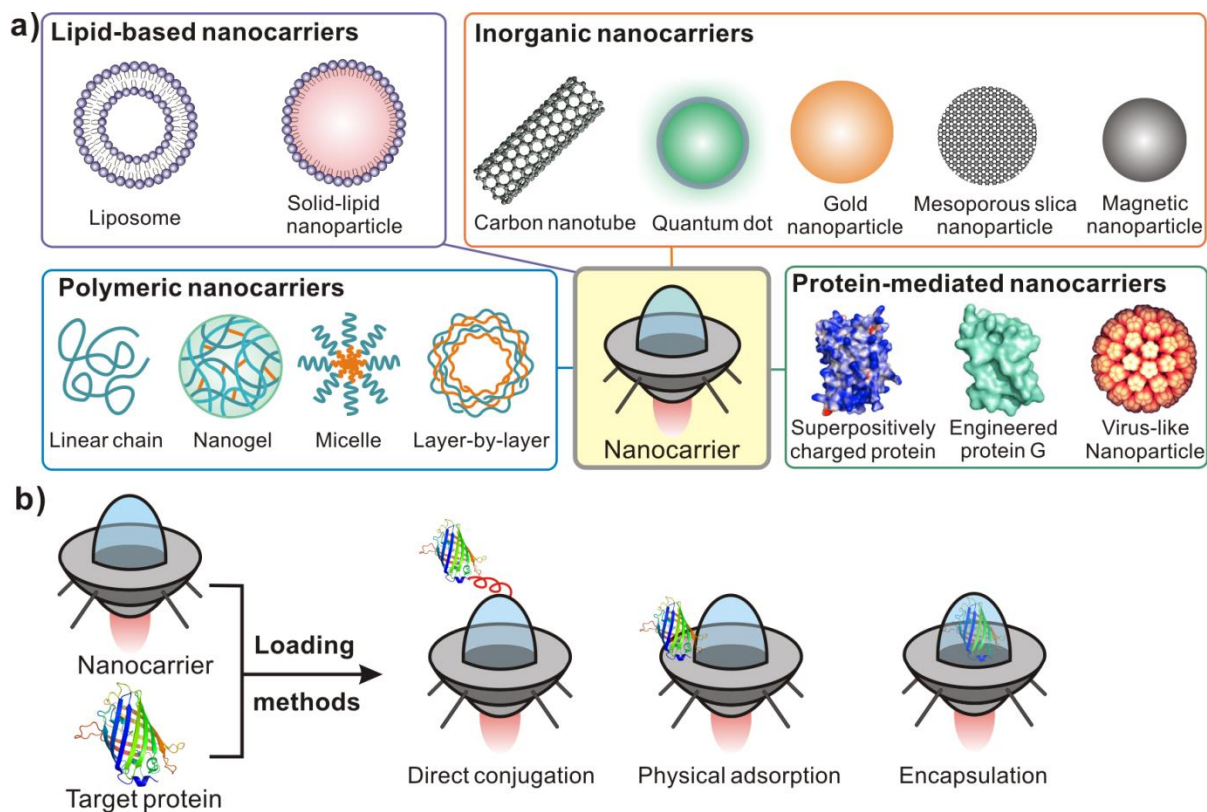


Figure 2. (a) Schematic of various types of nanocarriers used for protein intracellular delivery. (b) Schematic of three main loading methods for preparing protein/nanocarrier composites. Different nanocarriers are represented as a “space shuttle”.

1.2 Lipid-based nanocarriers

1.2.1 Liposomes

Liposomes are bilayered vesicles assembled from amphiphilic building blocks, such as lipids or phospholipids. The sizes of liposomes can range from ~ 20 nm to several microns. Liposomes can adhere to plasma membranes and enter the cell via endocytosis or liposome-cell fusion.¹⁵ Different liposome formulations have been explored as delivery vehicles for various hydrophilic or hydrophobic compounds³.

Debs *et al* demonstrated liposome-mediated carrier as a useful tool for functional

protein delivery. A mammalian transcriptional regulator, glucocorticoid receptor derivative T7X556, was encapsulated into the cationic liposomes DOTMA (*N*-[1-(2,3-dioleyloxy)propyl]-*N,N,N*-trimethyl-ammonium chloride).²⁰ They found T7X556 delivered using this strategy readily localized to the nucleus and specifically enhanced expression from glucocorticoid response element-linked promoters. Lenormand and coworkers utilized liposomes for intracellular delivery of therapeutic membrane proteins.²¹ The voltage-dependent anionic channel (VDAC) and the pro-apoptotic Bak were assembled into the lipid bilayer of liposomes (lipids were obtained from spinach Thylacoids), forming proteoliposome particles. They demonstrated that the internalization of integrated protein/liposomes into living cells induced apoptosis by release of cytochrome *c* and activation of caspases. Zelphati *et al.* developed a cationic lipid-mediated delivery system consisting of a trifluoroacetylated lipopolyamine (TFA-DODAPL) and dioleoyl phosphatidylethanolamine (DOPE).²² Various target proteins with different sizes and surface charges were successfully delivered into the cytosol of numerous adherent and suspension cells. The intracellular activity of β -galactosidase was prominently observed in X-gal-stained cells while the internalization of caspase-3, caspase-8 and granzyme B effectively triggered apoptosis. Zuber and coworkers applied an *in situ* dimerized amphiphile (CholCSper) along with DOPE to create an intracellular protein delivery vehicle.²³ CholCSper can generate disulfide linkers upon mild oxidation. Chemical conversion of gemini-like CholCSper amphiphiles led to stabilization and homogenous protein nanocomposites. This delivery approach resulted in a controlled, prolonged release of the encapsulated protein cargo. Dalkara *et al.* investigated the fundamental principles governing anionic protein delivery by lipospermine DOGS (dioctadecylglycylspermine).²⁴ They concluded that protein surface area rather than

electric charge ratio determines delivery properties. The intracellular delivery of anti- β -actin and anti- α -tubulin IgG's resulted in fiber depolymerization, which demonstrated successful delivery of antibodies to the internal compartments of cells.

Fretz *et al.* described photochemical internalization (PCI) as a tool to enhance endosomal escape of the liposome-mediated protein delivery of the cytotoxic protein saporin.²⁵ Human ovarian carcinoma (OVCAR-3) cells incubated with protein/liposome complexes and the photosensitizer (TPPS2a) were treated with illumination for various durations to carry out the photochemical internalization. While the amount of delivered saporin was important for cytotoxicity, the authors also found that increasing illumination time can lead to more effective endosomal escape and is also critical for the effective cytosolic delivery. Chiu and coworkers applied a single nanosecond pulse from a far-red laser (645 nm) to facilitate the release of lipid-based nanocarriers into the cytosol.²⁶ They delivered O6-alkylguanine-DNA alkyltransferase (AGT) fusion protein into Ba/F3 cells to induce apoptosis by inhibiting BCR-ABL, a key kinase in the apoptotic pathway.

Recently, several commercial lipid-based reagents have been utilized for protein delivery. For examples, Humpel and coworkers used lipid-mediated gene transfer (FuGENE6TM) and protein delivery reagent BioPORTERTM to deliver pro-apoptotic caspase-3 into malignant C6 glioma and immortalized rBCEC4 brain endothelial cells.²⁷ Caspase-3 induced TUNEL-positive cell death was observed in both cell lines. Weill *et al.* used a cationic amphiphile-based protein delivery reagent PULSinTM for cytosolic delivery of fluorescent proteins, R-phycoerythrin (R-PE) and Histone-H1-AlexaFluor®488.²⁸

1.2.2 Solid lipid nanoparticles

Solid lipid nanoparticles (SLNs) are lipid-based submicron colloidal particles that can be an alternative to liposomes.²⁹ Because of their relatively rigid core composed of hydrophobic lipids that are solid at room or body temperature, SLNs are more stable for biological applications in comparison to liposomes. Two primary preparation methods have been developed: 1) a high-pressure homogenization technique pioneered by Müller and Lucks and 2) a microemulsion technique explored by Gasco. Almeida *et al.* demonstrated protein incorporation into SLNs using lysozyme as a model enzyme.³⁰ The lysozyme remained intact and active through the entrapment process, as shown by gel electrophoresis, as well as the rate of lysis of *Micrococcus lysolideikticus*. This study opens avenue for the use of SLN as antigen carriers for vaccine delivery.

1.3 Polymeric nanocarriers

1.3.1 Direct attachment

The direct conjugation of polymers, such as poly(ethyleneglycol) (PEG), to proteins has been widely explored as a means to increase the systemic circulation of serum-based protein drugs. To date, various antibodies, cytokines and growth factors have been PEGylated³¹ and the resulting polymer/protein conjugates have received the Food and Drug Administration (FDA) approval for clinical use.³² Attachment of polymers to protein surfaces can be accomplished using well-established bioconjugation methods in literature. Reactive side chains on protein surfaces, such as amines, thiols, carboxylic acids and hydroxyl groups can all serve as the tethering site, depending on the coupling chemistry. Several methods using direct polymer attachment have also been developed to achieve intracellular delivery of target protein.

Yamada and coworkers have widely explored intracellular protein transduction by chemically conjugating polyethylenimine (PEI) to the surface of various proteins to create cationized macromolecules.^{33, 34} The authors were able to deliver a diverse array of proteins including ribonuclease (RNase), enhanced green fluorescent protein (EGFP) and IgG to the cytosol of murine and human fibroblast cells without observing significant differences in protein function. Proteins were internalized via receptor or transporter-independent endocytosis.³⁵ When PEI-EGFP was injected both intraportally and intraperitoneally *in vivo* to mice, cellular internalization was observed within 8 hours which was absent from mice treated with native EGFP. The system was further expanded by reversibly cationizing proteins by first incorporating disulfide bonds which can reduce under cytosolic conditions. Denatured human tumor-suppressor p53 was delivered to human osteogenic sarcoma-derived Saos-2 cells through a reversibly cationized complex and subsequent reduction of disulfide bonds in the cytosol and refolding into tetramers *in vitro* resulted in downstream intracellular events such as nuclear localization and induction of p53 target genes and eventual apoptosis.³⁶ The authors have since extended the direct PEI-attachment system to synthesize platform protein transduction carrier molecules for biotinylated proteins or antibodies by synthesizing PEI-cationized streptavidin, avidin or protein G.³⁷ They showed the utility of their engineered system by delivering functional protein simian virus 40 large T-antigen (SVLT-N), which inactivates retinoblastoma family proteins, by reversible biotinylation and complexation with PEI-cationized avidin.³⁸ Delivery of the complex to 3T3 fibroblast cells resulted in nuclear delivery of SVLT-N, interaction with cellular machinery and subsequent induction of cell proliferation.

Lackey *et al.* constructed a model system with an antibody conjugated to a pH-

sensitive poly(propylacrylic acid) (PPAAc) (Table 1), which can disrupt the endosomal membrane and aid delivery of the protein cargo to the cytosol.³⁹ Both the anti-CD3 antibody and the PPAAc polymer were first biotinylated, and complexed together in the presence of streptavidin. Confocal microscopy was used to determine that receptor-mediated endocytosis is the mechanism of cellular internalization for both the polymer-protein complex and the antibody itself. Visualization of the internalized ternary polymer-protein complex showed diffuse staining in the cytosol indicating endosomal escape, whereas antibody without conjugation of PPAAc showed punctate fluorescence, indicating no release from lysosomal or endosomal compartments. Recently the authors extended this strategy *in vivo* by directly conjugating PPAAc to the model antigen ovalbumin (OVA).⁴⁰ When the conjugates were delivered *in vivo* to an EG.7-OVA mouse tumor protection model, production of specific CD8+ T lymphocytes and antiovalbumin IgG increased 8-fold and 11-fold, respectively, resulting in robust inhibition of tumor growth.

More recently, Park and coworkers used glucose-coated polymeric beads to demonstrate delivery of EGFP into mouse embryonic stem (mES) cells and HeLa cells.⁴¹ The glucose coating was applied to establish interactions between beads and cell membrane. The monodispersed beads with a size of ~ 150 nm were obtained by dispersion polymerization in the presence of 6-*O*-glucosyl methacrylate, styrene, and acrylic acid (Table 1). The protein was then conjugated to the beads using the coupling EDC (1-ethyl-3-(3-dimethylaminopropyl) carbodiimide). Neither native EGFP alone nor EGFP-conjugated beads without glucose coating was found to be internalized into cells. However, the EGFP-conjugated, glucose-coated beads were clearly internalized into cells as visualized by fluorescence microscopy and transmission electron microscopy (TEM).

The transduction was inhibited at 4°C, indicating that the internalization process involved an endocytic pathway.

1.3.2 Physical adsorption and interaction

One major disadvantage of covalent conjugation of carrier to protein is that the cargo is chemically modified, often in a nonspecific fashion. This may lead to deleterious effects on the activities of the cargo. An alternate, commonly used method without covalent modification is the self-assembly between the protein and the nanocarrier. The spontaneous assembly is typically facilitated by physical adsorption, which is driven by electrostatic forces or van der Waals interactions. Hu *et al.* have utilized emulsion polymerization to generate pH-responsive core-shell nanostructures to load and deliver small molecules and proteins.⁴² The pH-sensitive core of nanoparticles was formed by a tertiary amine monomer (2-diethylamino ethyl methacrylate (DEAEMA); $pK_b \sim 7.0-7.3$) (Table 1) and a crosslinker (poly(ethylene glycol) dimethacrylate (PEGDMA; $pK_b \sim 11$); while the pH-insensitive hydrophilic shell layer was formed by the addition of a primary amine monomer (2-aminoethyl methacrylate (AEMA)). Highly monodisperse particles were synthesized with a diameter of ~205 nm at pH 7.4. Remarkably, these particles exhibited an abrupt size change between pH 7.0 and 6.8. The diameter increased by 2.8-fold upon moving from buffer solution with pH 7.4 (extracellular/cytosolic environment) to pH 5 (endolysosomal environment) at 37 °C, corresponding to a ~22-fold volume change. OVA was then mixed with core-shell nanoparticles via electrostatic adsorption. After incubation of protein-containing nanoparticles with bone marrow-derived dendritic cells (BMDCs) for 1h at 37 °C, fluorescently-tagged OVA was clearly observed in the cytosol and nucleus in BMDCs. As expected, DCs treated with OVA-loaded pH-

responsive nanoparticles elicited 4-fold more cytokine interferon- γ (IFN- γ) secretion compared to free OVA without carriers.

Akiyoshi and coworkers demonstrated the effective intracellular delivery of anionic proteins using self-assembled cationic nanogels.⁴³ The cationic nanogel matrix stabilized encapsulated protein molecules and prevented aggregation (Table 1). To enhance the cationic properties of the nanogel, the authors functionalized cholesteryl group-bearing pullulan (CHP) with an ethylenediamine group to form CHPNH₂. This in turn resulted in strong interaction with anionic FITC-BSA, and led to the formation of <50 nm nanoparticles by self-assembly in water. Flow cytometry analysis showed more efficient intracellular uptake into HeLa cells using CHPNH₂ nanogels compared to cationic liposomes and protein transduction domain-based carriers, both in the presence and absence of serum. Nanogels were observed to undergo macropinocytosis, escape into the cytosol, and dissociate into protein and CHPNH₂. Dissociation of the nanogel complex was attributed to an exchange mechanism resulting from substitution of protein with other intracellular hydrophobic substrates. Cell viability did not decrease after 24 h incubation of 100 nM nanogels, indicating the polymer vehicle is biocompatible. Sub-cellular delivery of target protein into nuclei by CHPNH₂ nanogels was also demonstrated using nuclear localization signal (NLS) tagged GFP. Recently, Kiyono and coworkers extended cationic CHP nanogels to construct an intranasal antigen-delivery vehicle for adjuvant-free vaccination.⁴⁴ They selected a non-toxic receptor-binding fragment of *C. botulinum* type-A neurotoxin subunit antigen Hc (BoHc/A) as a prototype vaccine antigen. They successfully demonstrated that CHP nanogels loaded with BoHc/A continuously attached to the nasal epithelium and were effectively internalized by CD11c⁺ dendritic cells. A strong botulinum-neurotoxin-A-specific mucosal IgA antibody

and serum IgG and secretory responses was effectively induced in the absence of co-administration of the mucosal adjuvant, whereas responses were not observed in mice immunized with naked BoHc/A or control PBS. Moreover, the authors validated that [^{111}In]-labelled BoHc/A nanogels did not accumulate in the olfactory bulbs or brain, which eliminated safety concerns of the potential internalization of antigens to the central nervous system (CNS).

Zimmerman and coworkers demonstrated effective intracellular delivery of copper/zinc superoxide dismutase (CuZnSOD), which can scavenge O_2^- intermediates resulting from aberrant AngII signaling in the central nervous system in a multitude of cardiovascular diseases.⁴⁵ “Nanozymes” were created by complexing CuZnSOD with a copolymer of PEI and PEG to create polyion complexes. When the nanozymes were delivered to mouse catecholaminergic CATH neurons, the increase in O_2^- intermediates caused by AngII was significantly inhibited compared to untreated neurons or neurons treated with native CuZnSOD. When CuZnSOD nanozymes were injected *in vivo* using an intracarotid injection into rabbits along with intracerebroventricular-delivered AngII, the responses of AngII were significantly inhibited without any toxic effects. In comparison, intracarotid injection of free CuZnSOD or PEI-PEG copolymer did not exhibit inhibition of AngII responses.

Yang and coworkers exploited biodegradable, cationic and amphiphilic copolymer poly(*N*-methyldietheneamine sebacate)-*co*-[(cholesteryl oxocarbonylamido ethyl) methyl bis(ethylene) ammonium bromide] sebacate) (P(MDS-*co*-CES)) (Table 1) to deliver lectin A-chain, an anticancer glycoprotein.⁴⁶ The nano-complexes had an average size of ~ 150 nm and ζ -potential of $\sim +30$ mV. Cytotoxicity assays of lectin A-chain delivered by polymeric nanoparticles were performed towards various cell lines. The IC_{50} values were

20, 50, 40 and 100 ppm for MDA-MB-231, HeLa, HepG2 and 4T1 cells, respectively. In comparison, lipid-based BioPorter/lectin A-chain complexes showed significantly weaker cytotoxicity indicating less efficient intracellular delivery of lectin A-chain. The difference can be attributed to greater cellular uptake, stability and endosomal buffering capacity of nanoparticle/lectin A-chain complexes.

Hasadsri *et al.* utilized polybutylcyanoacrylate (PBCA) as an effective carrier to deliver specific proteins to neurons.⁴⁷ PBCA nanoparticles undergo degradation *in vivo* due to enzymatic ester hydrolysis which produces a primary alcohol, butanol, and water soluble poly(2-cyanoacrylic acid). The nanoparticles (200-250 nm) were synthesized using anionic polymerization with dextran as a stabilizer. Incubation of nanoparticles with protein led to formation of the loaded delivery vehicle via adsorption. Effective delivery of three different proteins to neuronal cultures were demonstrated: recombinant *E.coli* β -galactosidase, recombinant human Myc-tagged rhoG and anti- α -synuclein mouse monoclonal antibody H3C. Each of the three protein cargo were shown to be successfully delivered indicated by positive staining for β -gal activity, morphological changes in response to rhoG, and immunostaining of α -synuclein. Notably, the nanoparticle delivery of rhoG led to neurite outgrowth and differentiation on PC12 cells after 2 days whereas genetic transfection of rhoG needs 4 days.

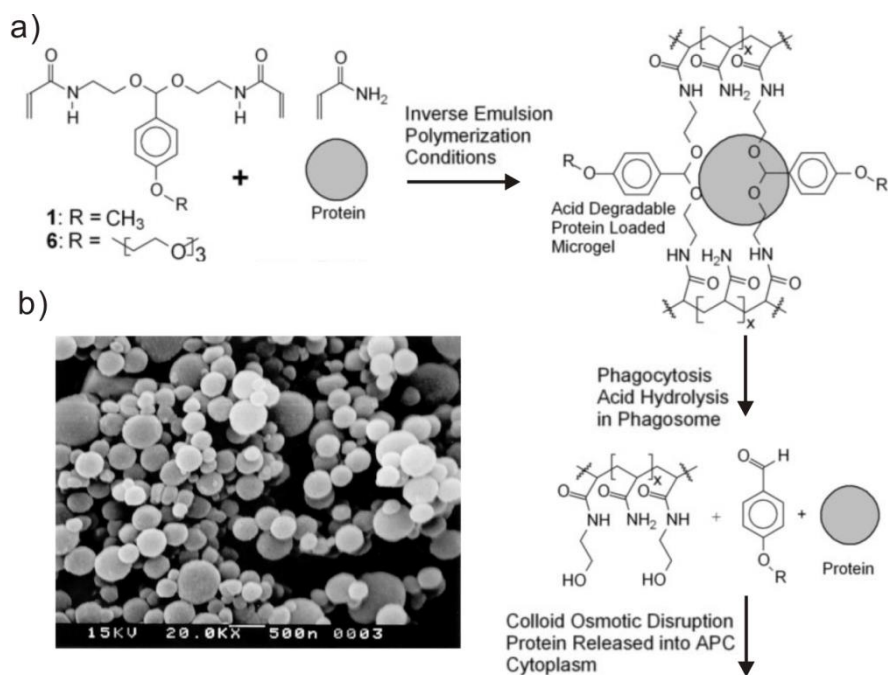


Figure 3. Microgels for protein delivery to antigen presenting cells (APCs) by Fréchet and coworkers. (a) Schematic of molecular design of microgels. (b) SEM image of ovalbumin (OVA)-loaded microgels made of acrylamide and (*N,N'*-Bisacryloyl-di-(2-aminoethoxy)-[4-(1,4,7,10-tetraoxaundecyl)phenyl]methane) (**6**) at 1.6 % crosslinking density. Reprinted with permission from ref. ⁴⁸. Copyright 2003 PNAS.

1.3.3 Emulsion-based encapsulation

Fréchet and colleagues have widely explored protein intracellular delivery through emulsion-based encapsulation that can degrade in the acidic environment of endosomes. Murthy *et al.* encapsulated OVA in particles sized from 200-500 nm using acrylamide as the monomer and an acid degradable crosslinker containing a hydrophilic triglyme moiety as shown in Fig. 3 and Table 1.⁴⁸ Particles were prepared using an inverse microemulsion technique where the aqueous phase (monomer, protein, and crosslinker) was dispersed via sonication in the organic phase (hexane and surfactants, Tween 80 and Span 80). After

free radical initiator was added, polymerization around the protein formed water-soluble microparticles. Whereas only 10% protein was released over 5 hours at pH 7.4, 80% of encapsulated protein was released at an acidic, endosomal pH 5.0. Acid-degradable protein nanoparticles activated three times more OVA-specific cytotoxic lymphocytes after delivery to antigen presenting cells compared to native OVA and showed 75% viability at 5 mg/mL. This study demonstrated acid-degradable nanoparticles as promising carriers for protein-based vaccines. To investigate the effect of particle size on the activation of T-cells with the treatment by antigen-presenting cells, Cohen *et al.* prepared OVA particles with mean diameters of 35 nm and 3.5 μm by emulsion and microemulsion based polymerization.⁴⁹ *In vivo* studies suggested that there was no significant difference for both sizes of particles in stimulating the proliferation of T-cells and both were able to generate antigen-specific cytotoxic T-cell response upon coadministration with immunostimulatory DNA. Furthermore, the double emulsion water/oil/water evaporation method was also explored, by incorporating biocompatible and degradable polymers, such as acetalated-dextran^{50, 51} and polyurethane⁵² with acetal moieties. In order to achieve high cell-penetrating ability and enhance subsequent activity, protein nanoparticles were conjugated with unmethylated CpG oligonucleotide ligands⁵³ or cell-penetrating peptides^{51, 54}.

Generally, microencapsulation techniques require multiple steps that may deteriorate protein stability and activity, including exposure to organic and aqueous interfaces, shear stress during homogenization of phases, and lyophilization. To combat these issues, Diwan *et al.* enhanced protein stability during encapsulation in PLGA microspheres by PEGylating the surface amine groups of lysozyme with methoxy-polyethylene glycol succinimidyl succinate.⁵⁵ Pegylated lysozyme formed less aggregates

during the encapsulation process and exhibited a near complete, sustained release of protein over 85 days compared to native lysozyme which suffered aggregation and a 65% burst release *in vitro*.

1.3.4 *In situ* polymerization

Different from emulsion-assisted encapsulation, *in situ* polymerization-based encapsulation occurs on the surface of core materials, similar to interfacial polymerization. Yan *et al.* have recently developed an intracellular delivery strategy based on nanocapsules that consist of a single-protein core and thin polymer shell anchored covalently to the protein core.⁵⁶ Briefly, polymerizable vinyl groups were covalently linked to the protein; subsequently, polymerization is performed in an aqueous solution containing monomers and crosslinker to wrap each protein core with a thin polymer shell that can protect the protein content from denaturation and proteolysis. This scheme enabled the synthesis of protein nanocapsules with non-degradable or degradable shells by using non-degradable or degradable crosslinker (Table 1), respectively. TEM and AFM images of horseradish peroxidase (HRP) indicated these nanocapsules were spherical with uniform diameter around 15 nm. By labeling each HRP molecule with a single 1.4 nm gold nanoparticle, most nanocapsules observed contained only one single gold nanoparticle, further confirming a single-protein core-shell structure. Nanocapsules encapsulating a wide variety of reporter and functional proteins including EGFP, HRP, BSA, superoxide dismutase (SOD), and caspase-3. Non-degradable nanocapsules exhibited long-term intracellular stability while degradable nanocapsules dissociated in the acidic environment in the endosome. The cells treated with EGFP nanocapsules

showed significantly higher fluorescence intensity than those with native EGFP and TAT-fused EGFP. Further cellular internalization studies suggested that the EGFP nanocapsules uptake was through a clathrin/caveolae-mediated endocytosis pathway. The authors also demonstrated *in vivo* stability of nanocapsules. EGFP nanocapsules remained intense fluorescence even 50 h after injection to nude mice, while HRP nanocapsules showed enzymatic activity 8 h after injection. Recently, Du *et al.* utilized the “single protein nanocapsule” concept to encapsulate HRP and decorate the polymeric shell of nanocapsules with quantum dots (QDs) for a bioluminescence study.⁵⁷ The bioluminescence generated from HRP-mediated oxidation of luminol can well-overlap with the absorbance wavelengths of QDs, which enables their effective bioluminescence resonance energy transfer (BRET). The maximum BRET efficiency can be achieved by adjusting the enzyme/QD conjugation ratio. Furthermore, Gu *et al.* developed a fluorescence resonance energy transfer (FRET)-based protease detection strategy, using a single-fluorescent-protein nanogel as donor and a dark quencher as acceptor linked by a photolabile caged-peptide.⁵⁸ Utilizing caspase-3 as a target protease, the authors demonstrated this design can be used for on-demand probing of protease activity within cells in a UV-responsive fashion.

Gu and Tang *et al.* conceived a new approach for preparation of single protein nanocapsules in which the protein was encapsulated by an enzymatically degradable polymeric network.⁵⁹ Instead of irreversible, pre-modification of protein surface, the protein cargo was reversibly encapsulated within a thin polymer shell through physical adsorption of monomers/crosslinkers and followed *in situ* polymerization, as illustrated in Fig. 4. The crosslinker that interconnected the polymeric matrix was a peptide linker that can be cleaved by a specific protease. Caspase-3 was selected as the model protein and

bisacrylated peptide crosslinker containing Asp-Glu-Val-Asp (DEVD), which is the substrate of caspase 3, was used to synthesize a self-degradable nanocapsule. The self-degradation progress was monitored in cell-free systems to occur at 37 °C compared to negligible degradation at 4 °C. Degradable nanogels were shown to induce apoptosis when delivered to a variety of mammalian cells in comparison to nanogels constructed with non-degradable crosslinker or native protein. To achieve a spatiotemporal control of caspase-3 nanocapsule degradation, the P1 aspartic acid was conjugated to a photolabile *o*-nitrobenzyl ester moiety. Only after decaging of the aspartic acid was caspase-3 able to recognize the peptide substrate and cleave the polymeric shell. In comparison, cells treated with only caspase-3 nanocapsules without UV or cells treated with only UV did not show significant cell death.

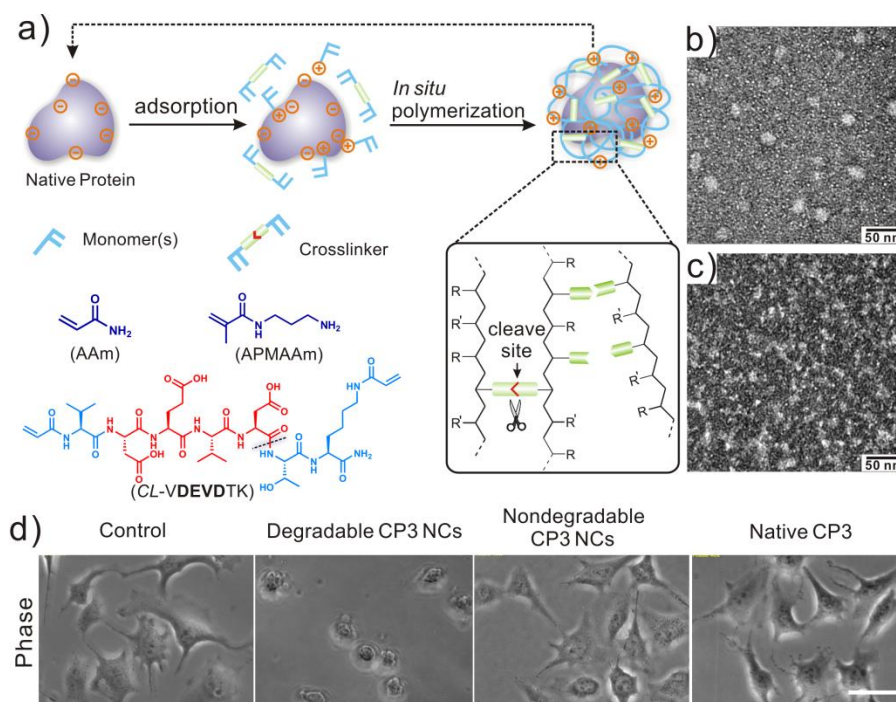


Figure 4. Enzymatically degradable single-protein nanocapsules for intracellular protein delivery by Tang and coworkers. (a) Schematic of the one-pot preparation of protein nanocapsules by in situ polymerization and typical monomers and crosslinker used in the caspase-3 (CP3) based nanocapsule study. (b) TEM images of fresh CP3 nanocapsules (CP3-NC13) and (c) the sample experienced self-degradation at 37 °C for 12 h in pH 7.4 PBS buffer. (d) Bright-field-microscopy images of HeLa cells treated for 24 h with i) saline; ii) 200 nM degradable CP3-NC; iii) nondegradable CP3 NCs and iv) native CP3. The scale bar is 50 μm. Reprinted with permission from ref. ⁵⁹. Copyright 2009 American Chemical Society.

The protease-assisted protein delivery was recently generalized through targeting of the essential endoprotease Furin, which is a ubiquitous proprotein convertase expressed in all eukaryotic organisms and most mammalian cells.⁶⁰ Protein cargos encapsulated using a furin-degradable peptide crosslinker of various sizes and tertiary structures were successfully delivered to various cell lines. Notably, furin-mediated intracellular delivery was used to achieve nuclear delivery of both fluorescent protein and transcription factor (TF) Klf4. It indicated the endoprotease-degradable nanocapsules were able to protect the

protein during cellular uptake and that the protein was released in active form and able to interact with cellular machinery. This study provides guideline of designing robust TF delivery system for reprogramming cell fate.^{61, 62}

1.3.5 Polymeric micelles

In 2009, Lee *et al.* reported a new delivery strategy based on 50 nm core-shell structured polyionic complex (PIC) micelles, which are formed via electrostatic interactions. Block copolymers were synthesized to incorporate both ionic and neutral regions and were subsequently allowed to associate with counterions of the charged region thereby creating micelles.⁶³ In this study, the cationic protein cytochrome *c* was modified with citraconic and *cis*-aconitic anhydrides to invert the surface charge and subsequently decrease the pI value as shown in Fig 5. Next PIC micelles were formed between charge-inverted cytochrome *c* and cationic block copolymer PEG-pAsp(DET) (Table 1). The micelles displayed a charge-conversional property since citraconic amides and *cis*-aconitic amides are stable at the physiological pH 7.4 but dissociate at endosome pH 5.5. PIC micelles showed efficient cytochrome *c* endosomal escape and subsequent diffusion to cytosol compared to non-charge-conversion control micelles which contained succinic amide modifications. The authors also demonstrated that the activity of cytochrome *c* was not compromised upon modification of the surface amine groups. This method demonstrated a stable PIC micelle protein delivery system without the use of cross-linking. Most recently, the authors have extended this technique to deliver a bioactive antibody, anti-NPC (nuclear pore complex) mouse IgG to human hepatoma cells.⁶⁴ They confirmed that the charge-conventional PIC micelles can successfully deliver IgG into cytosol and the

IgG recognition toward NPC was highly retained, further promoting applications in cellular imaging and therapeutic targeting of specific antigens.

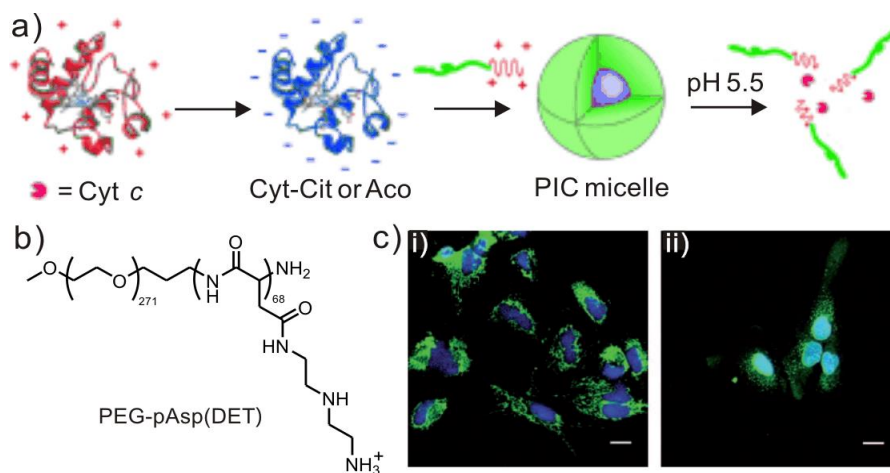


Figure 5. Polyionic complex micelles (PIC) for intracellular protein delivery developed by Kataoka and coworkers. (a) Schematic representation showing the preparation of the charge-conversional PIC micelles containing cytochrome *c* (Cyt *c*) and (b) diblock copolymer PEG-pAsp(DET), in which the ionic portion can interact with Cyt *c* forming micelles. (c) Recognition of NPC in fixed human hepatoma (HuH-7) cells by anti-NPC IgG-Cit after 4 h of incubation at i) pH 7.4 and ii) pH 5.5. Anti-NPC IgG-Cit was applied to the cells after fixation. The cell nuclei were stained by Hoechst 33258 (blue), and the anti-NPC IgG-Cit was detected by a secondary antibody (green). Scale bars: 20 μm . Reprinted with permission from ref. ^{63, 64}. Copyright 2009 Wiley-VCH.

Polymeric micelles were also synthesized by Kim *et al.* in which a positively-charged di-block copolymer conjugate of poly(L-lysine)-poly(ethylene glycol)-folate (PLL-PEG-FOL) was complexed to negatively charged FITC-BSA (Table 1).⁶⁵ This method targets specific cells which possess a folate receptor which is a marker for several cancers and could be used for tumor-selective drug delivery. Intracellular uptake was greatly enhanced for the 25 nm complexes made using PLL-PEG-FOL compared to PLL-

PEG. To confirm the uptake was due to folate receptor mediated endocytosis, a folate receptor deficient cell line (A549) and folate overexpressing line (KB) were compared. The comparative study showed only an enhanced cellular uptake for the KB cell line upon complexation of FITC-BSA and PLL-PEG-FOL versus PLL-PEG or native FITC-BSA.

Akagi *et al.* selected biodegradable poly(γ -glutamic acid) (γ -PGA) (Table 1) to deliver target proteins.⁶⁶ The β -carboxylate side chains of γ -PGA were modified with hydrophobic amino acid derivatives such as L-phenylalanine ethylester and L-tryptophan methylester. The resulting block copolymer was added to an equal volume of hydrophilic OVA or recombinant human immunodeficiency virus-1 gp120 to create 250-300 nm protein-loaded nanoparticles. When γ -PGA-gp120 nanoparticles were delivered intranasally to mice, antigen-specific immune responses were detected through induction of IFN- γ -producing splenocytes and antigen-specific CTL activity.

1.3.6 Layer-by-layer encapsulation

The layer-by-layer (LbL) encapsulation is based on the consecutive adsorption of oppositely charged polyelectrolytes around a sacrificial template core, which is followed by chemically dissolved. De Rose *et al.* applied the LbL strategy to load nanoengineered capsules with an oligopeptide vaccine (KP9 epitope).⁶⁷ The pair of polyelectrolytes included biodegradable thiolatedpoly(methacrylic acid) (PMA_{SH}) and poly(vinylpyrrolidone) (PVPON). The cysteine modified KP9 was first conjugated to PMA_{SH} through disulfide linkage, which can be cleaved inside cells for releasing KP9. The resulting KP9 carried polymer was adsorbed onto the amine-grafted silica template particles. PVPON and PMA_{SH} were then alternately assembled. Finally, KP9 encapsulated hollow particles were formed upon the removal of the

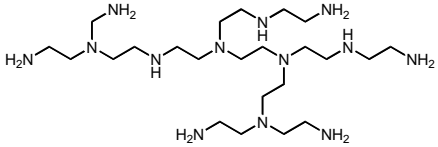
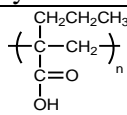
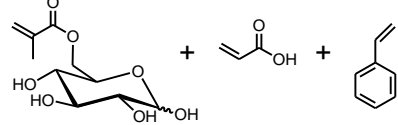
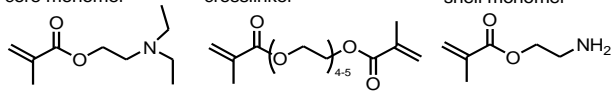
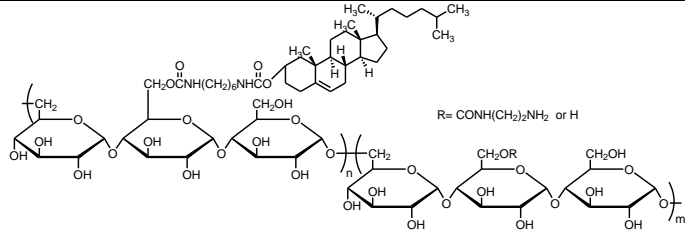
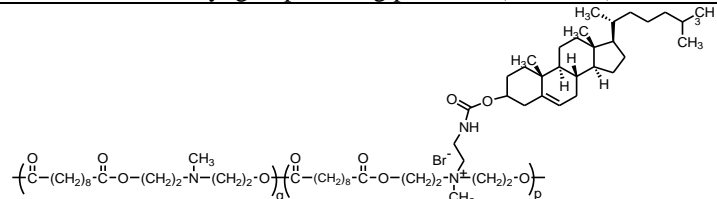
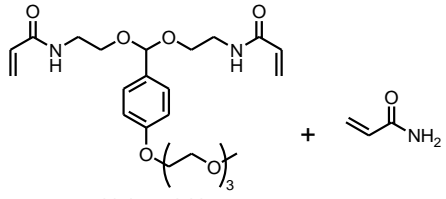
template. The authors demonstrated that the intracellular delivery of KP9 capsules stimulated a significant proportion of the KP9-specific CD8 T cells, which simultaneously expressed cytokines of IFN- γ and TFN- α .

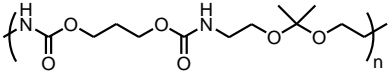
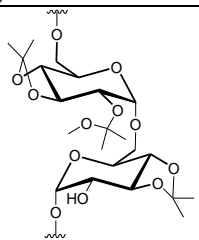
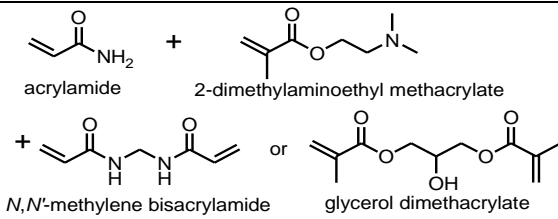
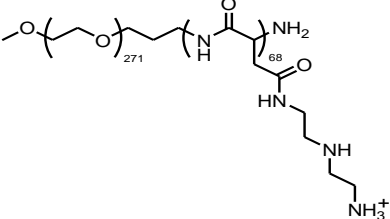
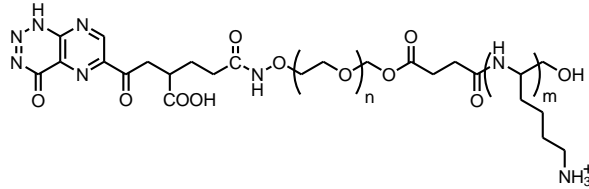
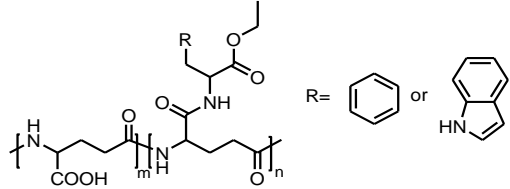
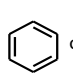
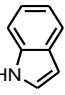
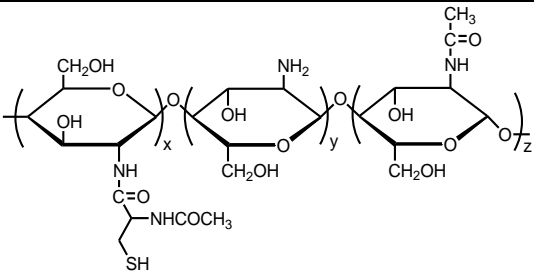
Using the LbL method, Parak and coworkers developed enzymatically degradable capsules for OVA delivery.⁶⁸ CaCO₃ particles coprecipitated with BODIPY dye conjugated OVA were selected as the template. Two bilayers, dextran sulfate/ poly-L-arginine (DEXS/pARG) and sodium poly(styrenesulfonate)/ poly(allylamine hydrochloride) (PSS/PAH) were selected to form degradable and nondegradable shells respectively. Because of the close proximity of dye molecules, the green fluorescence of BODIPY was self-quenched in the capsule cavity and showed red excimers. The authors presented that in the case of nondegradable capsules delivered towards embryonic NIH/3T3 fibroblasts, such red emission remained over incubation periods up to several days. In contrast, when using biodegradable DEXS/pARG capsules, the self-quenching of dyes was relieved and bright green emission appeared, indicating effective release of proteins upon harnessing of intracellular enzymes.

Recently, Shu *et al.* employed gradient shell cross-linked hollow polyelectrolyte nanocapsules for protein intracellular delivery.⁶⁹ The protein loaded polymeric outer shell consisting of dextran sulfate and chitosan decorated with cysteamine was formed by four steps: 1) loading target protein to the β -cyclodextrin functionalized silica spheres through physical adsorption; 2) LbL assembling polymers (Table 1) on silica spheres; 3) cross-linking thiols to generate polymeric matrix; and 4) removal of silica core-based templates. The authors demonstrated this disulfide bond gradient cross-linked nanocapsules had both reduction and pH sensitivity. Using BSA as a model protein, the release of protein from nanocapsules was performed in the buffer solution of pH 1.4 (simulating the pH in the

stomach) and 6.8 (simulating the extracellular pH). The authors demonstrated that the cross-linked nanocapsules can remain stable in physiological pH levels and protect the loss of protein in the gastric cavity. It is noteworthy that this approach can not only reduce the loss of protein in acidic environments, but also achieve the sustained release of protein in the cytosol.

Table 1. Selected polymers or monomers used for polymeric nanocarriers for the protein intracellular delivery.

Loading Methods	Polymer or Monomers	Ref.
Direct attachment	 <p style="text-align: center;">polyethyleneimine (PEI)</p>	33
	 <p style="text-align: center;">poly(propylacrylic acid) (PPAAc)</p>	39
	 <p style="text-align: center;">6-O-glucosyl methacrylate, acrylic acid and styrene</p>	41
Physical adsorption	 <p style="text-align: center;">core monomer crosslinker shell monomer</p> <p style="text-align: center;">DEAEMA PEGDMA AEMA</p>	42
	 <p style="text-align: center;">cholesteryl group-bearing pullulans (CHPNH₂)</p>	43
	 <p style="text-align: center;">Poly(<i>N</i>-methyldietheneamine sebacate)-<i>co</i>-[(cholesteryl oxocarbonylamido ethyl) methyl bis(ethylene) ammonium bromide] sebacate) (P(MDS-<i>co</i>-CES))</p>	46
Microemulsion-based encapsulation	 <p style="text-align: center;">acid-degradable crosslinker acrylamide</p>	48

	 <p>Polyurethane with acetal</p>	52
	 <p>Acetyl-derivatized dextran</p>	50
<i>in situ</i> polymerization	 <p>acrylamide + 2-dimethylaminoethyl methacrylate</p> <p>+ <i>N,N'</i>-methylene bisacrylamide or glycerol dimethacrylate</p>	56
	 <p>poly(ethylene glycol)-poly(<i>N</i>-[<i>N'</i>-(2-aminoethyl)-2-aminoethyl]aspartamide) (PEG-pAsp(DET))</p>	63
Polymeric micelles	 <p>poly(L-lysine)-poly(ethylene glycol)-folate (PLL-PEG-FOL)</p>	65
	 <p>(γ-PGA)-poly(L-phenylalanine ethylester) or (γ-PGA)-poly(L-tryptophan methylester)</p> <p>R =  or </p>	66
Layer-by-layer encapsulation	 <p>cysteine-conjugated chitosan</p>	69

1.4. Inorganic nanocarriers

1.4.1 Carbon nanotubes

Functionalized carbon nanotubes with water solubility and biocompatibility have been employed to deliver various therapeutic cargo into living cells, including small drugs, nucleic acids and peptides.⁷⁰ Particularly, the single-walled carbon nanotubes (SWNTs) can be applied as optical tags for biomedical imaging, due to their unique near-infrared (NIR) photoluminescence, Raman scattering, and high optical absorbance. Dai, Wender and their coworkers first utilized SWNTs to shuttle streptavidin into various cell lines, including nonadherent human promyelocytic leukemia (HL60) cells and human T (Jurkat) cells, as well as 3T3 fibroblast cells.⁷¹ Reactive carboxylates were first introduced onto the surface of SWNT using a oxidation/sonication procedure. Coupling of biotin onto the SWNT surface was followed by the binding of Alexa Fluor- labeled streptavidin. Dai *et al.* further investigated the uptake mechanism of proteins noncovalently conjugated to SWNT.⁷² The internalization of fluorescently labeled BSA or streptavidin absorbed onto SWNTs was confirmed by flow cell cytometry measurements, as well as by the exciting SWNT inside the cells by near infrared laser light. Further detailed analysis of the cellular internalization mechanism suggested a clathrin-mediated endocytosis pathway. HL-60 cells pretreated with either sucrose (hypertonic treatment) or a potassium ion-depleted medium, which can disrupt the formation of clathrin-coated vesicles, led to significant decreases in the uptake level of SWNTs-Protein. Similarly, Dai *et al.* also applied this strategy for intracellular delivery of cytochrome *c*.⁷³ As shown in Fig. 6, the successful delivery of cytochrome *c* using SWNTs was demonstrated and led to programmed cell death.

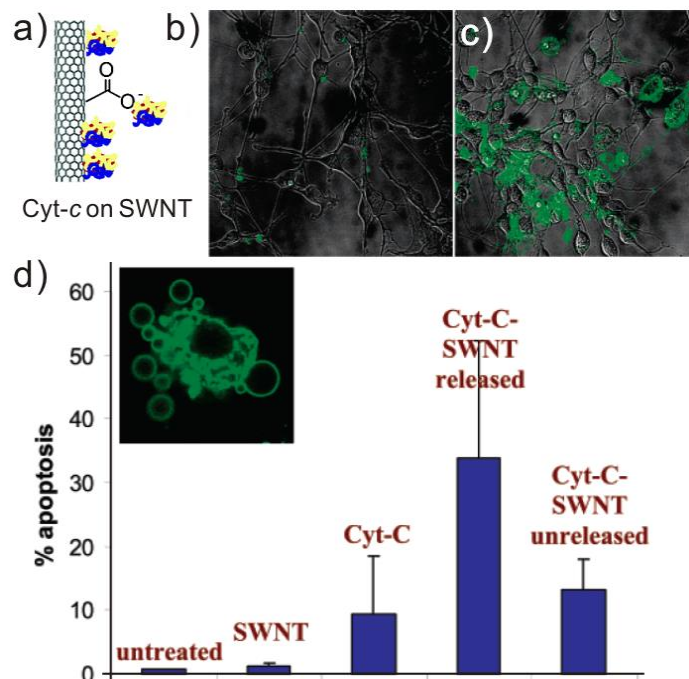


Figure 6. Single-walled carbon nanotubes (SWNT) as a vehicle for intracellular protein delivery developed by Dai and coworkers. (a) Schematic of cytochrome *c* complexed to SWNT. (b) Confocal image of NIH-3T3 cells after 3 h incubation in 50 μM cytochrome *c* alone and 20 min staining by Annexin V-FITC. (c) Images of cells after incubation in 50 μM cytochrome *c*-SWNTs in the presence of 100 μM chloroquine and after Annexin V-FITC staining. (d) Cell cytometry data of the percentages of cells undergoing early stage apoptosis after exposure to 100 μM chloroquine only (labeled “untreated”), SWNT + 100 μM of chloroquine, 10 μM cyt-*c* + 100 μM chloroquine, 10 μM cyt-*c*-SWNT + 100 μM chloroquine, and cyt-*c*-SWNT without chloroquine. The inset shows a representative confocal image of the blebbing of the cellular membrane (stained by Annexin V-FITC) as the cell undergoes apoptosis. Reprinted with permission from ref. ⁷³. Copyright 2005 American Chemical Society.

1.4.2 Quantum dots

Semiconductor quantum dots (QDs) have been widely utilized as fluorescent probes to visualize biological processes *in vitro* and *in vivo*.⁷⁴ Well-established merits of QDs

include narrow, tunable and symmetric emission spectra, as well as excellent thermal stability and resistance to photobleaching.⁷⁴ Russell and coworkers have explored a QD-based transduction method to shuttle the exogenous thin filament protein cardiac troponin C (cTnC) and a NLS peptide to myofibrillar and nuclei of living cardiac myocytes, respectively.⁷⁵ In order to achieve effective cellular internalization and efficient endosome escape, a peptide linker TAT-HA2 with a *N*-terminal cysteine residue (***CRRRQRRKKR-GGDIMGEWGNEIFGAIAGFLG***) was specifically designed. The TAT transduction domain (italicized) is responsible for membrane penetration, while the pH-sensitive and lipid membrane destabilizing HA2 sequence (underlined) facilitates escape of the complex from endosomes upon acidification⁷⁶. QD preattached to target protein ((QD)cTnc) was conjugated to the TAT-HA2 peptide via the *N*-terminus cysteine (bold). The authors demonstrated that no internalization signal from the QD was observed for samples treated with (QD)cTnC alone without the TAT domain. The (QD)cTnC-TAT complex was internalized but was not able to escape the endosome. In contrast, (QD)cTnC-TAT-HA2 with both TAT and HA2 distributed throughout the cell and associated with myofibrils. Lastly, the authors showed that QD-NLS peptide conjugated to TAT-HA2 was efficiently transduced into myocytes and was located in the nucleus.

Mattoussi *et al.* also demonstrated successful intracellular delivery of two QD-protein cargoes using cell penetrating peptides. The proteins were the monomeric yellow fluorescent protein (YFP, 27kDa) and multichromophore b-phycoerythrin complex (b-PE, 240kDa).⁷⁷ The attachment of proteins to QDs were based on 1) affinity between ZnS-overcoated CdSe QDs and inserted polyhistidine (His_n) in the proteins sequences; or 2) biotin-streptavidin binding. Endocytotic uptake was clearly shown as QD-protein conjugates were mostly distributed within endolysosomal compartments. Simultaneous

emission from both QDs and fluorescent proteins verified their colocalization and integrity inside living cells. These studies provide guidelines for live tracking and detection of exogenous proteins/peptide in a dynamic fashion.

1.4.3 Gold nanoparticles

Gold nanoparticles are useful in biological and medical applications due to their biocompatibility, tunable surface modifications and unique spectroscopical properties.⁷⁸ Rotello *et al.* exploited gold nanoparticles as effective carriers for intracellular delivery of β -galactosidase in several cell lines (Fig. 7).⁷⁹ Gold nanoparticles with a core diameter of ~ 2.5 nm were prepared and conjugated to ligands consisting of three functional domains: 1) the exterior peptide-tag (His-Lys-Arg-Lys); 2) a tethering section consisting of tetraethylene glycol (TEG) to prevent nonspecific binding; and 3) thiol-terminated alkyl chains that can anchor to the gold core. The positively-charged Lys-Arg-Lys moiety of the peptide ligand enables the particle to interact with the negatively-charged protein via electrostatic force and associate with plasma membrane. The imidazole group of the histidine residue can enhance endosomal escape of cargos with the “proton-sponge” effect. Gold nanoparticles with ~ 100 ligands were highly positively charged, with a ζ -potential of 32 ± 1 mV. When complexed with the nanocarriers (complex ratio is gold nanoparticle : protein = 2 : 1), the otherwise membrane-impermeable β -galactosidase was able to efficiently penetrate the cell membrane of HeLa cells and escape from endosomes. The retention of enzymatic activity of β -galactosidase after delivery was confirmed by treatment with a colorimetric reaction with X-gal (Fig. 7).

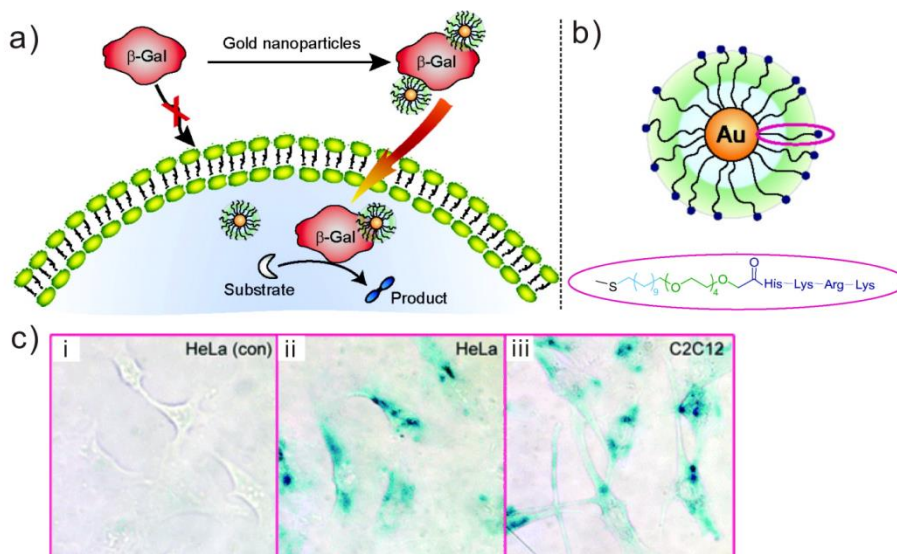


Figure 7. Gold nanoparticles-mediated intracellular protein delivery developed by Rotello and coworkers. (a) Schematic representation of intracellular delivery process. (b) Structure of the nanoparticle with attached ligands. (c) X-gal staining after transfection of i) HeLa cells with native β -galactosidase (β -Gal); ii) HeLa cells with gold nanoparticles/ β -Gal (100 nM/50 nM) and iii) C2C12 cells with gold nanoparticles/ β -Galactosidase (100 nM/50 nM). Reprinted with permission from ref. ⁷⁹. Copyright 2010 American Chemical Society.

1.4.4 Silica nanoparticles

Mesoporous silica nanoparticles (MSN) materials with large surface areas and pore volumes have been used as delivery vehicles for the controlled release of genes and membrane-impermeable chemicals.⁸⁰ Lin and coworkers first utilized a MSN with a large average pore diameter (5.4 nm) for intracellular delivery of cytochrome *c*.⁸¹ The encapsulation of protein into MSN was a diffusion-driven process, which was dependent on the solution concentration of cytochrome *c*. The authors validated that the enzymatic activity of the protein released from the MSNs was essentially identical compared to native proteins in catalyzing the oxidation of 2,2'-azino-bis(3-ethylbenzthiazoline-6-

sulfonate) (ABTS) in the presence of hydrogen peroxide. Interestingly, cell-free assays demonstrated that there was no obvious release of cytochrome *c* from MSN at pH 7.4 over 4 h, while immediate release was recorded at pH 5.2, which is suitable for controlled release in the endosome upon cellular internalization. The difference in the extent of release at these two pH values could result from the different ζ -potentials of MSN, which dropped significantly from -25.5 mV at pH 7.35 to -1.81 mV at pH 5.22. Flow cytometry analysis indicated an efficient internalization of FITC-tagged cytochrome *c* loaded in MSN in HeLa cells. Further confocal images clearly indicated that FITC-cytochrome *c* efficiently escaped from the endosomes within a few hours of endocytosis and diffused throughout the entire cytosol. The nanoparticles are thought to undergo nonspecific adsorptive endocytosis based on previous internalization studies on MSN.⁸² Recently, Dordick, Kane and coworkers explored hydrophobic silica nanoparticles functionalized with *n*-octadecyltrimethoxysilane (*n*-ODMS) for loading and delivering target proteins.⁸³ Specifically, delivery of ribonuclease A (RNase A) and the anti-phospho-Akt antibody towards human breast cancer MCF-7 cells and rat neural stem cells (NSCs) resulted in anticipated cell death.

1.4.5 Magnetic nanoparticles

Magnetic nanoparticles (MNPs) have been extensively investigated in the field of biomedical applications, including drug delivery, chemical and biochemical separation and enrichment of trace amounts of specific targets.⁸⁴ Particularly, magnetically-mediated delivery approaches can enhance the therapeutic profile by increasing localized concentration of target cargos and minimizing non-specific interactions.⁸⁵ Muzykantov *et*

al. investigated a biocompatible magnetic nanocarrier-based strategy for efficient encapsulation of two antioxidant enzymes, catalase and superoxide dismutase (SOD).⁸⁶ The enzyme-loaded MNPs were assembled through hydrophobic and electrostatic interactions between iron oxide MNPs and proteins. The average size of enzyme-loaded MNPs was from 300 to 400 nm, with a protein loading efficiency of 20-33%. To demonstrate antioxidant enzyme-loaded MNPs can rescue target cells from hydrogen peroxide toxicity, catalase-loaded MNPs were tested for intracellular delivery. Upon magnetic guidance, catalase-loaded MNPs with a negative net charge at pH 7.4 (-9.3 ± 1.1 mV) were efficiently taken up by bovine aortic endothelial cells (BAEC). A majority of cells that internalized catalase-loaded MNPs increased their resistance to oxidative stress and were rescued from hydrogen peroxide induced cell death. In the absence of magnetic field, only 10% cells were rescued.

1.5. Protein-mediated carriers

In addition to using polymer or inorganic nanocarriers, polypeptides have also served as guides for transducing target proteins to the intracellular space of cells. One example is to encapsulate proteins into virus-like particles consisting of polypeptide capsids. Abbing and coworkers efficiently encapsulated proteins or low molecular weight substances into recombinant polyomavirus-like nanoparticles.⁸⁷ The murine polyomavirus is a non-enveloped double-stranded DNA virus and can infect a number of eukaryotic cells. The outer shell is composed of 360 capsid protein VP1, while the inner core is composed of VP2 and VP3, which are not essential for capsid formation but have a tight binding affinity to the interior side of the VP1 cavity. The authors fused a conserved stretch of 49 amino acids, which is necessary for anchoring VP2 to VP1, to GFP. When self-assembled

with VP1, the loaded capsid-based nanoparticles showed regular morphology and had long-term stability. These nanoparticles were effectively internalized into 3T3 mouse fibroblasts, demonstrated by the detection of GFP and fluorescent detection of VP1 in endosomal compartments and the cytosol. The protein-loaded virions are thought to undergo caveolae-mediated internalization or macropinocytosis and subsequently degrade or disassemble in the cytosol, leading to release of protein.

Target proteins can also be fused to engineered protein delivery vehicles that have superior membrane penetrating properties. Liu and coworkers recently reported a novel intracellular delivery tool using superpositively charged GFP variants, which were extensively mutated at their surface-exposed residues.⁸⁸ They previously showed that superpositively charged GFP (Fig. 8) can internalize into a variety of cell lines through binding to anionic cell-surface proteoglycans and undergo endocytosis via an energy-dependent and clathrin-independent pathway. They further fused supercharged GFP to target proteins for intracellular delivery. Side-by-side comparisons of +36GFP and PTDs (Tat, oligoarginine (Arg₁₀) and penetratin) fused with mCherry or Cre recombinase revealed that using +36GFP as a vehicle resulted in significantly higher extent of internalization (up to ~ 100-fold). The delivered Cre recombinase also displayed dramatically higher efficiencies of Cre-induced recombination (up to ~ 10-fold) (Fig. 8). Ubiquitin-fused +36GFP was partially deubiquitinated when internalized, suggesting effective endosome escape. The supercharged GFP was also stable in serum and resistant to proteolysis, making it an attractive tool for delivering therapeutic agents.

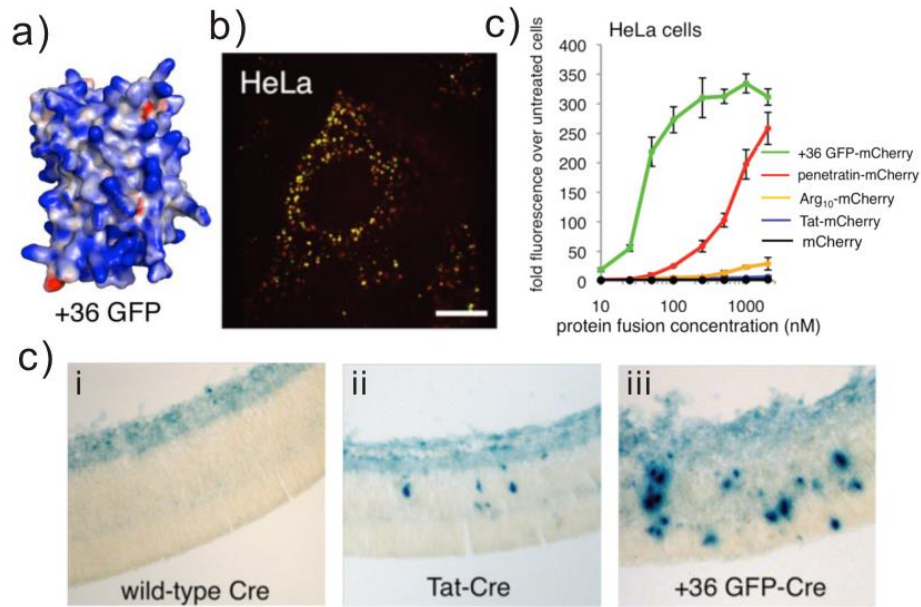


Figure 8. Superpositively charged GFP variants used for intracellular protein delivery developed by Liu and coworkers. (a) Calculated electrostatic surface potential of +36 GFP. (b) Confocal fluorescence microscopy of live cells incubated with 100 nM +36 GFP-mCherry for 4 h at 37 °C. Red color represents mCherry signal; green color represents +36 GFP signal. The scale bar is 15 μ m. (c) Flow cytometry of HeLa cells incubated in the presence of the specified concentrations of +36 GFP-mCherry, Tat-mCherry, Arg₁₀-mCherry, penetratin-mCherry, or wild-type mCherry alone for 4 h at 37 °C. (d) Retinal sections of neonatal RC::PFwe mouse pups harboring a nuclear LacZ reporter of Cre activity. Three days after injection of 0.5 μ L of 40 mM wild-type Cre, Tat-Cre, or +36 GFP-Cre, retinae were harvested, fixed, and stained with X-gal. Reprinted with permission from ref. ⁸⁸. Copyright 2010 American Chemical Society.

Lim *et al.* developed an engineered protein G system as a vehicle for non-invasive intracellular protein delivery.⁸⁹ The protein carrier contains three functional domains: 1) an N-terminus hexahistidine tag that can specifically bind to metal ions such as Ni(II) and Cu(II); 2) a C-terminus cell penetration peptide (CPPs) such as oligoarginines; 3) protein G itself which can strongly bind to IgG antibodies. This multifunctional protein G system

provides a convenient approach to capture Ni(II)-modified nanoparticles and antibodies without chemical attachment. The authors covalently attached anti-mitochondrial antibodies to the protein G system and bound the resulting conjugate to gold-coated iron oxide nanoparticles using Ni(II). They demonstrated that the antibody/nanoparticle complex can be easily internalized into HeLa cells and target mitochondria. The magnetic property of the nano complex also allowed facile separation of mitochondria from the lysates by using a permanent magnet.

1.6. Summary and outlook

Delivering functional proteins to the intracellular space of cells, whether healthy or cancerous, is a highly promising therapeutic approach. At the basic research front, it also enables direct investigation of the functions of recombinantly produced proteins on cellular processes. It is encouraging to recognize the substantial advances that have been made toward developing multifunctional nanocarriers for protein intracellular delivery. Table 2 summarizes examples of various nanocarriers recently reported. From the aspect of material design and fabrication, numerous synthesis strategies and protein loading techniques have been developed. Considerable insights into uptake and release mechanism, and delivery efficiency have been obtained.

Despite these efforts, intracellular delivery of target proteins is still in its infancy, and requires further development to fully realize its vast potential. Fig. 9 provides schematic guideline for engineering protein nanocarriers. Functional add-ons should be taken into account when constructing nanomaterial platforms. Meanwhile, the delivery performance of both *in vitro* and *in vivo* provides feedback to further tailor the structure. At present, many obstacles still need to be overcome to achieve effective and efficient

delivery. For example, covalent modifications to protein surfaces may cause irreversible changes to protein structure and subsequent loss of function whereas noncovalent strategies are often only weakly stable in serum.^{14, 16} Efficient intracellular transduction is still a challenge as many nanocarriers are unable to efficiently escape into the cytosol from the endosomal pathway.⁴

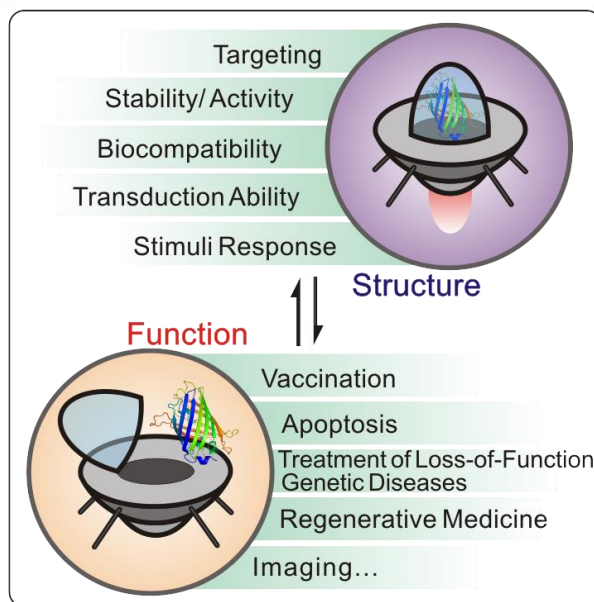


Figure 9. Schematic outline for engineering nanocarriers for intracellular protein delivery.

Another desired effect of nanocarriers is the controlled release of cargo through a timed mechanism instead of a burst release. This can be addressed through synthesis of stimuli-responsive nanocarriers to achieve release in an “on demand” fashion. It is desirable to further develop “smart” nanocarriers by designing materials with sensitive responses towards environmental conditions such as pH, redox, surrounding enzyme activity, temperature and externally applied physical signals such as magnetic field and light^{17, 18, 90, 91}.

Lastly, at the pinnacle of delivery goals is the targeting of specific cells or organs for disease-specific therapies. Under *in vivo* circumstance, protein nanocarriers encounter many barriers en route to their destination. It is crucial to allow vehicles to accumulate in the desired position either by the enhanced permeability and retention (EPR) effect mediated-passive targeting; or by active targeting through conjugating targeting moieties, such as antibodies, receptor ligands (peptides, vitamins, and carbohydrates) and aptamers.³ The efficacy of these nanocarrier systems can be assessed by previously accumulated empirical knowledge of nanomedicine in regards to biocompatibility, stability, uptake and biological interactions.⁹²

In conclusion, as described in this review, many advances, including vehicle tailoring and protein engineering, have been used to address these critical issues. We envision that significant progress will be made and new generations of protein nanocarriers will be developed in the near future as interdisciplinary research will lead to new approaches by the rational design of the material platform integrated with tailored functionalizations.

Table 2. Summary of recently reported nanocarriers for the protein intracellular delivery.

Types of Nanocarriers	Physical Properties	Delivered Protein	Cell Lines Used	Ref.	
Lipid-mediated	cationic lipid TFA-DODAPL:DOPE	positively charged	Phycoerythrin α -chain, β -chain; BSA; β -Galactosidase; Caspase-3; Caspase 8; Granzyme B; Cytochrome <i>c</i>	NIH-3T3; HeLa-S3; BHK-21; CHO-K1; B16-F0; 293; MDCK; P19; Jurkat; Ki-Ras 267 β 1	22
	DOGS (dioctadecylglycylspermine)	size: 500-900 nm; positively charged	BSA; β -Galactosidase; IgG(anti-actin); IgG(anti-tubulin); phycoerythrin	CHO; BHK; Jurkat	24
	FuGENE6 TM , BioPORTER TM	positively charged	β -Galactosidase; Caspase-3	C6 glioma cells; rBCEC4	27
	amphiphile (CholCSper)/DOPE	size: 200 nm; positively charged	phycoerythrin	BHK-21	23
Polymeric - based	PEI-cationized proteins through chemical conjugation	positively charged	RNase; eGFP; IgG; anti-S100C; p53; simian virus 40 large T-antigen	NIH-3T3; KMS-6; OUMS-36; HEK293; HeLa; K562; HFL-1; Saos-2	33-38
	PPAAc-NH ₂ /Streptavidin		biotinylated anti-CD3 antibody	Jurkat	39
	Glucose-coated beads	size: ~ 150 nm	EGFP	mES; Hela	41
	pH-responsive core-shell nanoparticles	size: ~ 200 nm at pH 7.4, ~ 580 nm below pH 6.8	ovalbumin (OVA)	BMDCs; dendritic DC2.4	42
	Self-assembled cationic nanogels	size: ~ 20-40 nm; positively charged	BSA; β -Galactosidase; Tat-NLS-GFP; BoHc/A	CHO-K1; cos-7; NIH-3T3; HeLa; Nasal mucosal dendritic cells	43, 44
	Acid-degradable particles by inverse emulsion polymerization	size: 200~500 nm	OVA	RAW309.1 CR macrophage	48
	Acid-degradable particles by double emulsion evaporation	size: ~250 nm	OVA	RAW309.1 CR macrophage	50, 52
	Single-protein nanocapsules	size: 8-20 nm; positively charged	GFP; BSA; HRP; SOD; Caspase-3; Klf4	HeLa; MCF-7; CHO; MEF	56, 59, 60
	Charge-conversional polyion complex (PIC) micelles	size: ~ 50 nm; positively charged	Cytochrome <i>c</i> ; anti-NPC mouse IgG	HuH-7	63, 64
Amphiphilic poly(amino acid) derivatives	size: 250-300 nm; negatively charged	OVA	Immature DCs	66	
Inorganic -	Single-walled carbon nanotubes (SWNT)	size: ~1-5 nm in diameter for SWNT	BSA; Streptavidin; Cytochrome <i>c</i>	HL60; Jurkat; CHO; NIH-3T3	71-73

based	Quantum dots	core diameter: ~20 nm	YFP; b-phycoerythrin	HEK 293T/17; COS-1	77
	Gold nanoparticles	core diameter: ~2.5 nm; positively charged	β -Galactosidase	HeLa; COS-1; MCF-7; C2C12	79
	Mesoporous silica nanoparticles (MSN)	size: ~200 nm; pore diameter: 5.4 nm	Cytochrome <i>c</i>	HeLa	81
	Hydrophobically functionalized silica nanoparticles	size: ~15 nm	anti-pAkt	MCF-7; NSCs	83
	Magnetic nanoparticles	size: 300-400 nm; negatively charged; magnetic moment at saturation: 14.3 emu/g	SOD; catalase	BAEC	86
Protein-mediated	Polyomavirus-like nanoparticles	size: 35 nm	GFP	Swiss 3T3	87
	Superpositively charged GFP variants	positively charged	Cre recombinase	HeLa; BSR; NIH-3T3; IMCD PC12	88
	Engineered protein G system		goat anti-mouse IgG	HeLa	89

Chapter 2 Redox-Responsive Nanocapsules for Intracellular Protein Delivery

2.1. Introduction

Protein therapeutics that functions intracellularly has enormous potential for the treatment of human diseases — especially those caused by the temporary or permanent loss of protein functions. For example, many cancer cells do not undergo programmed cell death because proteins in the apoptosis machinery are either defective in function or attenuated in expression.⁹³ Direct protein delivery to the cytosol of cells can therefore restore or replenish the functions of interest and lead to desired cell phenotypes. Additionally, introduction of recombinant proteins that can regulate transcription can exert artificial control of gene expression levels and lead to reprogramming of cell fate.⁹⁴ In comparison to gene therapy, which is currently the predominant choice of delivery for promising protein therapeutics, direct protein delivery can bypass the requirement of permanent or unintended changes to the genetic makeup of the cell, and is therefore a safer therapeutic alternative.⁹⁵

The development of intracellular protein therapeutics has been hampered by the limitations arising from the nature of proteins. These limitations include structural fragility, low serum stability and poor membrane permeability for most proteins that are negatively charged at pH 7.⁹⁶⁻¹⁰² All these obstacles require suitable protein delivery vehicles that can 1) protect the protein cargo from denaturation and proteolysis during circulation and endocytosis; 2) shield the negatively charged protein and provide an overall positive surface charge for internalization across the phospholipid membrane¹⁰³; and 3) release the protein cargo in native forms when the desired destination (i.e. the cytosol) is reached^{104, 105}. To address these requirements, a variety of nanoscale vehicles for cytosolic protein delivery have been reported to date, including lipid-based colloidal carriers¹⁰⁶⁻¹⁰⁹, nanogels^{43, 46, 48, 50, 97, 110-114},

micelles^{63, 64, 66}, inorganic nanoparticles^{77, 81, 115-117}, nanotubes¹¹⁸⁻¹²⁰ and protein-mediated carriers^{88, 89, 121}. While many of these methods have shown improved protein protection and membrane penetration, some of these techniques require covalent modification of proteins, which can disturb protein folding and impair biological activity^{122, 123}. On the other hand, noncovalent carriers may exhibit low delivery efficiency and encounter difficulties due to colloidal instability⁴³. Furthermore, depending on the formulations, various carriers may have different intracellular fates after internalization and those with a poor endosomal escaping ability may result in localization and degradation of the therapeutic proteins in lysosomes¹⁰³. Therefore, the ability of nanocarriers to escape from endosomes is also critical for effective intracellular delivery and improved efficacy of protein therapeutics¹²⁴.

We have previously developed a new strategy for intracellular protein delivery using single-protein nanocapsules (NCs)^{110, 125}. In this approach, the protein is encapsulated in a thin positively charged polymer shell, which serves as a protective layer. We exploited a protease-dependent degradation mechanism that allows disintegration of the peptide-based crosslinkers and release of the cargo. Notwithstanding this enzyme-responsive approach, a simple yet effective degradation strategy that can be triggered by changes in the chemical environment upon cellular entry is also desirable. Here, we report the use of a redox-responsive, disulfide-containing crosslinker in the preparation of the protein NCs. The cytosol has a low redox potential due to the abundance of reduced glutathione (GSH) in the millimolar concentration range, whereas the extracellular glutathione concentration falls in the micromolar range¹²⁶. To utilize this redox potential difference, a variety of gene delivery systems based on the dissociation of disulfide bonds have been reported¹²⁷⁻¹³¹. Similarly, we reason here that protein NCs interconnected by a disulfide-containing crosslinker through interfacial polymerization can maintain the integrity of the thin polymer shell under oxidative

conditions outside the cell, but it should undergo rapid degradation and cargo release after entry into the cytosol.

2.2 Materials and Methods

2.2.1 Materials

N-(3-aminopropyl) methacrylamide hydrochloride was purchased from Polymer Science, Inc. CellTiter 96® AQueous One Solution Cell Proliferation Assay (MTS) reagent was purchased from Promega Corporation. APO-BrdUTM TUNEL Assay Kit was purchased from Invitrogen. All other chemicals were purchased from Sigma-Aldrich and used as received. The deionized water was prepared by a Millipore NanoPure purification system (resistivity higher than 18.2 MΩ cm⁻¹).

2.2.2 Instruments

The Bradford protein assay was carried out on a Thermo Scientific GENESYS 20 spectrometer. Caspase 3 (CP-3) proteolysis activity was measured using a Beckman Coulter DU® 520 spectrometer. Far-UV circular dichroism (CD) spectra of proteins were tested using JASCO J-715 Circular Dichroism spectrometer. The size distributions and zeta potentials of NCs were measured on the Malvern particle sizer Nano-ZS. Transmission electron microscopy (TEM) images were obtained using Philips EM-120 TEM instrument. Fluorescent images were taken with Zeiss Axio Observer Z1 Inverted Microscope and Yokogawa spinning-disk confocal microscope (Solamere Technology Group, Salt Lake City, UT) on Nikon eclipse Ti-E Microscope equipped with a 60×1.49 Apo TIRF oil objective and a Cascade II: 512 EMCCD camera (Photometrics). An AOTF (acousto-optical tunable filter)

controlled laser-merge system (Solamere Technology Group Inc.) was used to provide illumination power at each of the following laser lines: 491 nm, 561 nm, and 640 nm solid state lasers (50 mW for each laser). FACSscan and FACSort (BD Bioscience) were used for flow cytometry analysis.

2.2.3 Methods

Protein Expression and Purification

The plasmid pHC332 for expression of the mature CP-3 was a generous gift from Dr. A. Clay Clark (North Carolina State University). Plasmid pHC332 was transformed into *Escherichia coli* BL21(DE3) cells and incubated at 37 °C overnight on LB agar plate with 100 µg/mL ampicillin. Colonies were picked and grown overnight at 37 °C with shaking (250 rpm) in 5 mL ampicillin-containing LB media. Overnight cultures were then inoculated in 1 L of LB media with 100 µg/mL ampicillin and allowed to grow under 37 °C until the absorbance of cell density (OD₆₀₀) reached 1.0. Isopropyl β-D-1-thiogalactopyranoside (IPTG) was added to a final concentration of 0.1 mM to induce protein expression. After overnight incubation at 16 °C, the *E. coli* cells were harvested by centrifugation (2,000 g, 4 °C, 15 min). Cell pellets were then resuspended in 30 mL Buffer A (50 mM Tris-HCl, pH 8.0, 2 mM dithiothreitol, 2 mM EDTA) and lysed by sonication. Cell debris and insoluble proteins were removed by centrifugation (20,000g, 4 °C, 30 min), followed by the addition of 1 mL Ni-NTA resin (Qiagen) into the cleared cell lysate and a binding period of 3 hours at 4 °C. Afterwards, the protein was then purified on a gravity column using Buffer A with increasing concentrations of imidazole (10, 20, and 250 mM). The protein concentration was qualitatively assessed by SDS-PAGE and quantitatively determined by the Bradford protein

assay using bovine serum albumin (BSA) as the standard. Enhanced green fluorescence protein (eGFP) was prepared following the procedures described above, except for the induction was carried out when OD₆₀₀ reached 0.4.

Single Protein Encapsulation

The concentration of protein (CP-3, eGFP and BSA) was diluted to 1 mg/mL with 5 mM sodium bicarbonate buffer at pH 9. Then 200 mg/mL acrylamide (AAm) monomer was added to 1 mL of protein solution with stirring at 4 °C. After 10 min, the second monomer, *N*-(3-aminopropyl) methacrylamide (APMAAm), was added while stirring. Different cross-linkers, *N,N'*-methylene bisacrylamide for nondegradable (ND) NCs and *N,N'*-bis(acryloyl)cystamine for disulfide-crosslinked NCs, was added 5 min after the addition of APMAAm. The polymerization reaction was immediately initiated by adding 30 µL of ammonium persulfate (100 mg/mL, dissolved in deoxygenated and deionized water) and 3 µL of *N,N,N',N'*-tetramethylethylenediamine. The polymerization reaction was allowed to proceed for 60 min. The molar ratio of AAm/APMAAm/cross-linker was adjusted to 12:9:1. Buffer exchange with phosphate-buffered saline (PBS) buffer (pH 7.4) was used to remove the remaining monomers and initiators. Rhodamine-tagged CP-3 NCs was obtained through encapsulation of CP-3 modified with 5-Carboxy-X-rhodamine *N*-succinimidyl ester (mass ratio (CP-3: rhodamine): 4:1).

Characterization of Protein NCs

Samples of NCs (0.05 mg/mL) for TEM imaging were negatively stained with 2 % uranyl acetate in alcoholic solution (50 % ethanol). The lamella of stained sample was prepared on carbon-coated electron microscopy grids (Ted Pella, Inc.). The degradation

process of S-S NCs was dynamically monitored by dynamic light scattering (DLS) in PBS buffer. Different amount of GSH were combined with 1 mg/mL S-S NCs in PBS buffer, to obtain final GSH concentrations of 0.5 mM and 2 mM. The average count rate at different time points were continuously monitored for 90 minutes at 25 °C. The release of CP-3 from S-S NCs and its activity were assessed using colorimetric substrate peptide Ac-DEVD-pNA (*p*-nitroanilide). Samples with 0.01 mg native CP-3 or S-S CP-3 NCs incubated with different concentrations of GSH (0.2 mM, 0.5 mM, 1 mM and 2 mM) were prepared in 1.0 mL PBS buffer. With the addition of 32 μM Ac-DEVD-pNA, the intensity of cleaved pNA was spectrometrically recorded at 409 nm for 120 min.

Cellular uptake, Internalization Pathway and Trafficking

HeLa cells (ATCC, Manassas, VA) were cultured in Dulbecco's Modified Eagle's Media (DMEM) (Invitrogen) supplemented with 10 % bovine growth serum (Hyclone, Logan, UT), 1.5 g/L sodium bicarbonate, 100 μg/mL streptomycin and 100 U/mL penicillin, at 37 °C with 98 % humidity and 5 % CO₂. To visualize NCs uptake, cells were seeded into 48-well plate, with a density of 5,000 cells/well in 250 μL of media with supplements. Once the confluency of 80% was reached, S-S NCs with eGFP and rhodamine-tagged CP-3 were added to a final concentration of 400 nM. After 3 hours of incubation, cells were washed with PBS twice, stained with DAPI Nucleic Acid Stain (Invitrogen) and imaged. To determine the internalization pathway of S-S NCs, HeLa cells were seeded into 12-well plates at a density of 50,000 cells/well. The plates were incubated at 37 °C overnight. The media was then replaced with 0.5 mL of fresh media containing 8 nM S-S eGFP NCs. After incubating at 4 °C and 37 °C for 2 hours, each well was washed with PBS and the cells were trypsinized and collected in PBS. After fixation using 2 % paraformaldehyde, samples were

analyzed via FACS with a 488 nm argon laser. The signal from the FL1 bandpass emission (530/30) was used for eGFP. Markers for different endosome stages were used for internalization trafficking. A concentration of 10 nM S-S eGFP NCs was added to HeLa cells at 4 °C for 30 min. The plates were moved to 37 °C and incubated for 30 min, 1 and 2 hours. Cells were then fixed with 4 % formaldehyde, permeabilized with 0.1 % Triton X-100, and stained with antibodies, mouse anti-EEA1 antibody against early endosomes and rabbit anti-CI-MPR antibody against late endosomes (Cell Signaling Technology, Inc.). Texas red goat anti-mouse IgG and Alexa Fluor® 647 goat anti-rabbit IgG (Invitrogen) were added as the secondary antibody.

Cytotoxicity Assay

Different cancer cells, HeLa, MCF-7 and U-87 MG cells (ATCC, Manassas, VA), were seeded into 96-well plates, each well containing 5,000 cells in 100 µL of DMEM with supplements. Different concentrations of protein and NCs were added into each well and the plates were incubated at 37 °C with 98 % humidity and 5 % CO₂ for 48 hours. The cells were washed with PBS solution twice and 100 µL of fresh cell culture media with supplements was added. Then 20 µL MTS solution (CellTiter 96® AQueous One Solution Cell Proliferation Assay, Invitrogen) was added into each well and the plates were incubated for 3 hours at 37 °C. The absorbance of product was read at 490 nm using a microplate reader (PowerWave X, Bio-tek Instruments, USA).

TUNEL Assay

Apoptosis of HeLa cells was detected using APO-BrdU Terminal Deoxynucleotidyl Transferase dUTP Nick End Labeling (TUNEL) assay kit. Cells were seeded at a density of

100,000 cells/well into a 6-well plate in 2 mL of cell culture media with supplements. Proteins and NCs were added after cells covered 80 % of bottom surface. After 24 hours of incubation, cells were fixed with 1 % paraformaldehyde in PBS, followed by the addition of DNA labeling solution containing terminal deoxynucleotidyl transferase and bromodeoxyuridine (BrdUrd). Cells were then stained with Alexa Fluor® 488 dye-labeled anti-BrdUrd antibody. Samples were deposited onto slides, which were later stained with propidium iodide (PI) solution containing RNase A. Images were obtained by fluorescence microscope (Zeiss, Observer Z1) using appropriate filters for Alexa Fluor 488 and PI.

2.3. Results and Discussion

2.3.1 Formation and characterization of protein NCs

The synthesis method for single-protein NCs is schematically shown in Figure 10a. Briefly, the target protein, which is either enhanced green fluorescent protein (eGFP), bovine serum albumin (BSA) or mature caspase 3 (CP-3), is mixed with acrylamide, positively charged *N*-(3-Aminopropyl) methacrylamide and the crosslinker. After the monomers are allowed to electrostatically adsorb onto the surface of the protein, *in situ* polymerization is initiated by the addition of free radical initiators. To render the crosslinking of the capsule reversible under reducing conditions, we choose to use the cleavable disulfide-bond containing *N,N'*-bis(acryloyl)cystamine (referred to as S-S crosslinker) (Figure 10b). When needed as a control as for the CP-3 studies, the target protein is also encapsulated using the nondegradable crosslinker *N,N'*-methylene bisacrylamide. Using this interfacial polymerization strategy, no covalent bond is formed between the resulting polymeric shell matrix and the core target protein, which ensures that the native protein is released upon

degradation. Following polymerization and encapsulation, the NCs were purified from unreacted monomers using AMICON centrifugal filters (molecular weight cutoff 30 kDa) and buffer exchanged into PBS buffer.

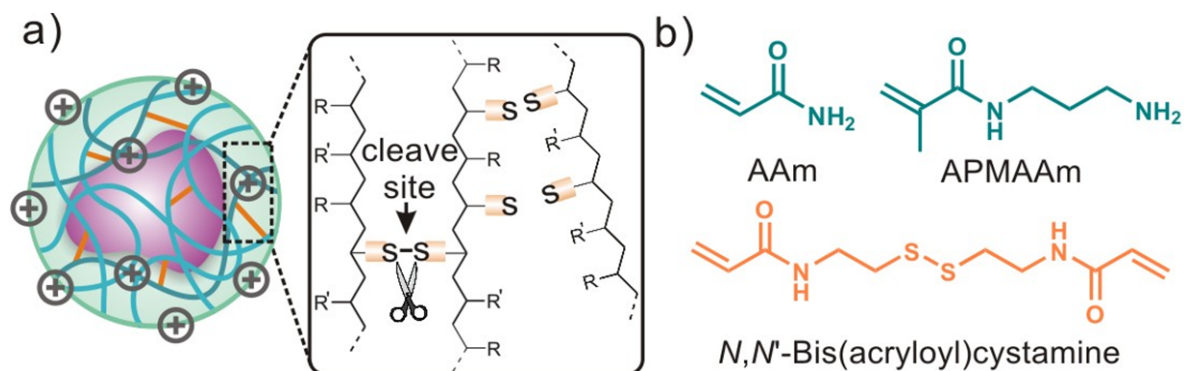


Figure 10. Formation of redox-responsive protein nanocapsules. **a)** Schematic of protein nanocapsules with redox-responsive polymeric matrix; and **b)** Chemical structures of monomers and crosslinker for S-S nanocapsules.

The surface charges of the NCs weaved with S-S crosslinkers (referred to as S-S NC) were assessed to be between 3.6 and 4.7 mV, confirming the necessary positive surface charge desired for cellular internalization (Table 3). The hydrodynamic sizes of the various NCs were measured by Dynamic Light Scattering (DLS) and are shown in Figure 11a and Table 1. Whereas native CP-3 protein had an average diameter of 5 nm, S-S NCs containing CP-3 had an average diameter of 11.3 nm with a relatively narrow size distribution. Similar sizes S-S NCs encapsulating eGFP and BSA were also observed. The narrow size distribution of S-S NCs was further confirmed by TEM, in which the NCs adopted a robust and consistent spherical shape in aqueous solution (Figure 11c). To ensure that the encapsulation process does not affect the folding of CP-3, circular dichroism was used to compare the secondary structures of native and encapsulated CP-3. As shown in Figure 11b, the two spectra both show the characteristic minima (208 and 222 nm) expected for the

predominantly α -helical CP-3. The nearly overlapping spectra validate that the secondary structure of CP-3 was well-preserved during the encapsulation process.

Table 3. Mean hydrodynamic sizes and zeta potentials of protein NCs

Abbreviation	S-S CP-3 NCs	S-S BSA NCs	S-S eGFP NCs	ND CP-3 NCs
Size (nm)	11.3	10.0	9.9	9.5
Zeta potential (mV)	3.6 \pm 0.1	4.7 \pm 0.4	3.6 \pm 0.7	4.0 \pm 0.4

To determine if the S-S NCs are degradable under reducing conditions, we treated S-S CP-3 NCs with the physiologically relevant GSH at 37 °C. As expected, after treatment with 2 mM GSH for 2 hours, the hydrodynamic size of the NCs decreased to an average size of 5.3 nm, which was highly consistent with that of native CP-3 protein before encapsulation (Figure 11a). This result suggests that the NCs have been nearly completely degraded upon reduction of the disulfide bonds. The degradation of S-S NCs was further substantiated by TEM, as no spherical particles were visible after GSH treatment (Figure 11d). To evaluate the kinetics of the disassembly process, we monitored the time-dependent decrease in the hydrodynamic sizes in the presence of different amount of GSH (Figure 12a). The relative scattering intensity of S-S CP-3 NCs decreased steadily in the presence of GSH, suggesting the continuous decrease of the particle size or the number of particles. At a GSH concentration as low as 0.5 mM, which is the lower limit of estimated intracellular concentration of GSH¹²⁶, CP-3 S-S NCs appeared to be completely degraded within 90 min, judged from the size decrease. At 2 mM GSH concentration, a much faster degradation process was observed. These results therefore strongly suggest that once delivered to the cytosol, the S-S NCs are expected to rapidly release the cargo protein under reducing conditions.

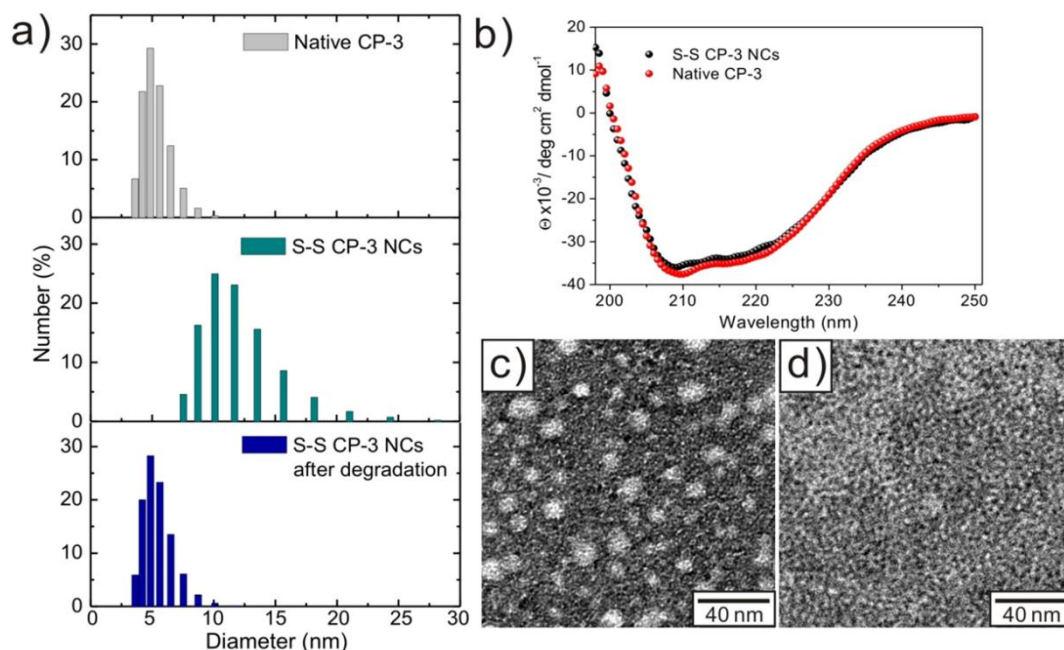


Figure 11. Characterization of S-S CP-3 nanocapsules. **a)** The hydrodynamic sizes of the native CP-3 (grey), S-S CP-3 NCs (green) and S-S CP-3 NCs after degradation (blue) measured by DLS; **b)** Far-UV CD spectra of native CP-3 (red), S-S CP-3 NCs (black); **c)** TEM images of S-S CP-3 NCs; and **d)** TEM images of S-S CP-3 NCs after treatment with 2 mM GSH for 2 hours at 37 °C.

To test the activity of encapsulated and released CP-3, we used a colorimetric assay employing a CP-3 peptidyl substrate mimic, Ac-DEVD-pNA (*p*-nitroanilide)¹³². As shown in Figure 12b, in contrast to free CP-3 protein that rapidly cleaved the substrate, CP-3 encapsulated in S-S NCs did not display any protease activity over the assay period in the absence of GSH. This result confirms that the *in situ* polymerization process completely shields CP-3 from the outside environment and that the peptidyl substrate is therefore inaccessible to the enzyme. This result also demonstrates that during storage and assay of the CP-3 S-S NCs, no significant diffusion of CP-3 across the polymer matrix, or spontaneous reduction of the S-S crosslinker occurs. When the degradation of the polymer shell was

triggered by addition of GSH, CP-3 activity was readily observed and the rate of proteolysis was linearly correlated with the amount of reducing agent present. In the presence of 2 mM GSH, complete digestion of the substrate can be observed within one hour. The controlled release of encapsulated CP-3 in the presence of GSH demonstrates the redox-responsiveness of the S-S NCs and also confirms the activity of the encapsulated protein is minimally affected during the entire assembly/disassembly process.

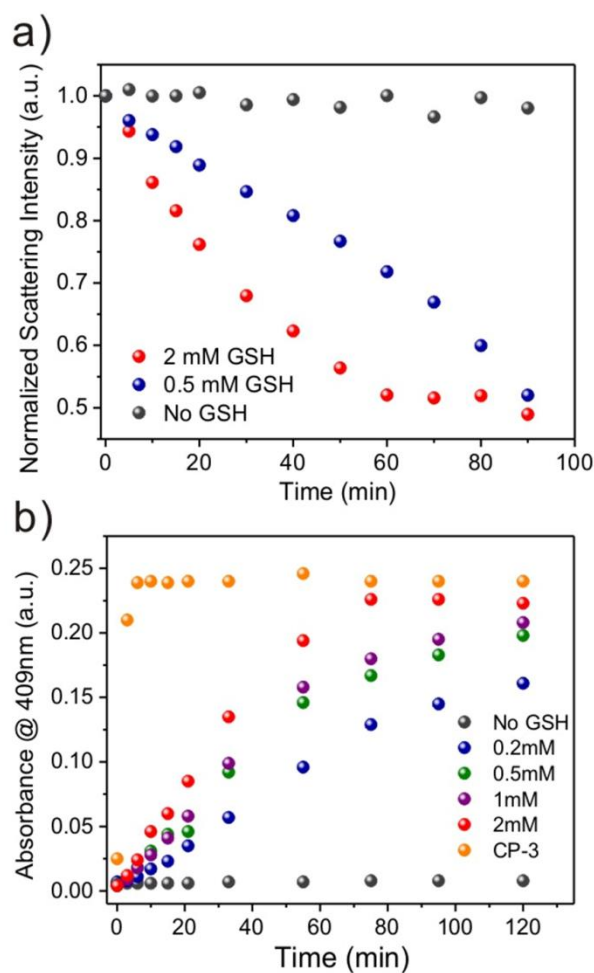


Figure 12. S-S CP-3 nanocapsules degradation and protein release. **a)** Degradation kinetics shown by normalized scattering intensity at 2 mM GSH (red), 0.5 mM GSH (blue) and no GSH (black); and **b)** Activity of CP-3 released from S-S CP-3 NCs towards colorimetric substrate Ac-DEVD-pNA (8.0 mM). The absorbance of cleaved pNA was measured at 409 nm.

2.3.2 Cellular uptake, Internalization Pathway and Trafficking of S-S NCs

Having confirmed the desired physical properties and chemical responsiveness of the S-S NCs, we next investigated the cellular uptake and trafficking mechanisms of NCs using eGFP as a fluorescent marker. The physical characteristics of the S-S eGFP NCs are shown in Table 1. Fluorescent microscopy image of HeLa cells incubated with 400 nM eGFP S-S NCs for 3 hours in media is shown in the left panel of Figure 13a. Compared to native eGFP, which cannot penetrate the cellular membrane, eGFP encapsulated in S-S NCs appears to be efficiently internalized by the cells and the eGFP fluorescent signals were diffusively visible in the cytosol. To investigate the mechanism of NC cellular internalization, HeLa cells were incubated with S-S eGFP NCs at different temperatures and analyzed by flow cytometry. The mean intensity of eGFP fluorescence at 4 °C dropped to ~ 20% of that at 37 °C (Figure 13b), indicating the likely involvement of the energy-dependent endocytosis for NC cellular uptake. The cellular trafficking of the internalized S-S eGFP NCs was then investigated for 2 hours by tracking the eGFP fluorescence at different time points and monitoring colocalization using markers for early and late endosomes (Figure 13c). At the onset of the internalization process, all the eGFP signals were localized at the membrane of the cells as expected (0 min). Overlap of eGFP (green) with early endosomal marker EEA1 (red) at ~ 60% colocalization was observed after 30 min of incubation, confirming that S-S eGFP NCs were trafficked into early endosomes upon cellular entry. While the degree of colocalization of eGFP and EEA1 signals decreased after 60 and 120 min, no significant colocalization of eGFP with late endosomal marker CI-MPR (blue) was detected, strongly suggesting that some of the NCs or proteins have been delivered into the cytosol (Figure 13c and 13d). Results from these imaging studies validate that S-S NCs can indeed be internalized by cells and at least a significant portion of the internalized NCs and the cargo can escape from the

endosomal compartment and reach the desired destination. Combined with the rapid degradation rate of the S-S NCs in the presence of GSH, release of the protein cargo into the cytosol of target cells can be expected to be highly efficient and completed within hours after the onset of internalization.

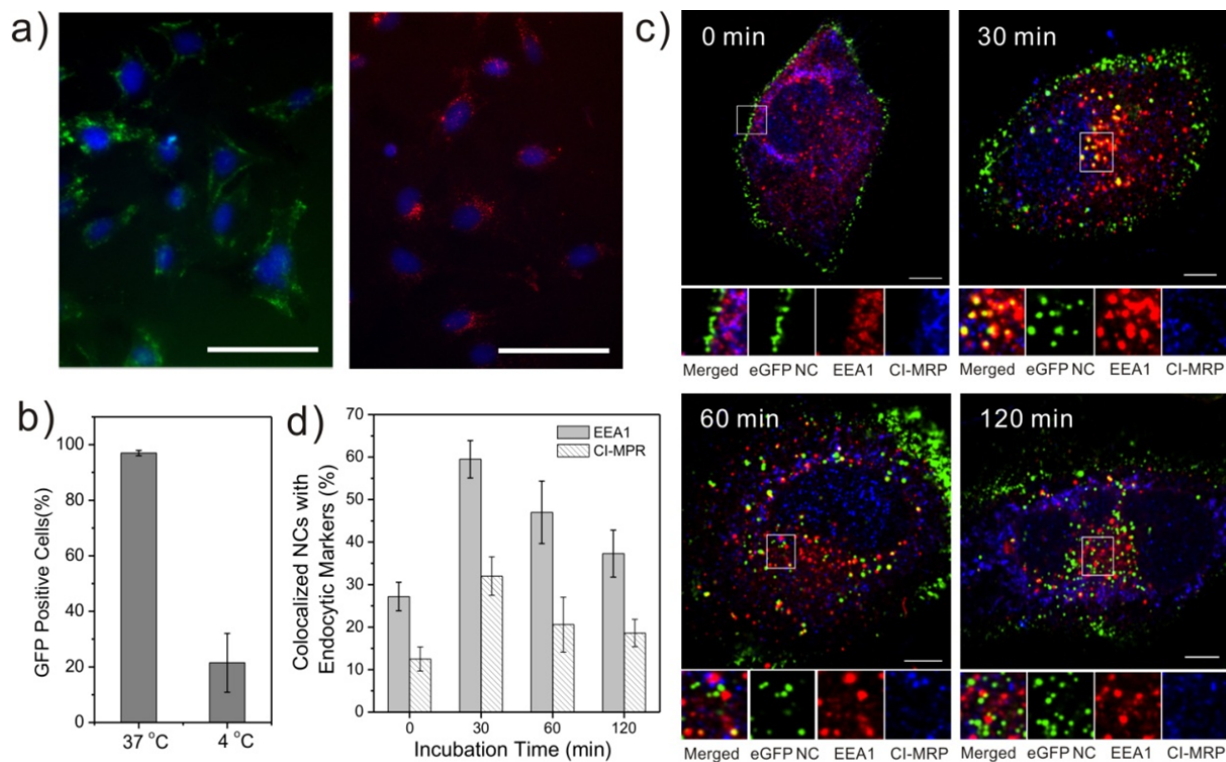


Figure 13. Cellular uptake and trafficking of S-S eGFP nanocapsules by HeLa cells. **a)** Fluorescence microscope images of HeLa cells after 3 hour incubation with 400 nM eGFP S-S NCs (left) and with 400 nM rhodamine-tagged S-S CP-3 NCs (right). Nuclei were stained with DAPI. The scale bar represents 100 μm ; **b)** Inhibition of the cellular internalization of S-S eGFP NCs (8 nM) by HeLa cells at 4 $^{\circ}\text{C}$. The mean fluorescence intensity was measured by flow cytometry and was represented as the percentage of fluorescence at 37 $^{\circ}\text{C}$; **c)** The trafficking of S-S eGFP NCs through endosomes. Cells were incubated with 10 nM S-S eGFP NCs at 37 $^{\circ}\text{C}$ for various time periods, 0, 30, 60 and 120 min. Early endosomes were detected by early endosome antigen 1 (EEA1, red). Late endosomes were detected by cation-independent mannose-6-phosphate receptor (CI-MRP, blue). The scale bar represents 10 μm ;

and **d**) Quantification of S-S eGFP NCs colocalized with EEA1+ (solid) or CI-MPR+ (stripe) endosomes at various incubation times. Colocalization coefficients were calculated using Manders' overlap coefficient (>10 samples). The error bars indicate standard deviation.

2.3.3 Apoptosis is observed following delivery of CP-3 S-S NCs

After confirming that NCs can be trafficked into the cytosol of cells, we next investigated the delivery of CP-3 as a functional protein using the redox-responsive NCs. CP-3 is a serine protease that can trigger rapid apoptosis, which is the desired phenotype upon successful delivery. Therefore, the S-S CP-3 NCs must be degraded once internalized to allow CP-3 to interact with its cytosolic macromolecular targets. The successful delivery of proteins— such as CP-3 to tumor cells— can also be a powerful method to resurrect a dysfunctional apoptotic pathway and directly induce tumor cell death^{95, 116}. To verify if S-S CP-3 NCs can indeed be internalized into cells, CP-3 was first tagged with NHS-modified rhodamine dye and was then encapsulated into an S-S NC. Delivery of the tagged CP-3 NCs into HeLa cells resulted in the appearance of dispersed red color throughout the cytosol after 3 hours of incubation (Figure 13a, right).

To evaluate the apoptotic potency of the designed NCs, HeLa cells were treated with S-S CP-3 NCs together with negative control samples: 1) native CP-3, which cannot be internalized; 2) S-S BSA NCs, which cannot trigger the apoptosis pathway; and 3) CP-3 encapsulated in nondegradable NCs, which shield CP-3 and prevent it from interacting with its substrates. After 48 hours of treatment, the cytotoxicity of the different protein and NCs samples were assessed using the MTS assay. As shown in Figure 14a, HeLa cells treated with S-S CP-3 NCs exhibited prominent cell death and had an IC_{50} ~300 nM. In comparison, cells treated with each of the three control samples did not display significant cell death. The

robust cell viability of the S-S BSA NCs also illustrates the polymeric material that constitutes the delivery vehicle does not have significant cytotoxicity towards human cell lines. To demonstrate the S-S NCs can be delivered to a variety of cell lines, breast cancer cell line MCF-7 (Figure 14b) and brain cancer cell line U-87 MG (Figure 14c) were also treated with the different NCs. Similar to the assay results from HeLa cells, both cell lines treated with S-S CP-3 NCs for 48 hours showed prominent cell death, but remained viable when treated with the three control NCs. The S-S CP-3 NCs displayed an IC_{50} value of ~ 300 nM and ~600 nM towards U-87 MG and MCF-7 cells, respectively.

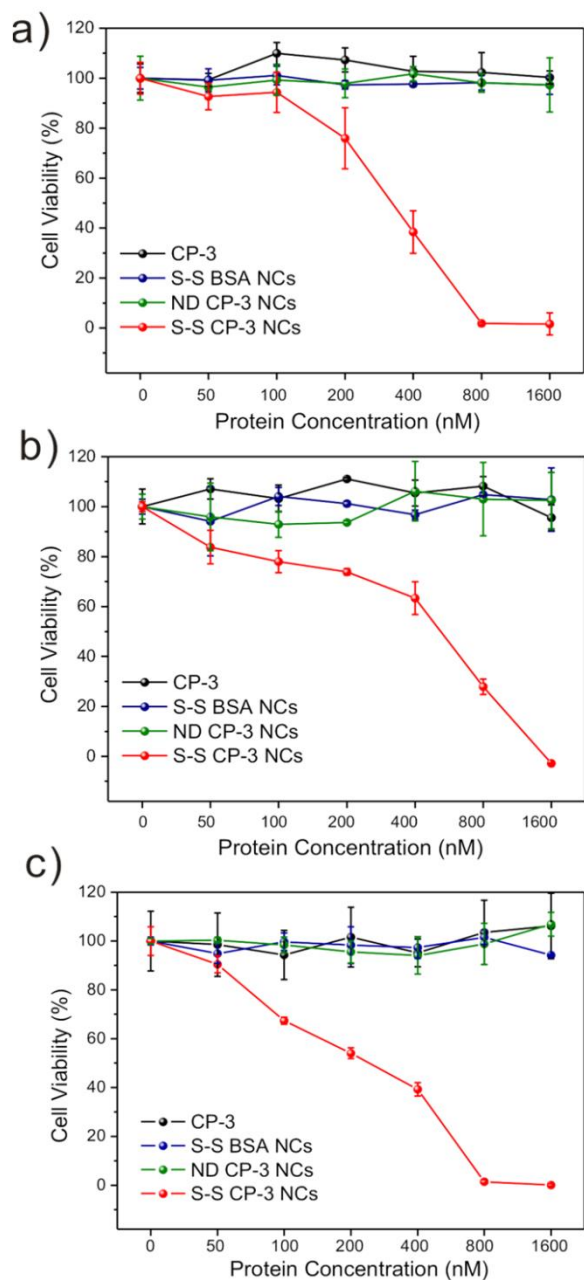


Figure 14. Cytotoxicity of S-S CP-3 nanocapsules toward different cancer cell lines. For each cell line, the cells were treated for 48 hours with native CP-3, S-S BSA NCs, nondegradable CP-3 NCs and S-S CP-3 NCs at concentrations of 50 nM, 100 nM, 200 nM, 400 nM, 800 nM and 1600 nM. Cell viability was measured by using the MTS assay. Cell lines used were **a)** HeLa; **b)** MCF-7; and **c)** U-87 MG.

To confirm the cell death incurred after treatment with S-S CP-3 NCs was indeed apoptosis, we examined the cell morphology under bright field microscopy. As shown in Figure 15a, only HeLa cells incubated with S-S CP-3 NCs showed apoptotic properties such as membrane blebbing and cell shrinkage. In contrast, no morphology change was observed in cells treated with control proteins or NCs. Another signature feature of apoptosis is the fragmentation of the nucleosome upon CP-3 cleavage of the caspase-activated-deoxyribonuclease inhibitor (ICAD)⁹³, which can be detected by the TUNEL assay¹³³. To visualize nicked DNA, the cells were detached, fixed and stained with Alexa Fluor 488 (green), while total cellular DNA was stained with propidium iodide (red). As shown in Figure 15b, HeLa cells treated with 800 nM S-S CP-3 NCs underwent extensive apoptotic DNA fragmentation. In contrast, cells treated with the negative control samples did not display any apoptosis characteristics. Collectively, these results demonstrate that CP-3 encapsulated in the S-S NCs can 1) be internalized into the various cancer cell lines; 2) be delivered into cytosol upon entry; and 3) be released in functional forms and trigger apoptosis. Our results with the CP-3 NCs further demonstrate the potential of using nanocarriers to delivery protein-based cancer therapeutics¹³⁴. Other proteins that can lead to programmed cell death in cancer cells, such as the tumor suppressor p53¹³⁵ and tumor-selective killing proteins¹³⁶, may be similarly formulated in the methods described in this work and be delivered to tumors as potential anticancer therapeutics.

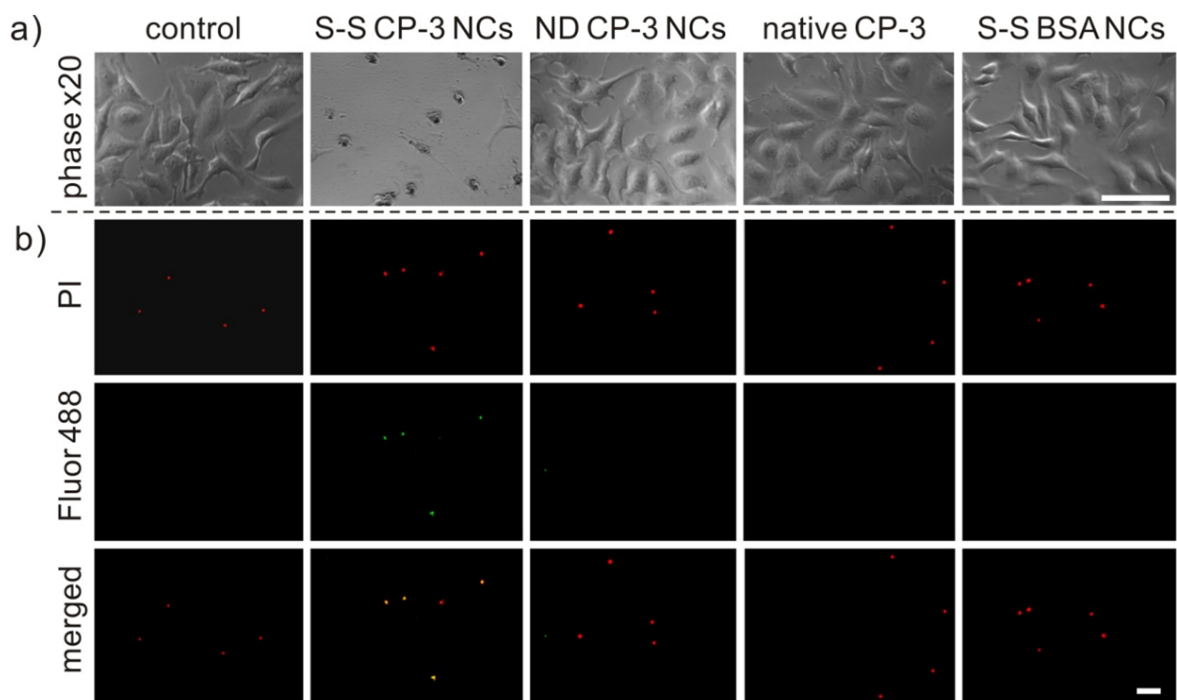


Figure 15. Apoptosis induced by S-S CP-3 nanocapsules. **a)** Bright-field-microscopy images of HeLa cells treated for 24 hours with (i) control (saline); (ii) 800 nM S-S CP-3 NCs; (iii) 800 nM nondegradable CP-3 NCs; (iv) native CP-3; and (v) 800nM S-S BSA NCs. The scale bar represents 100 μm ; and **b)** Apoptotic fragmentation of the nucleosome detected by APO-BrdUTM TUNEL assay with treatment of 800 nM S-S CP-3 NCs for 24 hours. Red fluorescence represents the propidium-iodide-stained total DNA, and green fluorescence represents the Alexa Fluor 488-stained nick end label, the indicator of apoptotic DNA fragmentation. The merged pictures combine the PI-stained nuclei and the Alexa Fluor 488-stained nick end label. The scale bar represents 100 μm .

2.4 Conclusion

We have developed a new method to encapsulate single protein in a polymeric nanocapsule, which can reversibly release the protein in the reducing environment of the cytosol. We demonstrate that these S-S NCs can be rapidly degraded when treated with physiologically relevant concentrations of GSH, can be internalized into cells and escape from endosomes,

and can deliver functional proteins. CP-3 delivered using S-S NCs were able to induce apoptosis in human cancer cell lines including HeLa, MCF-7 and U-87 MG. Therefore, the redox-responsive encapsulation strategy is a simple yet effective method of intracellular protein delivery.

Chapter 3 Degradable Polymeric Nanocapsule for Efficient Intracellular Delivery of a High Molecular Weight Tumor-Selective Protein Complex

3.1. Introduction

The most desirable anticancer therapy is both potent and specific towards tumor cells^{137, 138}. Many conventional small molecule chemotherapeutics do not discriminate between cancerous and normal cells, cause damage to healthy tissues, and are therefore unable to be administered at high dosage. In contrast, cytoplasmic and nuclear proteins that selectively alter the signaling pathways in tumor cells, reactivate apoptosis and restore tissue homeostasis, can delay tumor progression with less collateral damage to other tissues¹³⁹⁻¹⁴². Using stimuli-responsive nanocarriers for the intracellular delivery of such proteins, including human tumor suppressors¹⁴³ and exogenous tumor-killing proteins¹⁴⁴⁻¹⁴⁶, is attractive as a new anti-cancer therapy modality.

Apoptin is a 121-residue protein derived from chicken anemia virus¹⁴⁵. When transgenically expressed, apoptin can induce p53-independent apoptosis in a variety of tumor and transformed cells^{147, 148}, while leaving normal and untransformed cells unaffected¹⁴⁹. Apoptin exists as a globular multimeric complex, composed of thirty to forty subunits, with no well-defined secondary structure^{150, 151}. While the exact mechanism of the tumor selectivity is unresolved, apoptin is known to translocate to the nucleus where tumor-specific phosphorylation at residue Thr108 takes place, leading to accumulation of apoptin in nucleus and activation of the apoptotic cascade in tumor cell¹⁵². In normal cells, apoptin is not phosphorylated at Thr108 and is located mostly in the cytoplasm, where it aggregates and undergoes degradation¹⁵³. Because of the high potency in inducing this exquisite tumor-selective apoptosis, apoptin has been investigated widely as an anti-tumor therapeutic

option¹⁴⁵. Different gene therapy approaches have been used to administer apoptin to mouse xenograft tumor models, in which significant reduction in tumor sizes and prolonged lifespan of mice have been observed without compromising the overall health¹⁵⁴⁻¹⁵⁶. However, as with other gain-of-function therapy candidates, *in vivo* gene delivery approaches using viral vectors may lead to unwanted genetic modifications and elicit safety concerns¹⁵⁷. While protein transduction domain (PTD)-fused apoptin has been delivered to cells^{158, 159}, this approach suffers from inefficient release of the cargo from endosomes and instability of the unprotected protein¹⁶⁰. Development of nanoparticle carriers to aid the functional delivery of apoptin to tumor cells is therefore desirable¹¹.

We chose to work with recombinant maltose-binding-protein fused apoptin (MBP-APO) that can be solubly expressed from *Escherichia coli*, whereas native apoptin forms inclusion bodies¹⁵¹. MBP-APO has been shown to similarly assemble into a multimeric protein complex, which exhibits the essential functions and selectivity of native apoptin¹⁵¹. Nanoparticle-mediated delivery of functional MBP-APO poses unique challenges¹⁶¹. First, MBP-APO preassembles into large complex with an average diameter of ~40 nm and molecular weight of ~2.4 MDa¹⁵¹. To achieve nanocarrier sizes that are optimal for *in vivo* administration (~100 nm)⁹², a loading strategy that forms compact particles is desirable. Second, in order to maintain the multimeric state of functional MBP-APO, the protein loading and releasing steps need to take place under very mild, physiological conditions in the absence of surfactants. Lastly, the nanocarrier must completely disassemble inside the cell to release the MBP-APO in its native and unobstructed form to ensure the correct spatial presentation of key residues within the apoptin portion, including the nuclear localization/export signals, the phosphorylation site and other elements important for downstream signaling.

In the current study, we selected a polymeric nanocapsule (NC) strategy for the functional delivery of MBP-APO, in which the protein complex is noncovalently protected in a water soluble polymer shell (Figure 18). This slightly positively-charged shell shields the MBP-APO from serum proteases and surrounding environment, while enabling cellular uptake of the polymer-protein complex through endocytosis¹⁶². The polymeric layer is weaved together by redox-responsive cross-linkers containing disulfide bond (S-S) that can be degraded once the NCs are exposed to the reducing environment in cytoplasm¹⁶³. No covalent bonds are formed between the protein cargo and the polymer shell, which ensures complete disassembly of the capsule layer and release of native MBO-APO inside the cell. Using this approach, we show that MBP-APO can be efficiently delivered to induce apoptosis in cancer cell lines selectively both *in vitro* and *in vivo*.

3.2. Materials and Methods

3.2.1. Materials

N-(3-aminopropyl) methacrylamide hydrochloride was purchased from Polymer Science, Inc. CellTiter 96® AQueous One Solution Cell Proliferation Assay (MTS) reagent was purchased from Promega Corporation. APO-BrdUTM TUNEL Assay Kit was purchased from Invitrogen. *In situ* Cell Death Detection Kit, POD; was purchased from Roche Applied Science. Female athymic nude (*nu/nu*) mice, 6 weeks of age, were purchased from Charles River Laboratories (Wilmington, MA). All other chemicals were purchased from Sigma-Aldrich and used as received.

3.2.2 Instruments

The Bradford protein assay was carried out on a Thermo Scientific GENESYS 20 spectrometer. The size distribution and ζ -potential of NCs were measured on the Malvern particle sizer Nano-ZS. Transmission electron microscopy (TEM) images were obtained using Philips EM-120 TEM instrument. Fluorescent images were taken with Zeiss Axio Observer Z1 Inverted Microscope and Yokogawa spinning-disk confocal microscope (Solamere Technology Group, Salt Lake City, UT) on Nikon eclipse Ti-E Microscope equipped with a 60 \times 1.49 Apo TIRF oil objective and a Cascade II: 512 EMCCD camera (Photometrics). An AOTF (acousto-optical tunable filter) controlled laser-merge system (Solamere Technology Group Inc.) was used to provide illumination power at each of the following laser lines: 491 nm, 561 nm, and 640 nm solid state lasers (50 mW for each laser).

3.2.3. Protein Expression and Purification method

The pMalTBVp3 plasmid for expression of the MBP-APO was a generous gift from Dr. C. Backendorf and Dr. M. Noteborn (Leiden University). MBP-APO plasmid was transformed into *Escherichia coli* BL21(DE3) cells and incubated at 37 °C overnight on LB agar plate with 100 μ g/mL ampicillin. Colonies were picked and grown overnight at 37 °C with shaking (250 rpm) in 5 mL ampicillin-containing LB media. Overnight cultures were then inoculated in 500 mL of TB media with 100 μ g/mL ampicillin and allowed to grow under 37 °C until the absorbance of cell density (OD₆₀₀) reached 1.0. Isopropyl β -D-1-thiogalactopyranoside (IPTG) was added to a final concentration of 0.1 mM to induce protein expression. After overnight incubation at 16 °C, cells were harvested by centrifugation (2,000 g, 4 °C, 15 min). MBP-APO protein was purified according to procedure described in

previous literature¹⁵⁰. Cell pellets were first resuspended in 30 mL lysis buffer (25 mM Tris-HCl, 500 mM NaCl, 10% glycerol pH 7.4) and lysed by sonication. Cell debris and insoluble proteins were removed by centrifugation (17,000 rpm, 4 °C, 30 min), followed by filtering through 0.22 µm filters to clear the cell lysate further. Protein was then purified on an amylose column (New England BioLabs), which was passed over 5 times with lysate under gravity flow at 4 °C then washed with wash buffer (20 mM Tris-HCL, 50mM NaCl, 1 mM EDTA, pH 7.4) to remove unbound protein. MBP-APO was eluted from the column with 10 mM maltose buffer and buffer exchanged into PBS. The protein concentration was qualitatively assessed by SDS-PAGE and quantitatively determined by the Bradford protein assay using bovine serum albumin (BSA) as the standard.

3.2.4. Protein nanocapsule preparation

The concentration of protein was diluted to 1 mg/mL with 5 mM sodium bicarbonate buffer at pH 9. Then 200 mg/mL acrylamide (AAM) monomer was added to 1 mL of protein solution with stirring at 4 °C. After 10 min, the second monomer, *N*-(3-aminopropyl) methacrylamide (APMAAm), was added while stirring. Different cross-linkers, *N,N'*-methylene bisacrylamide for ND NC and *N,N'*-bis(acryloyl)cystamine for S-S NC, were added 5 min after the addition of APMAAm. The polymerization reaction was immediately initiated by adding 30 µL of ammonium persulfate (100 mg/mL, dissolved in deoxygenated and deionized water) and 3 µL of *N,N,N',N'*-tetramethylethylenediamine. The polymerization reaction was allowed to proceed for 60 min. The molar ratios of AAM/APMAAm/cross-linker used were 1.5:1:0.14, 2:1:0.14, 4:1:0.14, and 8:1:0.14. Buffer exchange with phosphate-buffered saline (PBS) buffer (pH 7.4) was used to remove the remaining

monomers and initiators. Rhodamine-labeled APO NCs was obtained through encapsulation of MBP-APO modified with 5-carboxy-X-rhodamine *N*-succinimidyl ester (mass ratio (MBP-APO: rhodamine): 4:1).

3.2.5. Characterization of protein nanocapsules

The mean hydrodynamic size and ζ -potential of NC were determined by dynamic light scattering (DLS) in PBS buffer. Samples of NCs (0.05 mg/mL) for TEM imaging were negatively stained with 2 % uranyl acetate in alcoholic solution (50 % ethanol). The lamella of stained sample was prepared on carbon-coated electron microscopy grids (Ted Pella, Inc.).

3.2.6. Cellular uptake and localization of nanocapsules

MDA-MB-231, HeLa, MCF-7, and human foreskin fibroblast (HFF) cells (ATCC, Manassas, VA) were cultured in Dulbecco's Modified Eagle's Media (DMEM) (Invitrogen) supplemented with 10% bovine growth serum (Hyclone, Logan, UT), 1.5 g/L sodium bicarbonate, 100 μ g/mL streptomycin and 100 U/mL penicillin, at 37 °C with 98% humidity and 5% CO₂. To visualize NCs uptake, MDA-MB-231 cells were seeded into 48-well plate, with a density of 10,000 cells/well in 250 μ L of media with supplements. S-S Rho-APO NC and ND Rho-APO NC were added to a final concentration of 20 nM. After 1 hour and 24 hours of incubation, cells were washed with PBS twice, stained with DAPI Nucleic Acid Stain and imaged. For internalization of S-S Rho-APO NC with different ζ -potentials, MDA-MB-231 cells were incubated with 20 nM NCs for 2 hours before nuclei staining. Markers for early and late endosomes were used for internalization trafficking study. A concentration of 20 nM S-S Rho-APO NCs was added to HeLa cells and incubated for 30 min, 60 min and 120 min under 37 °C. Cells were then fixed with 4 % formaldehyde, permeabilized with 0.1 % Triton X-100, and stained with antibodies, mouse anti-EEA1 antibody against early

endosomes and rabbit anti-CI-MPR antibody against late endosomes (Cell Signaling Technology, Inc.). Texas red goat anti-mouse IgG and Alexa Fluor® 647 goat anti-rabbit IgG (Invitrogen) were added as the secondary antibody. To determine the cellular localization of the protein delivered, confocal images were taken with HeLa, MCF-7, and HFF cells incubated with 20nM of S-S Rho-APO NC or ND Rho-APO NC at 37 °C for 24 hours. Nuclei were then counterstained with DAPI. The Z-stack images of cells were imaged at 0.4- μ m intervals and analyzed by Nikon NIS Element software. Fluorescent microscopy images were acquired on a Yokogawa spinning-disk confocal scanner system (Solamere Technology Group, Salt Lake City, UT) using a Nikon eclipse Ti-E microscope equipped with a 60 \times /1.49 Apo TIRF oil objective and a Cascade II: 512 EMCCD camera (Photometrics, Tucson, AZ, USA). An AOTF (acousto-optical tunable filter) controlled laser-merge system (Solamere Technology Group Inc.) was used to provide illumination power at each of the following laser lines: 491 nm, 561nm, and 640 nm solid state lasers (50mW for each laser).

3.2.7. Cytotoxicity Assays

Different cancer cells lines, HeLa, MCF-7 and MDA-MB-231, as well as noncancerous HFF, were seeded into 96-well plates, each well containing 5,000 cells in 100 μ L of DMEM with supplements. Different concentrations of protein and NCs were added into each well and the plates. After incubation of 48 hours at 37 °C, the wells were washed with PBS solution twice and 100 μ L of fresh cell culture media with supplements was added. Then 20 μ L MTS solution (CellTiter 96® AQueous One Solution Cell Proliferation Assay) was added into each well and the plates were incubated for 3 hours at 37 °C. The absorbance of each well was read at 490 nm using a microplate reader (PowerWave X, Bio-tek Instruments, USA). Apoptosis was detected using APO-BrdU Terminal Deoxynucleotidyl

Transferase dUTP Nick End Labeling (TUNEL) assay kit. MDA-MB-231 and HFF cells were seeded at a density of 100,000 cells/well into a 6-well plate in 2 mL of cell culture media with supplements. Proteins and NCs were added after cells covered 80% of bottom surface. After 24 hours of incubation, cells were fixed with 1% paraformaldehyde in PBS, followed by the addition of DNA labeling solution containing terminal deoxynucleotidyl transferase and bromodeoxyuridine (BrdUrd). Cells were then stained with Alexa Fluor® 488 dye-labeled anti-BrdUrd antibody. Samples were deposited onto slides, which were later stained with propidium iodide (PI) solution containing RNase A. Images were obtained by fluorescent microscope (Zeiss, Observer Z1) using appropriate filters for Alexa Fluor 488 and PI.

3.2.8. *In vivo studies with MCF-7 xenograft model*

All mice were housed in an animal facility at the University of Southern California in accordance with institute regulations. Female athymic nude (*nu/nu*) mice were subcutaneously grafted on the back flank with 5×10^6 MCF-7 tumor cells. Afterwards, tumor size was monitored by a fine caliper and the tumor volume was calculated as the product of the two largest perpendicular diameters and the vertical thickness ($L \times W \times D$, mm^3). When the tumor volume reached 100-200 mm^3 , mice were randomly separated into different groups. From day 0, mice were treated with intratumoral injection of native MBP-APO or S-S APO NC (200 μg per mouse) every other day. PBS and S-S BSA NC were included as the negative controls. When the tumor volume exceeded 2500 mm^3 , the mice were euthanized by CO_2 according animal protocol. The average of tumor volumes was plotted as the tumor growth curve in respective treated groups. For histology study, treated tumor samples were collected and fixed in 4% paraformaldehyde, and processed for staining using the *In Situ* Cell

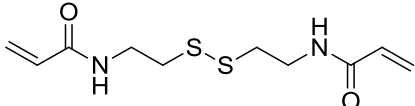
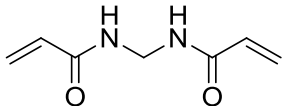
Death Detection Kit. The stained tumor slides were observed under microscope, and representative pictures were taken for analysis. Paraformaldehyde-postfixed frozen tumor sections (5- μ m thick) were permeabilized with 0.1% triton X-100 and stained with TUNEL assay kit (In Situ Cell Death Detection Kit, POD; Roche Applied Science, Indianapolis, IN) in accordance with the manufacturer's instructions. DAPI was used for nuclear counterstaining.

3.3. Results and Discussion

3.3.1. Synthesis and characterization of apoptin nanocapsules

MBP-APO (pI = 6.5) was first purified from *E. coli* extract using an amylose-affinity column (Figure 16 and Figure 17). Dynamic Light Scattering (DLS) measurement revealed an average hydrodynamic radius of 36.1 nm (Figure 17), consistent with the reported size for the recombinant MBP-APO complex¹⁵¹. Transmission Electron Microscopy (TEM) analysis of MBP-APO showed similarly sized protein complexes (Figure 18c and enlarged in Figure 18d). Interestingly, MBP-APO complexes appear to adopt a disk-shaped structure despite the lack of defined secondary structure from the apoptin component. Since the apoptin portion of the protein can self-assemble into the ~40-mer complex, we propose a three dimensional arrangement of MBP-APO in which the C-terminal apoptin forms the central spoke of the wheel-like structure (Figure 18b), with the larger MBP portion distributes around the apoptin. The planar arrangement allows the apoptin portion of the fusion protein to remain accessible to its protein partners, which may explain how the MBP-APO fusion retains essentially all of the observed functions of native apoptin.

Table 4. Mean hydrodynamic size and ζ - potential of protein NC

	S-S APO NC	S-S BSA NC	ND APO NC
Size (nm)	74.71	10	79.58
ζ-potential (mV)	2.8 \pm 0.2	4.7 \pm 0.4	1.6 \pm 0.4
Crosslinker	<i>N,N'</i> -bis(acryloyl)cystamine 	<i>N,N'</i> -methylene bisacrylamide 	

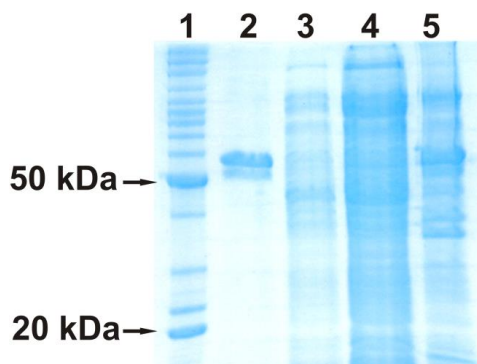


Figure 16. SDS-PAGE of MBP-APO purification using amylose affinity chromatography. Lane 1: Molecular weight marker; Lane 2: Purified MBP-APO (56 kDa) as eluted with 10 mM maltose; Lane 3: Wash fraction; Lane 4: Unbounded cell lysate proteins; Lane 5 Insoluble fractions from lysed *E. coli* cells.

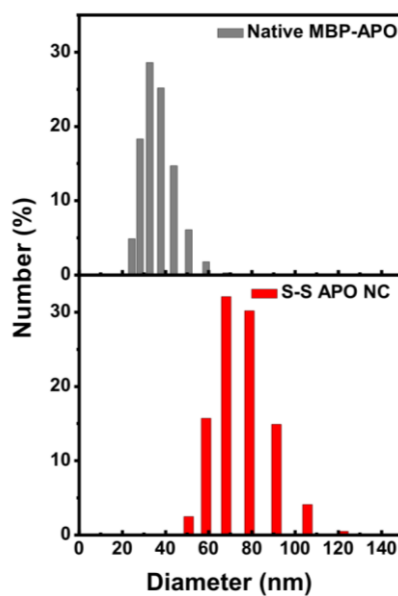


Figure 17. Size distribution of native MBP-APO and S-S APO NC. The hydrodynamic sizes of the native MBP-APO (grey) and S-S APO NC (red) were determined by DLS.

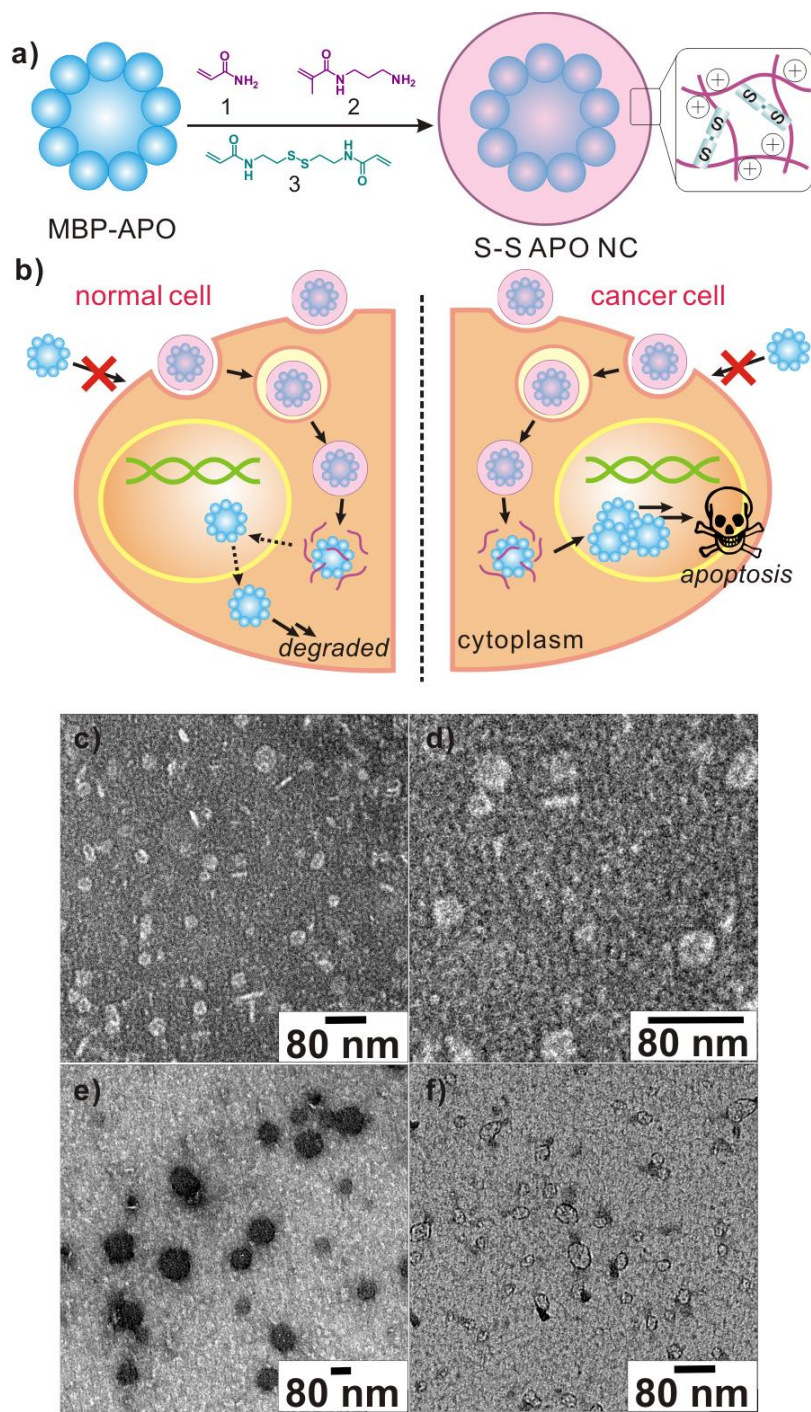


Figure 18. Degradable nanocapsules for apoptin delivery. a-b) Schematic diagram of synthesis of degradable apoptin nanocapsules (S-S APO NC) and delivery into tumor cells to induce apoptosis; TEM images of c) native MBP-APO; d) enlarged image of MBP-APO; e) S-S APO NC; and f) degraded S-S APO NC after treatment with 2 mM GSH for 6 hours at 37 °C;

The reversible encapsulation strategy for producing apoptin NCs is shown in Figure 18a. Following electrostatic deposition of the monomers acrylamide (**1** in Figure 18a) and *N*-(3-aminopropyl)methacrylamide (**2**), and the cross-linker *N,N'*-bis(acryloyl)cystamine (**3**), at a molar ratio of 1.5:1:0.14, onto MBP-APO (1 mg) in carbonate buffer (5 mM, pH 9.0), *in situ* polymerization was initiated with the addition of free radical initiators and proceeded for one hour. The molar ratio and the time of reaction reported were optimized to minimize protein aggregation and precipitation, as well as to maximize the solution stability of the resulting NCs (designated below as S-S APO NC). Excess monomers and cross-linkers were removed using ultrafiltration and S-S APO NC was stored in PBS buffer (pH 7.4). DLS clearly showed increase in average diameter of the sample to ~75 nm with a slightly positive ζ -potential value of 2.8 mV (Table 3). TEM analysis of the S-S APO NC confirmed the nearly doubling in diameter of the spherical particle (Figure 18e). Unexpectedly, the NCs displayed dark contrast upon uranyl acetate staining, which hints that the cores of the particles were very densely packed. As expected from the incorporation of redox-responsive cross-linker **3**, the reduction of NCs size can be seen upon treatment of the reducing agent glutathione (GSH) (2 mM, 6 hours, 37 °C). As shown in Figure 18f, the densely packed NCs were completely dissociated into ~30 nm particles, confirming the reversible nature of the encapsulation process. As a control, we also synthesized nondegradable MBP-APO NCs (ND APO NC) using *N,N'*-methylene bisacrylamide as the cross-linker with same monomer and protein concentrations under identical reaction conditions. Whereas similarly sized NCs were formed, no degradation of ND APO NC can be observed in the presence of GSH.

3.3.2. Cellular uptake and localization of nanocapsules

We next examined the cellular uptake of the S-S APO NC and cellular localization of the cargo. If the unique tumor selectivity of MBP-APO is maintained following the encapsulation and release processes, we expect the delivered MBP-APO to either accumulate in the nuclei of the tumor cells, or to localize in the cytoplasm of noncancerous cells. Prior to the polymerization process, the MBP-APO protein was conjugated to amine-reactive rhodamine (Rho-APO). Subsequent encapsulation yielded similarly sized NCs as unlabeled S-S APO NCs. Fluorescent microscopy showed all NCs readily penetrated the cell membrane and are present in the cytoplasm of MDA-MB-231 cells within one hour (Figure 19). When the relative amounts of positively-charged monomer **2** were reduced in the NC shell, corresponding decreases in ζ -potentials of the NCs were measured by DLS, which led to decreases in cellular internalization (Figure 20).

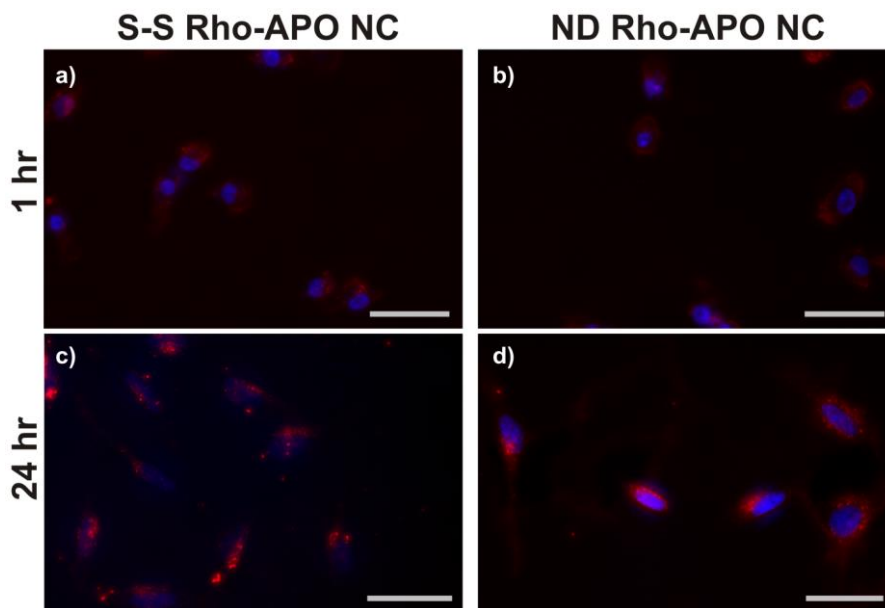


Figure 19. Internalization of S-S APO NC and ND APO NC. Fluorescent microscopy images of MDA-MB-231 cells after 1 and 24 hours incubation with 20 nM S-S Rho-APO NCs and with 20 nM ND Rho-APO NCs. Nuclei were stained with DAPI. The scale bars represent 50 μm .

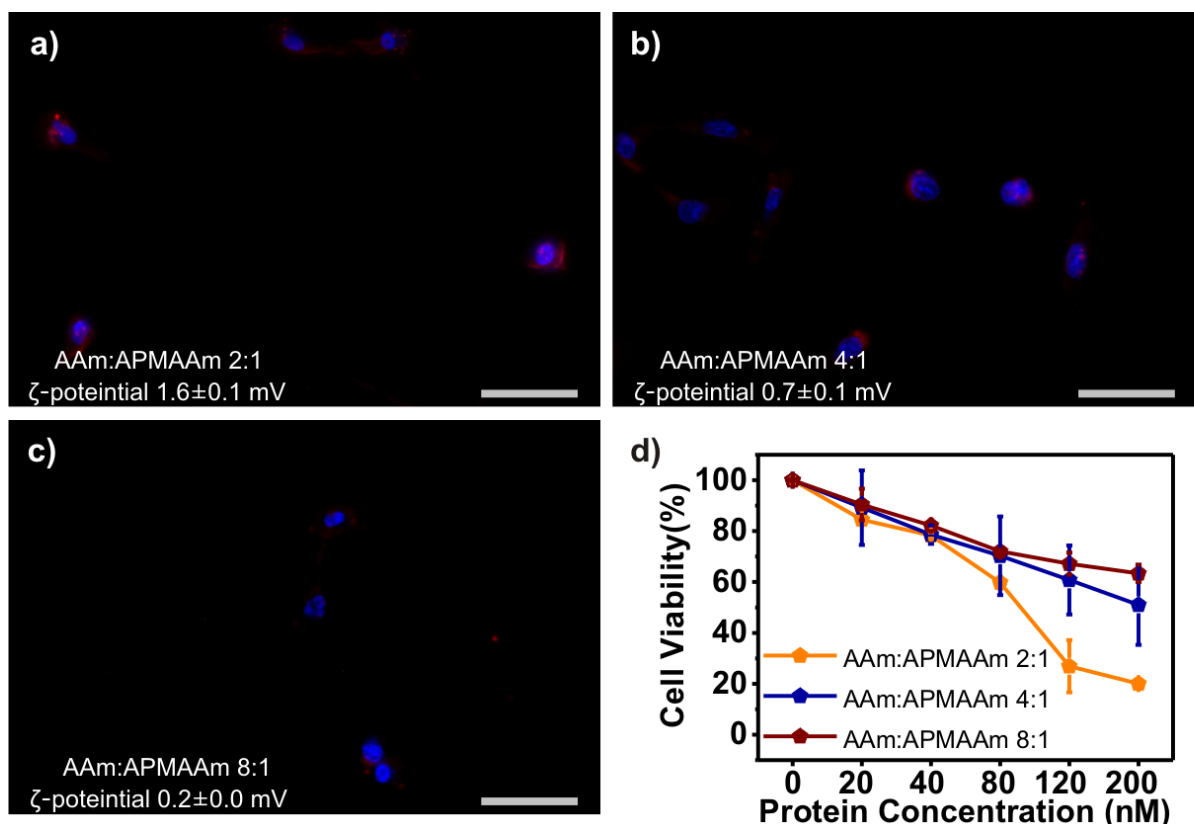


Figure 20. Internalization and cytotoxicity of S-S APO NCs with different ζ -potentials. Fluorescent microscopy images of MDA-MB-231 cells after 2 hours incubation with 20 nM S-S NCs of different M1 to M2 ratios a) 2:1; b) 4:1; and c) 8:1. Nuclei were stained with DAPI. The scale bars represent 50 μ m; d) Cell viability curves for MDA-MB-231 cells treated with various concentrations of S-S APO NC with different ζ -potentials.

The cellular trafficking of the internalized S-S Rho-APO NCs in HeLa cells was investigated for 2 hours by monitoring colocalization using fluorescent markers for early and late endosomes (Figure 21a). Colocalization of Rho-APO with early endosomes was detected at the highest levels after 30 minutes and decreased at later time points. In contrast, colocalization of Rho-APO with late endosome remained low throughout the trafficking studies. Colocalization of Rho-APO with nuclei became evident after 2 hours, indicating endosomal escape and nuclear entry of the released apoptin protein. These results suggested that S-S Rho-APO NCs were trafficked into early endosomes upon internalization and at least

a significant portion of the internalized NCs and the cargo can escape from the endosomal compartment.

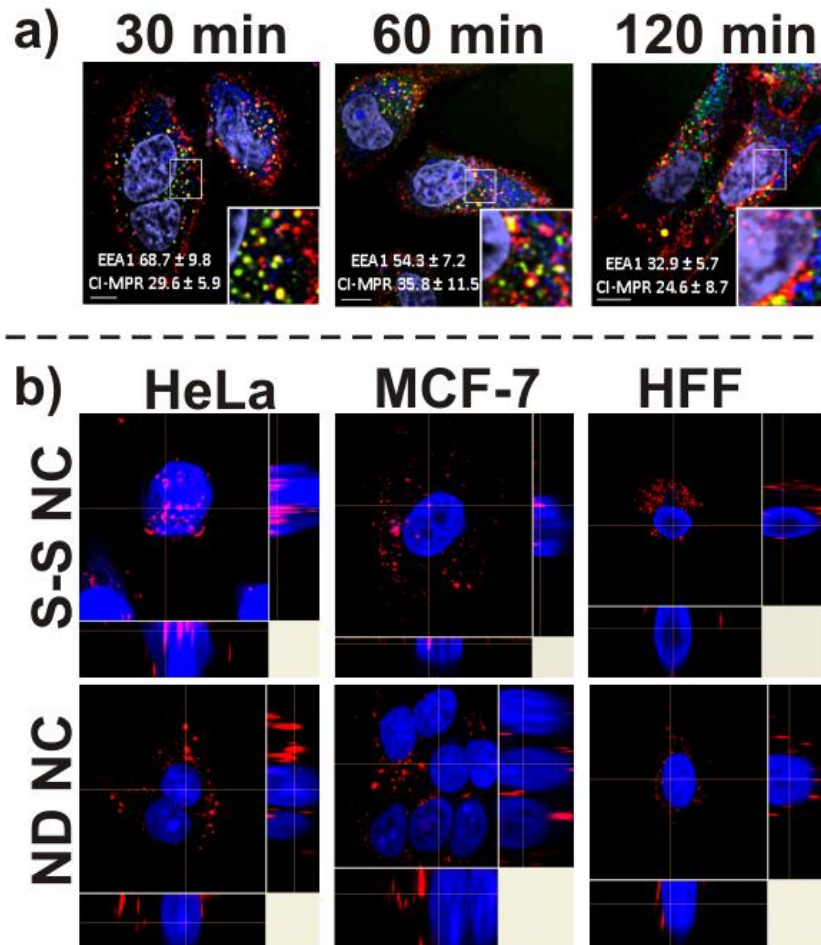


Figure 21. Protein nanocapsule cellular trafficking and localization. a) The trafficking of Rho-APO in S-S NCs through endosomes. HeLa cells were incubated with 20 nM S-S Rho-APO NCs (red) at 37 °C for various time periods, 30, 60 and 120 min. Early endosomes were detected by early endosome antigen 1 (EEA1, green). Late endosomes were detected by cation-independent mannose-6-phosphate receptor (CI-MPR, blue). Nuclei were stained with DAPI and shown as purple. The scale bar represents 10 μm. The percentage of fluorescence colocalization was quantified by calculating colocalization coefficients using Manders' overlap coefficient (>10 samples) and shown in each figure; b) confocal microscopy of cellular localization of Rho-APO encapsulated in S-S NC and ND NC to cancer cell lines HeLa and MCF-7, and noncancerous HFF. Nuclei were stained with DAPI (blue). The scale bar is 20 μm.

To analyze protein localization using confocal microscopy, two cancer cell lines HeLa and MCF-7, together with the noncancerous human foreskin fibroblast (HFF), were treated with either S-S Rho-APO NC or ND Rho-APO NC (Figure 21b). In the case of ND Rho-APO NCs, red fluorescence signals remained in the cytoplasm for all three cell lines, indicating the encapsulated Rho-APO proteins were well-shielded by the nondegradable polymer shell and the internal nuclear localization sequences were not accessible to the transport machinery. In stark contrast, when HeLa cells were treated with S-S Rho-APO NC, strong red fluorescence of rhodamine was present in the nuclei, resulting in intense pink color as a result of overlapping of rhodamine and DAPI fluorescence. Z-stacking analysis confirmed the Rho-APO to be localized inside of the nuclei. Similar results were observed with MCF-7 cells, although the fluorescence intensity was not as strong as in the HeLa cells. These results confirmed that the Rho-APO delivered can indeed be released in native forms inside the cytoplasm and enter the nuclei. More importantly, the tumor-specificity of delivered apoptin proteins towards cancer cell lines were demonstrated in the confocal analysis of noncancerous HFF cells treated with S-S Rho-APO NC, as all of the dye signals remained in the cytoplasm and no nuclear accumulation was observed.

3.3.3. Tumor-selective cytotoxicity of apoptin nanocapsules

We then investigated whether the MBP-APO protein delivered still possesses its function to induce tumor-selective apoptosis. The potency and selectivity of S-S APO NC were tested on various cell lines including HeLa, MCF-7, MDA-MB-231, and HFF (Figure 22). MTS assay was used to measure cell viability 48 hours after addition of the protein and NC. For each cell line, ND APO NC and native MBP-APO were used as negative controls. When S-S

APO NC was added to a final concentration of 200 nM, all three cancer cell lines had no viable cells, whereas ~75 % of the HFF had survived. The IC₅₀ values were 80 and 30 nM for HeLa and MDA-MB-231, respectively. The IC₅₀ for MCF-7 was higher at ~110 nM, which may be due to the deficiency in the terminal executioner caspase 3 and reliance on other effector caspases for apoptosis^{164, 165}. As expected, native MBP-APO and ND APO NC did not significantly decrease the viability of any cell lines tested, consistent with the inability to enter cells and release MBP-APO in cytoplasm, respectively. The IC₅₀ values of S-S APO NC towards MDA-MB-231 increased as the surface charge of the NC became more neutral (Figure 20), suggesting more efficient internalization can improve S-S NCs cytotoxicity. The morphologies of MDA-MB-231 and HFF cells were examined under various treatments. Only the S-S APO NC treated MDA-MB-231 cells exhibited blebbing and shrinkage, which are hallmarks of apoptotic cell death (Figure 22e and Figure 23). Using TUNEL assay, S-S APO NC treated MDA-MB-231 also showed nuclear fragmentation associated with apoptosis, whereas cells treated with native MBP-APO and ND APO NC at the same concentration (Figure 23), as well as HFF treated with 200 nM S-S APO NC (Figure 22e), had no sign of apoptosis. Collectively, these results demonstrated that the recombinant MBP-APO delivered by the degradable NCs retains the potency and selectivity as the transgenically expressed apoptin in previous studies¹⁴⁵.

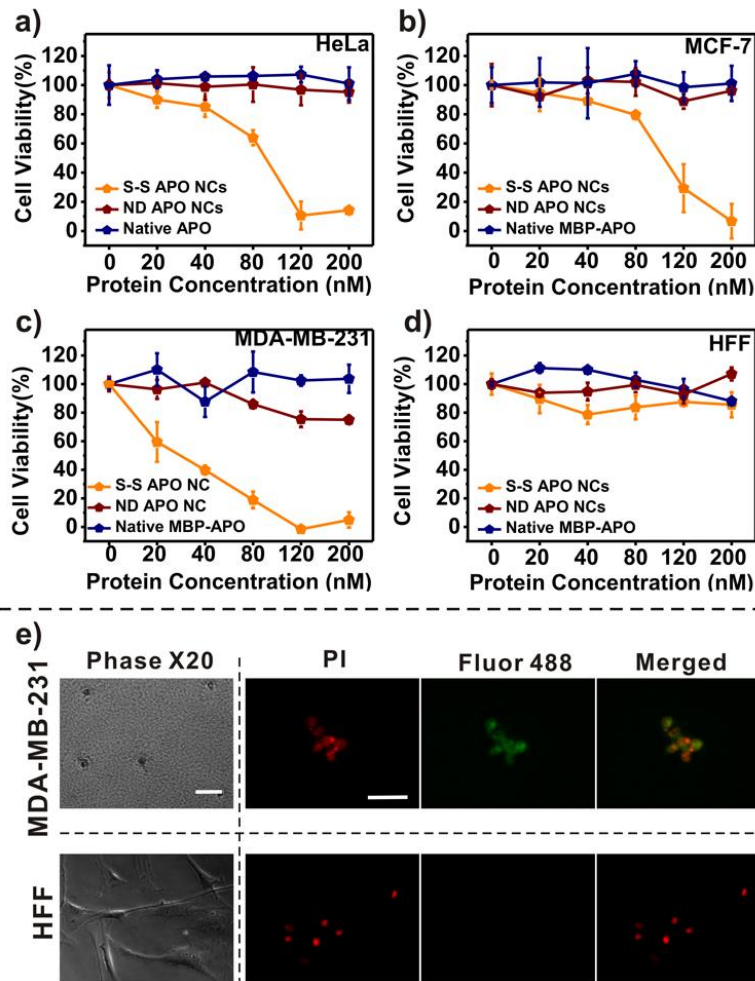


Figure 22. Cytotoxicity and apoptosis observed following nanocapsule delivery. (a) HeLa; (b) MCF-7; (c) MDA-MB-231; or (d) HFF cells with treatment of different concentrations of S-S APO NC, ND APO NC, and native MBP-APO. (e) Apoptosis induced by S-S APO NC determined by TUNEL assay. Images on the left are bright field microscopy images of MDA-MB-231 and HFF cells treated for 24 hours with 200 nM S-S APO NC. The scale bar represents 50 μm. Images right of the dash line shows detection of apoptotic fragmentation of the nucleosome after same treatment using APO-BrdUTM TUNEL assay kit. The scale bar represents 50 μm. Red fluorescence represents the propidium-iodide (PI)-stained total DNA, and green fluorescence represents the Alexa Fluor 488-stained nick end label, the indicator of apoptotic DNA fragmentation. The merged pictures combine the PI-stained nuclei and the Alexa Fluor 488-stained nick end label. (Note the bright field images do not overlap with the fluorescent microscopy images; cells were detached and collected for TUNEL assay after treatment).

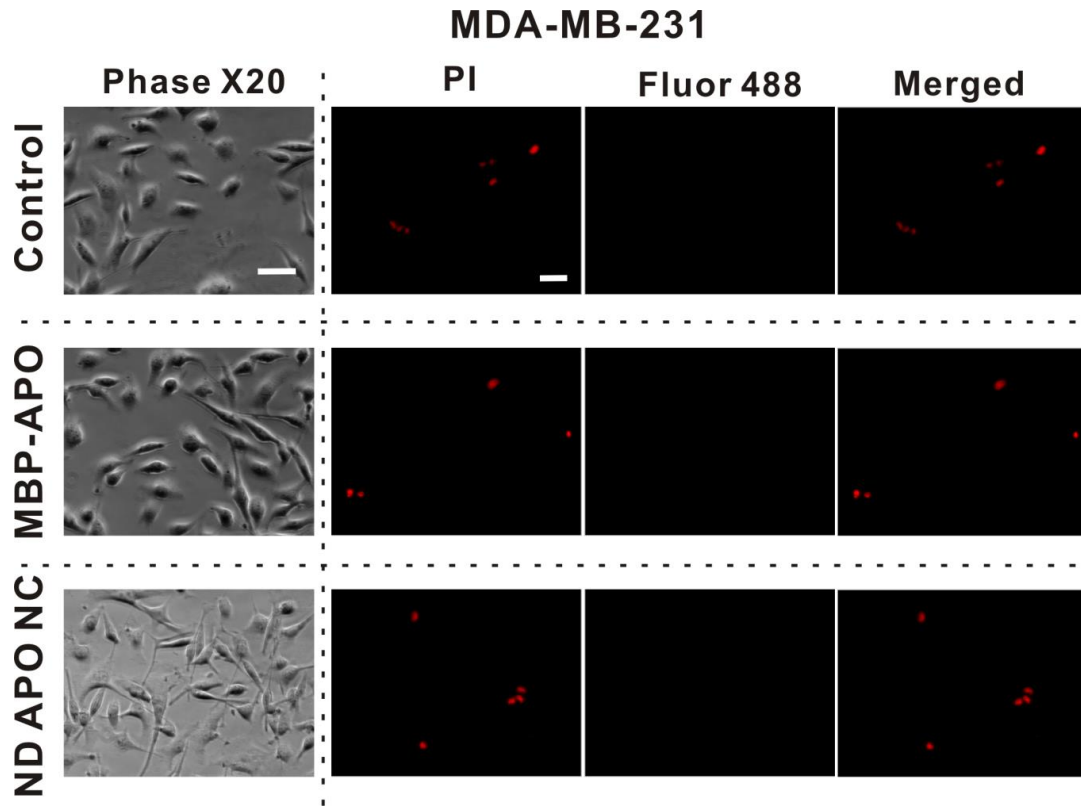


Figure 23. TUNEL assay of MDA-MB-231 cells treated with control samples. Images left of dash line are bright-field-microscopy images of MDA-MB-231 treated for 24 hours with (i) control (saline); (ii) 200 nM native MBP APO; (iii) 200 nM ND APO NC. The scale bars represent 50 μm ; Images right of dash line are apoptotic fragmentation of the nucleosome detected by APO-BrdUTM TUNEL after same treatment as above. The scale bars represent 50 μm . Red fluorescence represents the PI-stained total DNA, and green Alexa Fluor 488 fluorescence represents apoptotic DNA fragmentation. The merged pictures combine the PI-stained nuclei and the Alexa Fluor 488-stained nick end label. Note the bright field images do not overlap with the fluorescent microscopy images.

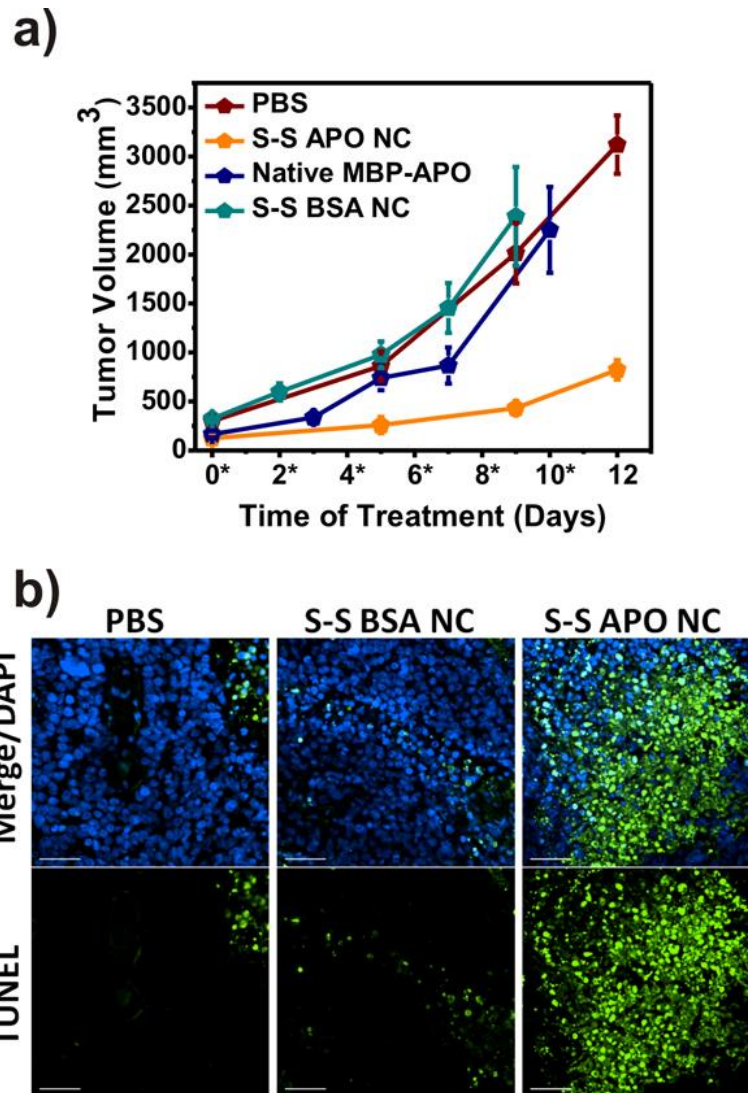


Figure 24. Treatment of apoptin nanocapsules resulted in tumor growth retardation. a) Significant tumor inhibition was observed in the mice treated by S-S APO NC. Female athymic nude mice were subcutaneously grafted with MCF-7 cells and treated with intratumoral injection of MBP-APO (n=4) or S-S APO NC (n=4) (200 $\mu\text{g}/\text{mouse}$) every other day. PBS (n=3) and S-S BSA NC (n=4) were included as negative controls. The average tumor volumes were plotted vs. time. Asterisks indicate injection days. b) Detection of apoptosis in tumor tissues after treatment with different NCs. Cross-sections of MCF-7 tumors were stained with fluorescein-dUTP (green) for apoptosis and DAPI for nucleus (blue). The scale bars represent 50 μm .

3.3.4. *In vivo* evaluation of apoptin nanocapsules

We further examined the potency of S-S APO NC in a mouse xenograft model. Female athymic nude (*nu/nu*) mice were subcutaneously grafted on the back flank with 5×10^6 MCF-7 breast cancer cells. When the tumor volume reached 100-200 mm³ (day 0), mice were randomly separated into different groups and treated with intratumoral injection of PBS, MBP-APO, S-S APO NC. In addition, S-S NC with bovine serum albumin (S-S BSA NC) was added as a nonlethal protein cargo control to test the effects of the S-S NC polymer component on tumor cells *in vivo*. Tumors treated with saline, S-S BSA NC or native MBP-APO expanded rapidly and reached the maximum limit (>2500 mm³) within 12 days. In sharp contrast, tumor growth was significantly delayed when treated with S-S APO NC (Figure 24a). Fixed tumor tissues collected from each treatment group was examined for DNA fragmentation using *in situ* TUNEL assay. The images revealed the highest level of cell apoptosis for the tumor harvested from mice treated with S-S APO NC, correlating well with the significantly delayed tumor growth observed for this treatment group and confirming that tumor growth inhibition was indeed due to apoptin-mediated apoptosis (Figure 24b). Collectively, the xenograft study verified that the degradable NCs effectively delivered MBP-APO proteins to tumor cells *in vivo*, which was highly effective in limiting tumor progression. Upon further optimization of the pharmacokinetics of the S-S APO NC, including surface derivatization with active targeting ligands, these particles may be intravenously administered as an anticancer therapy¹⁶⁶.

3.4. CONCLUSIONS

We were able to deliver the high molecular weight complex of the tumor-selective MBP-APO using a redox-responsive polymeric NC *in vitro* and *in vivo*. The choice and design of the sub-100 nm NC is well-suited for diverse protein targets because of its mild preparation conditions, reversible encapsulation, efficient membrane penetration, and cytoplasmic release of the protein cargo. Our application here further illustrates how intracellular protein delivery using nanoscale system can provide new possibilities for achieving selective anticancer therapy.

Chapter 4 Clickable Protein Nanocapsules for Targeted Delivery of Recombinant p53

4.1 Introduction

Virtually all human cancer cells have elaborate anti-apoptotic strategies to overcome apoptosis, which is a vital cellular mechanism to obstruct tumor progression⁹³. The most commonly mutated gene in tumor cells is the tumor suppressor gene *TP53*, the protein product of which promotes apoptosis of aberrant cells through both transcription-dependent and independent mechanisms¹⁶⁷. In this manner, the genome guardian p53 is critically important in eliminating possible neoplastic cells incurred during DNA damage. About 50% of all the human tumors have mutant p53 proteins, whereas ~30% of breast cancer cell lines are mutated in p53¹⁶⁸. Therefore, restoring p53 function can be a highly effective option for cancer treatment. While functional copies of p53 can resurrect the apoptotic circuitry, it will also sensitize the tumor cells towards other various treatments (radio- and chemotherapy)¹⁶⁹. Different strategies pursuing this goal have been intensively investigated, including small molecules, peptides that overcome p53 mutations and adenovirus/p53 gene delivery vectors¹⁷⁰⁻¹⁷³. While restoring p53 functions in cancer cells has been a tantalizing approach towards combating cancer, the lack of effective delivery method has undermined its potential as an anti-cancer therapeutic.

Intracellular protein delivery using “Smart functional nanomaterials” has emerged as an attractive method to deliver various cargos to cells of interest. In particular, water soluble polymer-based nanoparticles that encapsulate the protein of interest to aid the penetration of cellular membrane, while capable of releasing the material upon various cellular stimuli, have been demonstrated to be effective in functional delivery of protein¹⁷⁴. Nanocapsules that can be triggered to release protein cargo in response to changes in temperature, light, pH, redox

potential and enzymatic activities have been reported^{60, 162, 163, 175, 176}. As a result, nanocapsules-mediated delivery of recombinant p53 to cancer cells may be a direct method of reactivating the apoptosis pathway and induce programmed cell death. In our previous formulations, the nanocapsules are synthesized with a positively charged monomer that enables nonselective entry across cellular membrane. However, since the level of p53 is tightly regulated in normal cell lines, targeted delivery of p53 using functionalized nanocapsules that restricts entry to only cancer cell lines is highly desirable. Hence, new methods that allow facile modification of the polymer-based carrier are needed.

To functionalize the nanocapsules with cancer-targeting ligands such as peptides and antibodies that can enable receptor mediated endocytosis, the surface of the nanocapsules must be decorated with reactive handles that facilitate facile, aqueous-based chemistry. The chemistry utilized must be nondenaturing and maintaining the native form of protein cargo. This is especially important for p53 delivery since the protein forms a tetrameric complex that is prone to aggregation and loss of function. The reaction must also be orthogonal to the nanocapsule synthesis chemistry and compatible with the designed degradation strategy of the nanocapsules, such as disulfide mediated redox degradation. One of the most versatile reactions that is compatible with a protein-based cargo is the Copper-free Click Chemistry that utilizes azides and aryl cyclooctynes. Click chemistry has been used for modification of nanoparticles for directed conjugation of ligands and chromophores¹⁷⁷. In this report, we demonstrate that protein nanocapsules containing reactive azido on the surface can be synthesized, which allows facile conjugation to various ligands. More importantly, we show that recombinant p53 can be selectively delivered to specific cancer cell lines using nanoparticles clicked with targeting ligands.

4.2. Material and methods

4.2.1. Construction, expression and purification of proteins

The plasmid for expression of the full length human p53 protein was purchased from Addgene (Plasmid 24859). The purification and refolding of p53 was performed as described in S. Bell *et al.* Biophysical Chemistry 2002. Briefly, the plasmid was transformed into *Escherichia coli* BL21(DE3) cells and incubated at 37 °C overnight on LB agar plate with 100 µg/mL ampicillin. Colonies were picked and grown overnight at 37 °C with shaking (250 rpm) in 5 mL ampicillin-containing LB media, which were then inoculated into 500 mL of TB media with 100 µg/mL ampicillin and allowed to grow under 37 °C until the absorbance of cell density (OD₆₀₀) reached 0.9. Isopropyl β-D-1-thiogalactopyranoside (IPTG) was added to a final concentration of 0.1 mM to induce protein expression. After overnight incubation at 16 °C, the *E. coli* cells were harvested by centrifugation (3,750 rpm, 4 °C, 15 min). Cell pellets were then resuspended in 50 mL lysis buffer (0.1 mM Tris-HCl, 1mM EDTA, pH 7) and lysed by sonication. Inclusion bodies (IB) were harvested by centrifugation (31,000 g, 4 °C, 30 min), followed by sequential washes remove cell debris and other proteins at 4 °C (Wash 1: 60 mM EDTA, 6% triton X-100, 1.5 M NaCl, pH 7; Wash 2: 0.1 M Tris-HCl, 30 mM EDTA, 3% Triton X-100, 0.8M NaCl, pH 7; Wash 3: 0.1M Tris-HCl, 20 mM EDTA, pH 7). IB pellet was collected by centrifugation (31,000 g, 4 °C, 10 min) between wash buffers and was washed until a clean band of p53 can be seen on SDS-PAGE. Afterwards, the IB pellet was solubilized in solubilization buffer (100 mM Tris-HCl, 6 M Guanidinium Chloride, 50 mM DTT, pH 8) at room temperature for 2 hours. After adjusting the pH to 2 using HCl, centrifugation was used to separate solubilized p53 from any insoluble material (31,000 g, 4 °C, 30 min). The concentration of solubilized p53 was determined using Bradford protein assay and solubilized protein was aliquoted for -80 °C storage.

Renaturation of solubilized p53 was carried out in renaturation buffer at 4 °C (50 mM Sodium Pyrophosphate, 1 M L-arginine, 2 mM DTT, 0.2 mM Zinc Chloride, pH 8). Solubilized p53 protein was diluted in renaturation buffer using step-wise addition with 90 min interval, yielding final protein concentration about 1 mg/mL. The entire renaturation volume was then dialyzed against dialysis buffer at 4 °C (50 mM Sodium Pyrophosphate, 2 mM DTT, pH 8), followed by centrifugation to remove any precipitates (31,000 g, 4 °C, 1 hour). The clear protein solution was concentrated and buffer exchanged into buffer containing 100 mM NaCl and 10 mM Sodium Pyrophosphate, pH 7.5. The final protein concentration was qualitatively assessed by SDS-PAGE and quantitatively determined by the Bradford protein assay. The Bradford protein assay was carried out on a Thermo Scientific GENESYS 20 spectrometer.

Mutant S121F was constructed from Plasmid 24859 by PCR with the following primers,

5'-TTGCATTCTGGGACAGCCAAGTTTGTGACTTGCACGTACTCCCCT-3', and

5'-AGGGGAGTACGTGCAAGTCACAAACTTGGCTGTCCCAGAATGCAA-3'.

The PCR product was verified by sequencing, and then transformed into BL21(DE3) cells. Expression and purification of S121F follows the same procedure for wild type p53 protein described above.

Gene sequence encoding single-chain variable fragment of the anti-HER2 antibody was synthesized by Genscript, NJ. based on protein sequence shown below,

MGGSEVQLVESGGGLVQPGGSLRLSCAASGFNIKDTYIHWVVRQAPGKGLEWVARIYP
TNGYTRYADSVKGRFTISADTSKNTAYLQMNSLRAEDTAVYYCSRWGGDGFYAMDY
WGQGTLLVTVSSGGGGSGGGGSGGSADIQMTQSPSSLSASVGDRVTITCRASQDVNTA

VAWYQQKPGKAPKLLIYSASFLYSGVPSRFSRSGTDFTLTISSLQPEDFATYYCQQH
YTPPTFGQGTKVEIKRASGCGPE

The DNA sequence was subsequently cloned into pET28a vector for expression of single chain HER2 antibody. Single chain HER2 antibody was purified using standard Ni-NTA resin protocol.

4.2.2. Synthesis of *N*-(azidoethyl-decaethylene glycol)-acrylamide

O-(2-Aminoethyl)-*O'*-(2-azidoethyl)nonaethylene glycol was purchased from Sigma and used as received. A mixture of *O*-(2-Aminoethyl)-*O'*-(2-azidoethyl)nonaethylene glycol (1.06 g, 2.01 mmol) and 5 mL dry DCM was added into a flame-dried round bottom flask. Next, 197 μ L acryloyl chloride (2.44 mmol) and 2.5 mL dry DCM were mixed and slowly added by drops into the round bottom flask at 0 $^{\circ}$ C with stirring, after which 337 μ L triethylamine (2.42 mmol) was added. The reaction was carried out at room temperature under nitrogen protection for 4 hours. After solvent removal with rotary evaporation, THF was used to precipitate the side product, which was then removed from the mixture by filtration. THF was subsequently removed by rotary evaporation again and the crude product was further injected and purified by HPLC, which was equipped with a Phenomenex Luna 10 μ 150 x 21.2 mm C18 reverse-phase column at a flow rate 5 mL/min and using a linear gradient of 30-80% solvent B over 30 min (Solvent A: water, solvent B: acetonitrile). LC-MS was conducted to verify the product formation and purity with a Shimadzu 2010 EV Liquid Chromatography Mass Spectrometer using both positive and negative electrospray ionization monitoring the *m/z* range 100-1400. Samples were separated on a Phenomenex Luna 5 μ 100 x 2 mm C18 reverse-phase column using a flow rate of 0.1 mL/min on a linear

gradient of 5-95% solvent B in 30 min followed by isocratic 95% solvent B for another 15 min (solvent A: water with 0.1% (v/v) formic acid, solvent B: acetonitrile with 0.1% (v/v) formic acid).

4.2.3. Protein nanocapsule preparation

Before the encapsulation reaction, the concentration of protein was diluted to 1 mg/mL with cold 5 mM sodium bicarbonate buffer (pH 9). Then 200 mg/mL monomer **1** was added to 1 mL of the diluted protein solution while stirring at 4 °C. After 10 min, monomer **2** was added while stirring. Different cross-linkers, *N,N'*-methylene bisacrylamide for ND NC and *N,N'*-bis(acryloyl)cystamine for S-S NC, were added 5 min after. The polymerization reaction was immediately initiated by adding 30 µL of 100 mg/mL ammonium persulfate and 3 µL of *N,N,N',N'*-tetramethylethylenediamine. The reaction was allowed to proceed for 60 min. The molar percentage of monomer **1**, monomer **2**, and cross-linker used were 93.5%, 1.5% and 5%, respectively. Unreacted monomers and initiators are removed by centrifugation, followed by buffer exchange with phosphate-buffered saline (PBS) buffer pH 7.4.

To Conjugate DBCO-TAMRA (Invitrogen) onto nanocapsule with azide functional groups, DBCO-TAMRA was added in excess into protein nanocapsule solution at a molar ratio of 15:1. The reaction was carried out for overnight at with stirring at 4 °C. Excess DBCO-TAMRA was removed by consecutive dialysis in PBS buffer. To conjugate targeting ligand onto the azide-containing nanocapsule, the ligand was first coupled onto the DBCO-containing linker first. To couple LHRH peptide (American Peptide Company) to DBCO-PEG4-NHS ester linker (Click Chemistry Tools), LHRH peptide was first dissolved in 20mM HEPES buffer pH9.0. The linker was dissolved in DMSO, and was added into the peptide

solution to achieve a final peptide to linker molar ratio of 3:1. The reaction was allowed to proceed for 3 hrs at room temperature and the coupled product was then purified on HPLC and verified by LCMS, followed by lyophilization to dry powder. The coupled peptide-linker was conjugated onto the nanocapsule in PBS buffer with stirring overnight at 4 °C, with a peptide-linker to protein molar ratio of 15:1. Excess peptide-linker was removed by consecutive dialysis using PBS buffer. HER2 single chain antibody was coupled onto DBCO-PEG4-Maleimide linker (Click Chemistry Tools), at a linker to antibody molar ratio of 5:1 in PBS pH7.0 buffer with stirring for overnight at 4 °C. The product was recovered using Zeba Spin desalting column 7K MWCO. The coupled product was conjugated onto the nanocapsule in PBS buffer with stirring overnight at 4 °C, with a peptide to protein molar ratio of 10:1. The conjugated nanocapsule was recovered using Zeba Spin desalting column 40K MWCO. Rhodamine-labeled NCs was obtained through encapsulation of protein modified with 5-carboxy-X-rhodamine *N*-succinimidyl ester, with a mass ratio of protein to rhodamine 100:1.

4.2.4 Characterization of protein nanocapsules

Transmission electron microscopy (TEM) images were obtained using Philips EM-120 TEM instrument. Samples of NCs (0.05 mg/mL) for TEM imaging were negatively stained with 2 % uranyl acetate in alcoholic solution (50 % ethanol). The lamella of stained sample was prepared on carbon-coated electron microscopy grids (Ted Pella, Inc.). The size distribution and ζ -potential of NCs were measured on the Malvern particle sizer Nano-ZS. The mean hydrodynamic size and ζ -potential of NC were determined by dynamic light scattering (DLS) in PBS buffer. Fluorescence spectra were recorded on Spectrofluorometer-SPEX. ELISA assay was performed to detect protein release from nanocapsules. The

nanocapsules samples were incubated with 2 mM DTT at 37 °C for each time point. The ELISA assay was performed using *TransAM*[™] p53 kit (Active Motif) following the kit instruction.

4.2.5 Internalization and trafficking of nanocapsules

All cell cultures used in the study were purchased from ATCC. MDA-MB-231, HeLa, SK-OV-3 and human foreskin fibroblast (HFF) cells were cultured in Dulbecco's Modified Eagle's Media (DMEM) (Invitrogen) supplemented with 10% bovine growth serum (Hyclone, Logan, UT), 1.5 g/L sodium bicarbonate, 100 µg/mL streptomycin and 100 U/mL penicillin, at 37 °C with 98% humidity and 5% CO₂. To visualize NCs uptake, MDA-MB-231 cells were seeded into 48-well plate, with a density of 10,000 cells/well in 250 µL of media with supplements. Different GFP nanocapsules were added to a final concentration of 400 nM. After 12 hours of incubation, cells were washed with PBS twice, stained with DAPI Nucleic Acid Stain and imaged. To compare the extent of internalization using FACS, MDA-MB-231 cells were seeded into 12-well plates at a density of 50,000 cells/well. The plates were incubated at 37 °C for overnight. The medium was then replaced with 0.5 mL of fresh medium containing 400 nM of different protein samples. After incubated at 37 °C for 12 hours, each well was washed with PBS and the cells were trypsinized and collected in PBS. After fixation using 2% paraformaldehyde, samples were analyzed via FACS with a 488 nm argon laser. The signal from the FL1 bandpass emission (530/30) was used for GFP. To study the trafficking of nanocapsules, markers for early and late endosomes were used on MDA-MB-231 cells. A concentration of 800 nM LHRH GFP NCs was incubated with cells for 30 min, 60 min and 120 min under 37 °C. Cells were then fixed with 4 % formaldehyde, permeabilized with 0.1 % Triton X-100, and stained with antibodies, mouse anti-EEA1

antibody against early endosomes and rabbit anti-CI-MPR antibody against late endosomes (Cell Signaling Technology, Inc.). Texas red goat anti-mouse IgG and Alexa Fluor® 647 goat anti-rabbit IgG (Invitrogen) were added as the secondary antibody.

4.2.6. Localization of protein delivered by nanocapules

To determine the cellular localization of the protein delivered, confocal images were taken with MDA-MB-231 cells incubated with 200nM of LHRH ND Rho-p53 or LHRH S-S Rho-p53 at 37 °C for 6 hours. Nuclei were then counterstained with DAPI. The Z-stack images of cells were imaged at 0.4- μ m intervals and analyzed by Nikon NIS Element software. Fluorescent microscopy images were acquired on a Yokogawa spinning-disk confocal scanner system (Solamere Technology Group, Salt Lake City, UT) using a Nikon eclipse Ti-E microscope equipped with a 60 \times /1.49 Apo TIRF oil objective and a Cascade II: 512 EMCCD camera (Photometrics, Tucson, AZ, USA). An AOTF (acousto-optical tunable filter) controlled laser-merge system (Solamere Technology Group Inc.) was used to provide illumination power at each of the following laser lines: 491 nm, 561nm, and 640 nm solid state lasers (50mW for each laser). ELISA assay was performed using *TransAM*TM p53 kit (Active Motif) following the kit instruction. Cytoplasmic and nuclear fraction of MDA-MB-231 cells were obtained using Nuclear Extract kit (Active Motif) following the kit instruction.

4.2.7. Cytotoxicity Assays and Apoptosis detection

CellTiter 96® AQueous One Solution Cell Proliferation Assay (MTS) reagent was purchased from Promega Corporation. Different cells lines, MDA-MB-231, HFF and SK-OV-3 were seeded into 96-well plates, each well containing 5,000 cells in 100 μ L of DMEM with supplements. Different concentrations of samples were added and the samples were incubated for 48 hours at 37 °C. The plates were washed with PBS solution twice and 100 μ L

of fresh media with 20 μ L MTS was added. The plates were incubated for 3 hours at 37 $^{\circ}$ C. The absorbance of each well was measured at 490 nm using a microplate reader (PowerWave X, Bio-tek Instruments, USA). APO-BrdUTM TUNEL Assay Kit (Invitrogen) was used to detect apoptosis. MDA-MB-231 cells were seeded at a density of 100,000 cells/well into a 6-well plate in 2 mL of cell culture media with supplements. After incubating overnight at 37 $^{\circ}$ C, PBS and LHRH S-S S121F were added to a final concentration of 800nM. After 24 hours of incubation, cells were fixed with 1% paraformaldehyde in PBS, followed by the addition of DNA labeling solution containing terminal deoxynucleotidyl transferase and bromodeoxyuridine (BrdUrd). Cells were then stained with Alexa Fluor[®] 488 dye-labeled anti-BrdUrd antibody. Samples were deposited onto slides, which were later stained with propidium iodide (PI) solution containing RNase A. Images were obtained by fluorescent microscope (Zeiss, Observer Z1) using appropriate filters for Alexa Fluor 488 and PI.

4.3 Results and Discussion

4.3.1 Synthesis of nanocapsules with clickable monomer

Our synthesis strategy for protein nanocapsules is shown in Figure 25. Monomers and redox-sensitive crosslinkers are polymerized in situ around the target protein to form a noncovalent shell that encapsulates the protein. The monomer acrylamide (**1**) is used as a general building block of the water-soluble shell. The nanocapsules are crosslinked with *N,N'*-bis(acryloyl)cystamine (**3**), which is designed to degrade under high reducing conditions such as the cytosol, thereby releasing the protein cargo intracellularly. To synthesize a neutral polymer shell that does not enter cells via electrostatic interactions with the membrane, we first eliminated the use of positively charged monomers employed in previous designs, such as *N*-(3-Aminopropyl) methacrylamide. Instead, we chose *N*-(azidoethyl-decaethylene glycol)-acrylamide (**2**) as the second monomer (Figure 25a). The neutral **2** contains a terminal azido group that can be used as the reactive site for cross-coupling via copper-free click reaction. The ten ethylene glycol unit serves as a water soluble spacer at the surface of the nanocapsules, and provides flexibility to the conjugated targeting ligand. Through copolymerization of **1** and **2**, the azido functionalities can be displayed on the surface of the nanocapsules for subsequent modification. Monomer **2** was readily prepared by reacting *O*-(2-Aminoethyl)-*O'*-(2-azidoethyl)nonaethylene glycol with acryloyl chloride. Following purification and MS characterization of monomer **2** (Figure 26), we performed the *in situ* polymerization process using green fluorescent protein (GFP) as the cargo. The mole fraction of **2** was kept at 1.5% of total monomers. Following one hour of polymerization, uniformly sized nanoparticles were synthesized, with an electrostatic potential of -0.93 mV, and an average size of 9.1 ± 0.8 nm.

To verify the presence of azido groups on the surface of the nanocapsules, we performed the copper-free reaction between dibenzylcyclooctyne TAMRA (DBCO TAMRA, **4**) and the GFP nanocapsules prepared from monomers **1** and **2**. As a control, nanocapsules synthesized from **1** alone were also mixed with **4**. After overnight stirring at 4 °C, the reaction was subjected to repeated dialysis and ultrafiltration (30K MWCO) to remove any unreacted **4**. The conjugation of TAMRA to the protein nanocapsules were detected by fluorescence emission scan (Figure 25b). Whereas nanocapsules synthesized with both **1** and **2** exhibited the characterized emission peak at 580 nm of TAMRA, the control sample with only **1** showed nearly no signal. We previously established that most of the nanocapsules prepared via this method contain a single copy GFP. Assuming that each nanocapsules synthesized here also contained one GFP molecule on average, the number of TAMRA conjugated per nanocapsules was approximated through the comparison of relative intensities of GFP and TAMRA fluorescent intensity. At a mole fraction of 1.5% monomer **2**, we established that approximately each nanocapsules were conjugated with four TAMRA molecules through the click reaction to accessible azido functional groups.

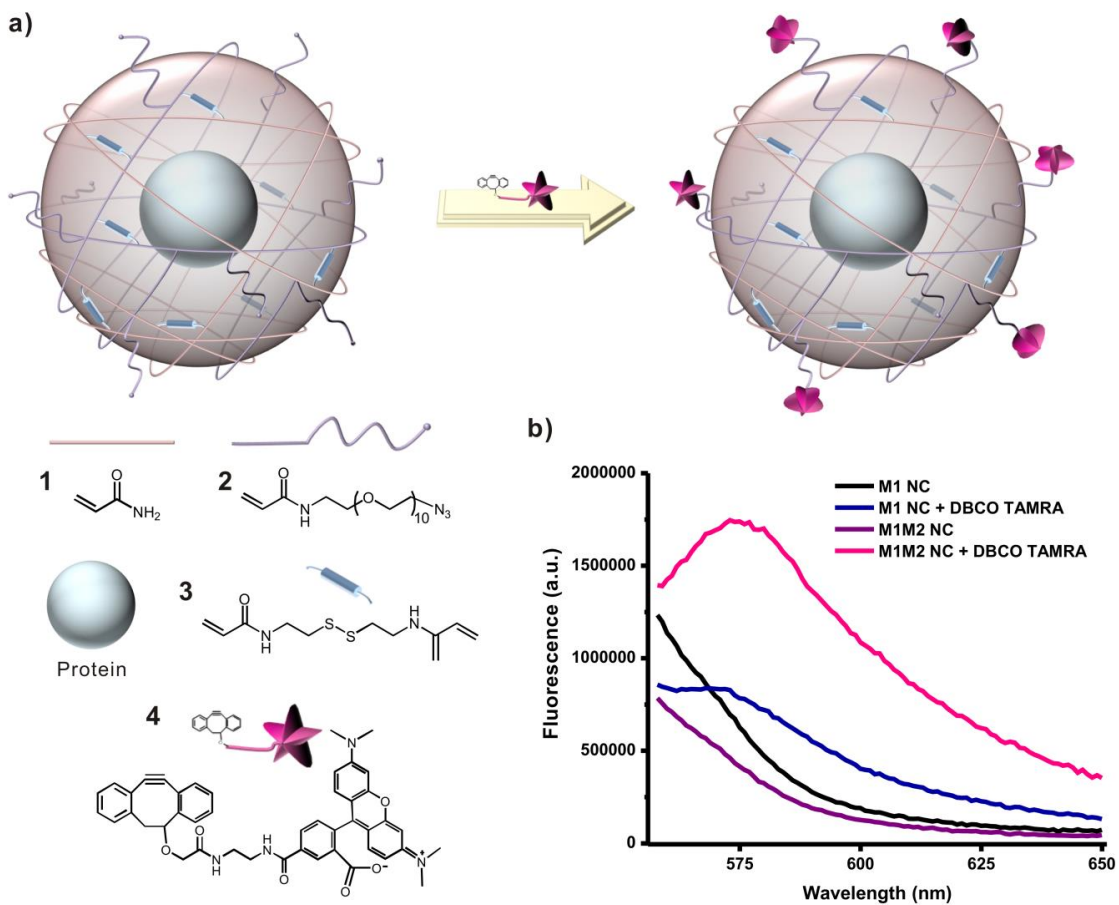


Figure 25. Clickable nanocapsules. a) Schematic diagram of clickable, redox-responsive protein NC, and scheme of clickable NC conjugated to DBCO TAMRA. b) Fluorescence spectra of NC samples before and after copper-free click conjugation with DBCO TAMRA.

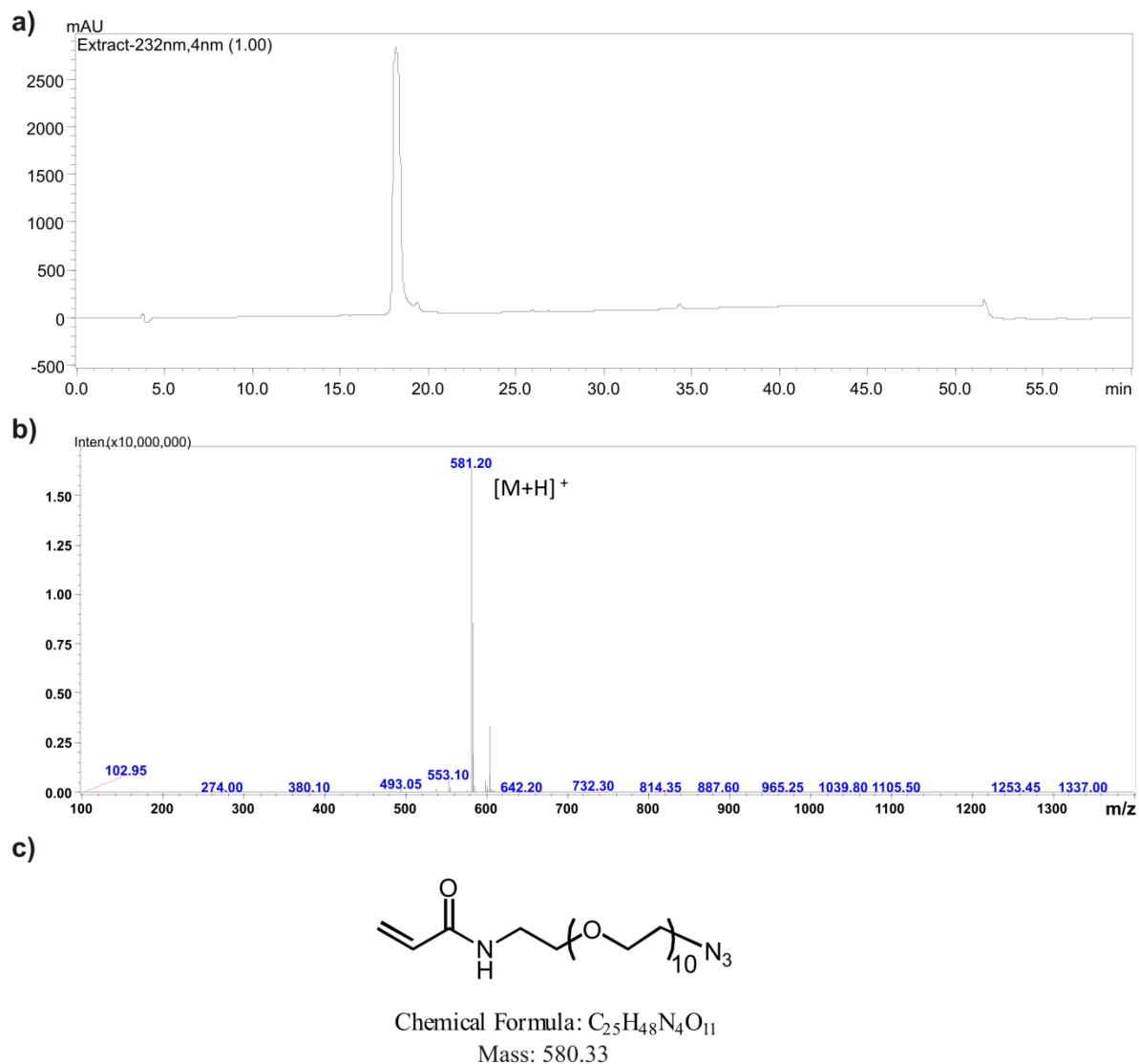


Figure 26. Purification and MS characterization of purified monomer **2**.

4.3.2. Conjugation of nanoparticles with ligands

After confirming the successful “clicking” of cyclooctyne moieties onto the surface of azido-functionalized nanocapsules, we then developed methods to conjugate cancer targeting ligands. We selected the luteinizing hormone releasing hormone (LHRH) peptide **5** (Glp-His-Trp-Ser-Tyr-D-Lys-Leu-Arg-Pro-NHEt, Figure 27a), which binds to LHRH receptors that are overexpressed in various hormonal related cancers, such as breast and prostate cancers¹⁷⁸.

LHRH receptors are not expressed detectably in most visceral organs and have been targeted in the delivery of small molecules^{179, 180}. The bifunctional dibenzocyclooctyne-PEG4-N-hydroxysuccinimidyl ester (DBCO-PEG4-NHS ester, **6**) was chosen as the tether (Figure 27a). The peptide **5** was first conjugated to the NHS terminus of **6** through the internal D-Lys designed to serve as a site for coupling. The adduct **8** was verified by LC-MS and purified by HPLC to homogeneity (Figure 28). Subsequently, **8** was added to the azido-functionalized GFP nanoparticles at a molar ratio of 15:1 and allowed to react overnight at 4 °C. Following the click reaction, unreacted **8** was removed through ultrafiltration and the nanoparticles were dialyzed with PBS. To test the LHRH receptor mediated endocytosis of nanocapsules, we added the LHRH functionalized nanocapsules to the MDA-MB-231 cell line, which is known to overexpress the receptor. As controls we also added GFP nanocapsules that are i) positively charged that are expected to be internalized; ii) azido-functionalized but not conjugated to LHRH; and iii) same as ii but with unconjugated LHRH peptide in solution. After overnight incubation, the internalization of nanocapsules was visualized by fluorescent microscope. As can be seen from Figure 27b, the positively charged particles well-internalized as expected. In contrast, the neutral, azido-functionalized particles were completely not internalized either with or without the free LHRH peptides. LHRH-functionalized GFP nanocapsules, however, were efficiently internalized as can be seen from the GFP fluorescence in the cytosol. To quantify the LHRH-receptor mediated endocytosis, FACS was performed on the samples shown in Figure 29a. The level of internalization through LHRH receptor mediated endocytosis is ~70% level of that observed with positively charged nanocapsules. More importantly, azido-functionalized nanoparticles without LHRH conjugation did not exhibit noticeable internalization compared to no treatment or native GFP controls. Particle trafficking experiments were performed for the LHRH-targeted GFP particles (Figure 29b,c).

Localization in the early endosomes was observed within 30 minutes, while release into the cytosol was detected at one and two hours after delivery. No significant localization of GFP in the late endosome was observed.

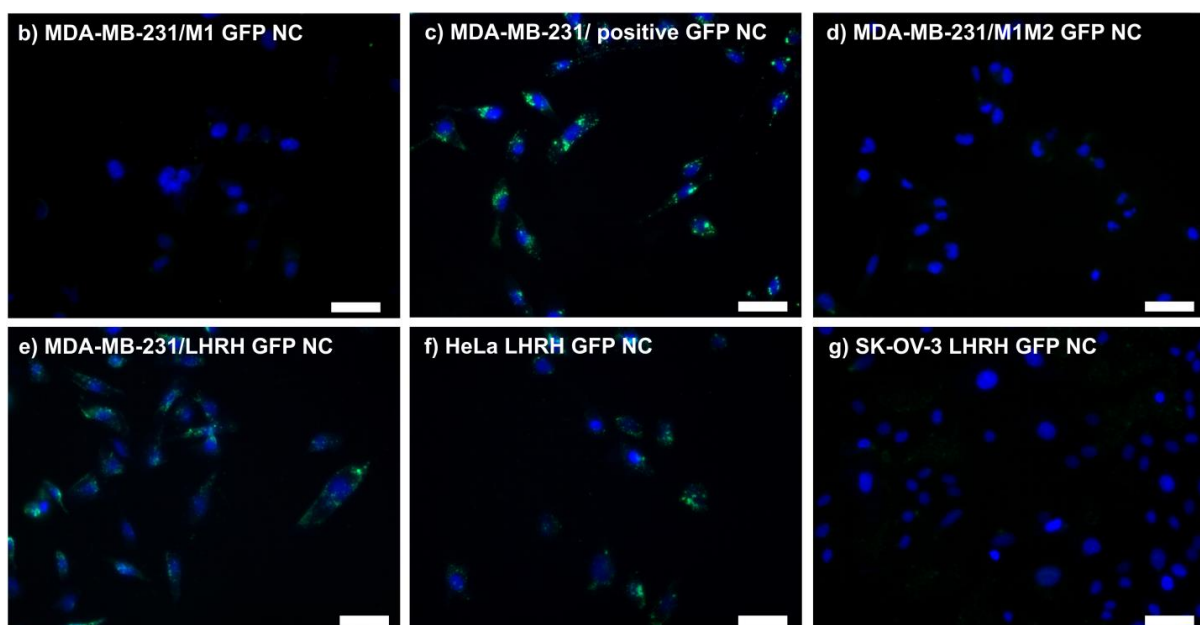
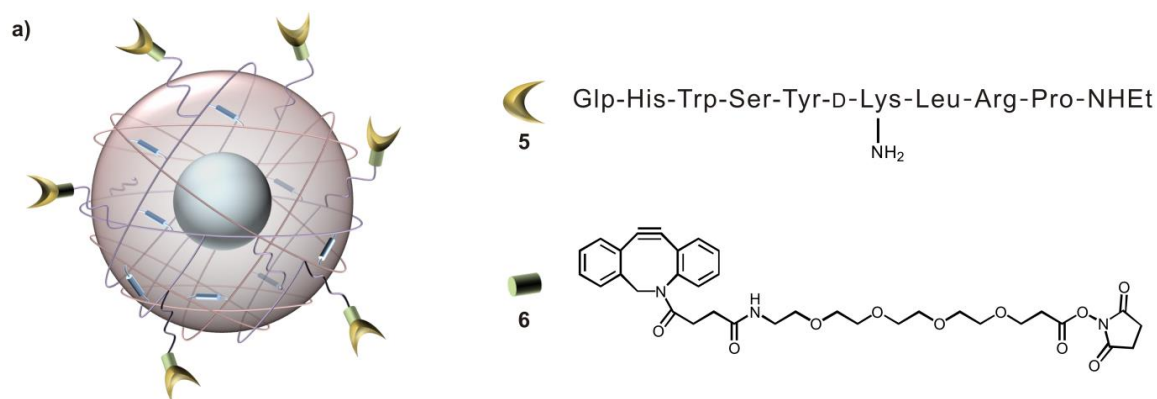


Figure 27. LHRH conjugated nanocapsule. a) Scheme of LHRH S-S NC. Glp is cyclized glutamine; Fluorescent microscopy images of 400nM GFP NC on different cell lines. b) MDA-MB-231 with monomer 1 GFP NC; c) MDA-MB-231 with positive GFP NC; d) MDA-MB-231 with monomer 1 and 2 GFP NC (no targeting ligand); e) MDA-MB-231 with LHRH GFP NC; f) HeLa with LHRH GFP NC; g) SK-OV-3 with LHRH GFP NC. Nuclei were stained with DAPI. The scale bars represent 50 μ m.

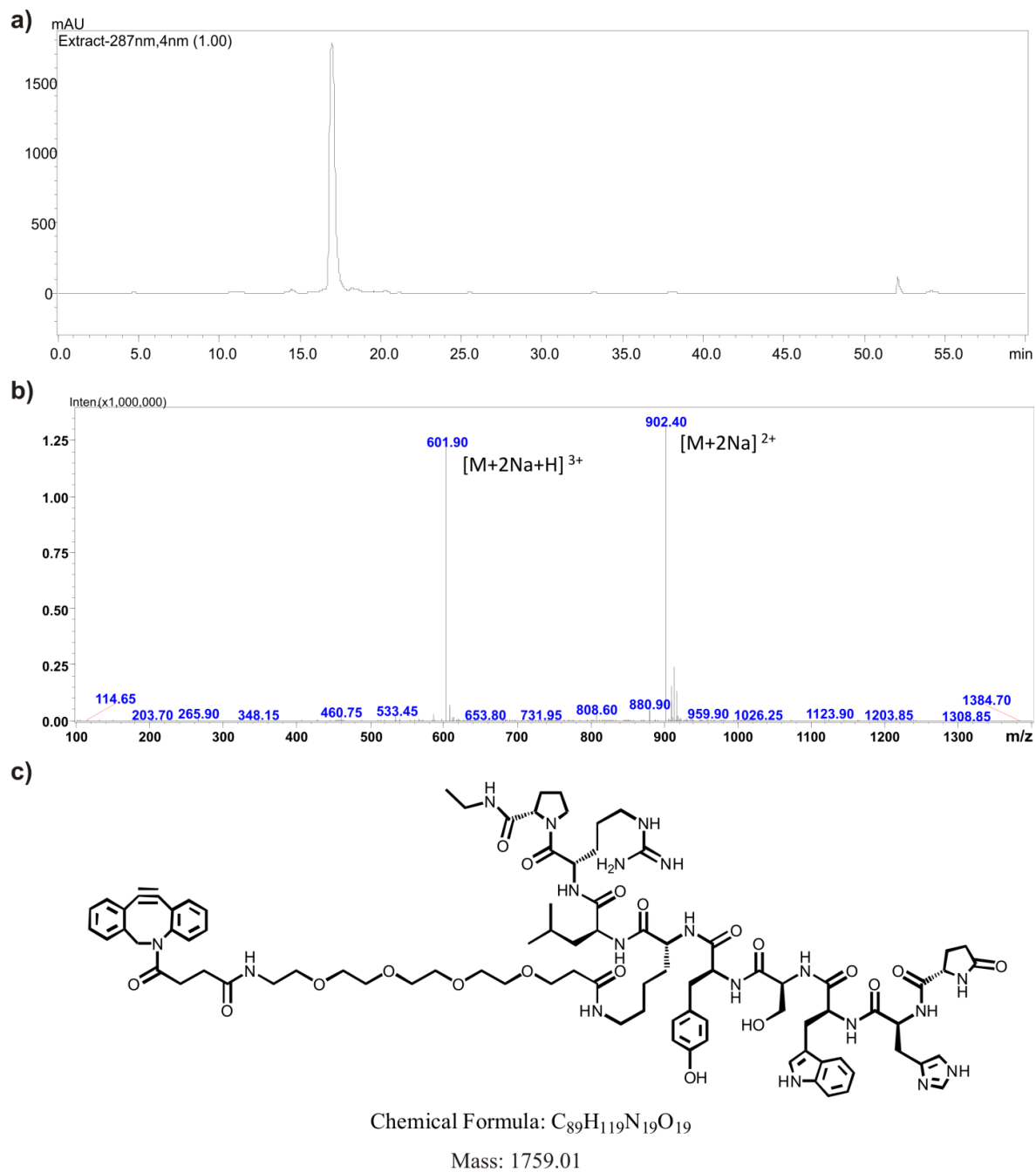


Figure 28. Purification and MS characterization of purified adduct 8.

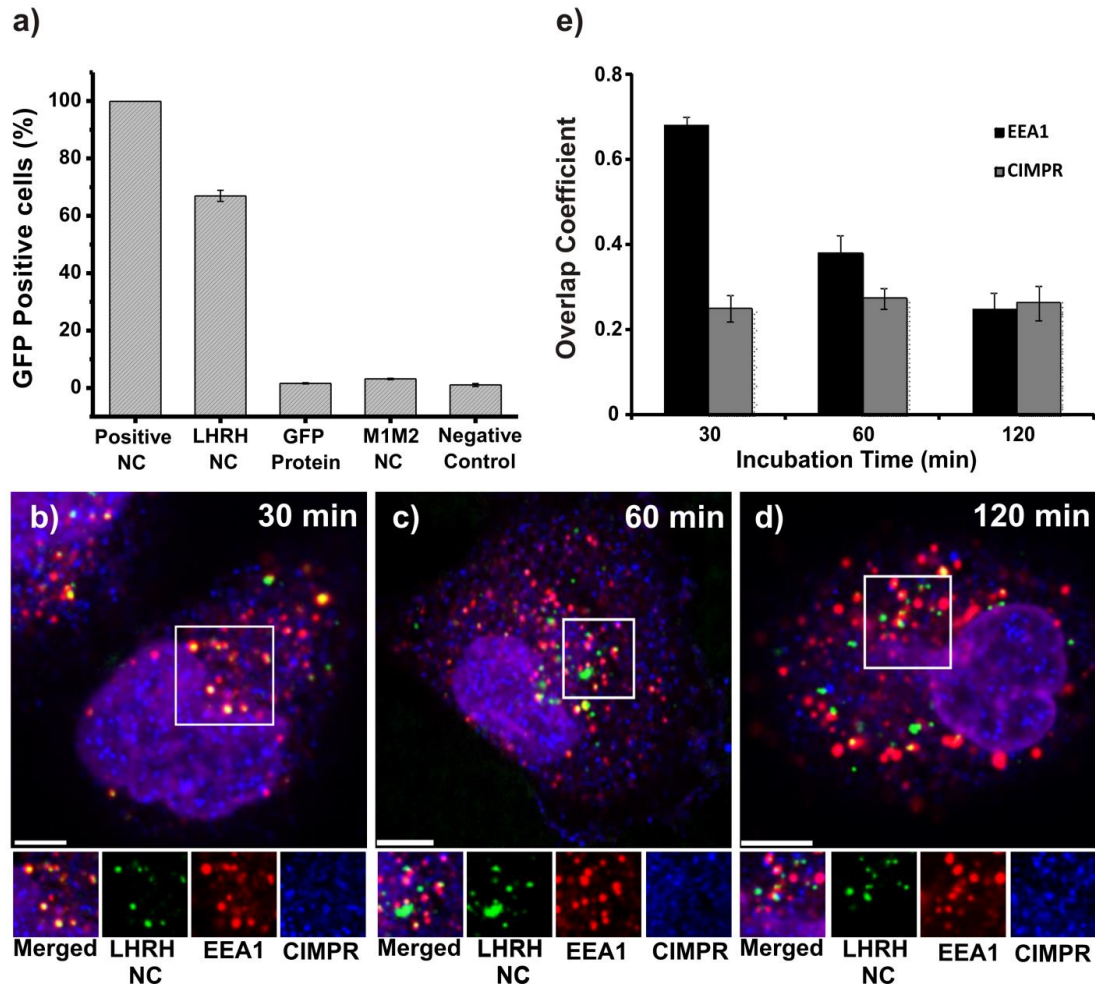


Figure 29. Cellular uptake and trafficking of LHRH nanocapsule by MDA-MB-231 cells. a) Different extent of the cellular internalization of 400 nM GFP protein or NC by MDA-MB-231 cells at 37 °C for 12 hours. The mean fluorescence intensity was measured by flow cytometry and was represented as the percentage of fluorescence from MDA-MB-231 cells incubated with positive NC. b) The trafficking of LHRH GFP NC through endosomes. MDA-MB-231 cells were incubated with 800 nM LHRH GFP NC at 37 °C for various time periods, 30, 60 and 120 min. Early endosomes were detected by early endosome antigen 1 (EEA1, green). Late endosomes were detected by cation-independent mannose-6-phosphate receptor (CI-MPR, blue). Nuclei were stained with DAPI and shown as purple. The scale bar represents 10 μm. e) Quantification of LHRH GFP NC colocalized with EEA1 or CI-MPR endosomes at various incubation times. Colocalization coefficients were calculated using Manders' overlap coefficient (>10 samples). The error bars indicate standard deviation.

To further test the cell selectivity of the protein delivery, we added the LHRH-functionalized to various cell lines with varying levels of LHRH receptor expression. When added to HeLa cells that have comparable levels of expression the amount of internalization were similar to that of MDA-MB-231. No internalization was seen in the SK-OV-3, which is a LHRH receptor-negative ovarian cancer cell line. Furthermore, we conjugated the single-chain variable fragment of the anti-Her2 antibody to the azido-functionalized GFP nanocapsules through a maleimide containing bifunctional linker **9** that conjugates to cysteine residue on the antibody. When administered to cell lines, internalization of GFP nanocapsules is only observed in SK-BR-3 that overexpresses the HER2 receptor, and no fluorescence can be seen in triple negative breast cancer cell line MDA-MB-231, cervical cancer cell line HeLa or primary human foreskin fibroblasts (HFF) (Figure 30). Collectively these data illustrate the polymerization, conjugation and internalization steps are all effective as designed.

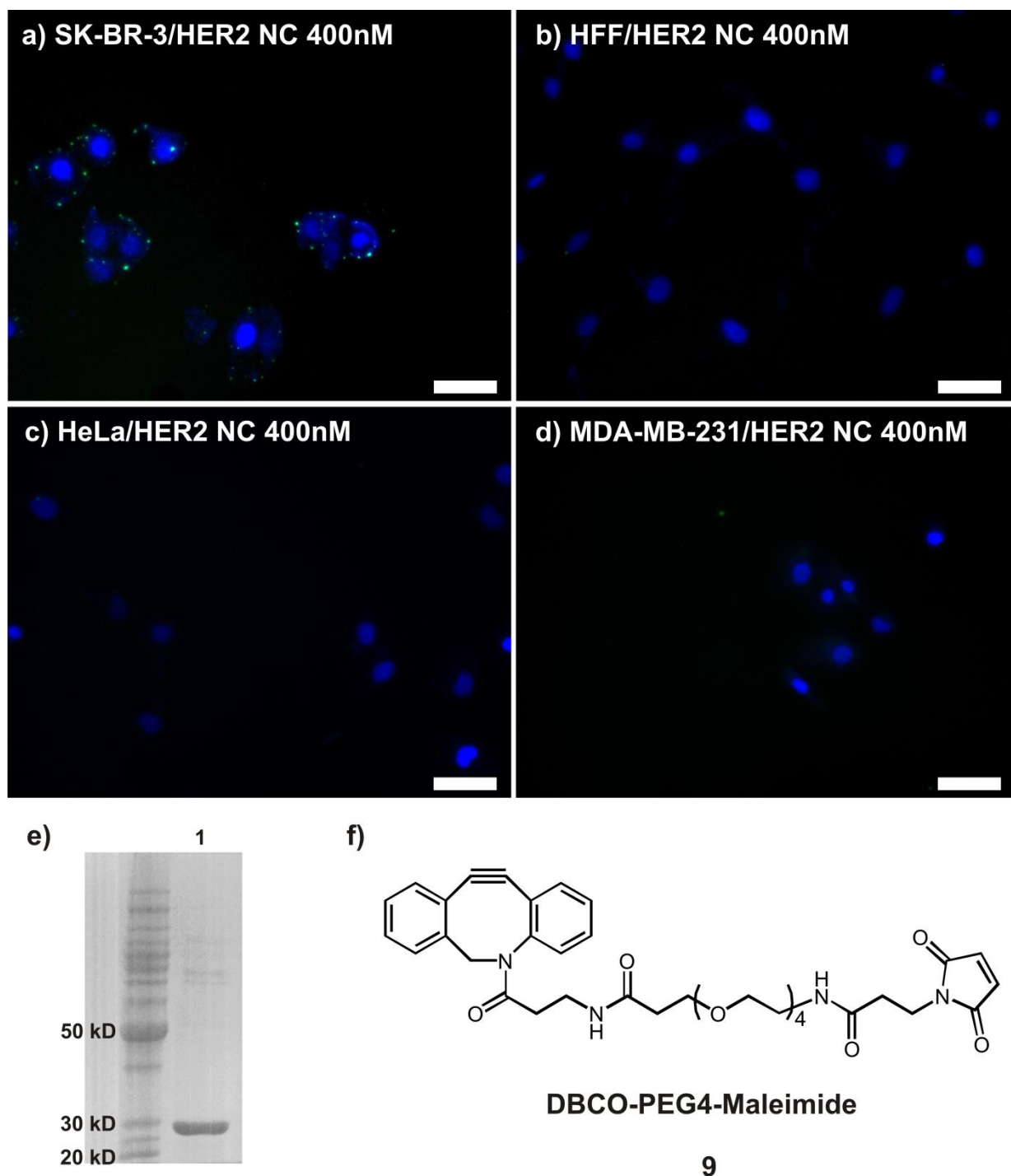


Figure 30. Internalization of HER2 NC. Fluorescent microscopy images of a) SK-BR-3 cells; b) HFF cells; c) HeLa cells; d) MDA-MB-231 cells incubated overnight with 400 nM HER2 NC containing GFP protein. Nuclei were stained with DAPI. The scale bars represent 50 μm . e) SDS-page of purified single-chain variable fragment of anti-HER2 antibody (lane 1). f) Structure of DBCO-PEG4-Maleimide.

4.3.3. Synthesis of clickable p53 nanocapsules

We then applied the nanocapsule synthetic steps towards the targeted delivery of p53 to cancer cells. Delivery of recombinant p53 poses significant challenges as the tetrameric complex can readily aggregate and lose activity in non-ideal condition. The three-dimensional structure of p53 is also not well resolved, and has been shown to be loosely organized, especially in the absence of DNA. Recombinant p53 was expressed from *E. coli*, purified from inclusion bodies and refolded as soluble protein (Figure 31a). The in situ polymerization using monomers **1** and **2**, as well as crosslinker **3** was optimized to minimize aggregation and precipitation of the soluble P53. A final molar fraction of 1.5% of **2** was used in the monomers, while 5% **3** was added as crosslinkers. We found that p53 concentration must be kept at below 0.7 mg/mL and all steps must be performed in sodium bicarbonate containing buffer. After encapsulation, the nanocapsules (S-S p53 NC) were buffer-exchanged and concentrated in PBS buffer. Successful encapsulation was monitored by both DLS and TEM as shown in Figure 31b and Figure 31c, respectively. The native p53 tetramer exhibited hydrodynamic diameter of ~8 nm, consistent with other structural characterizations^{181, 182}. Upon encapsulation the average diameter increased to $\sim 27.5 \pm 0.5$ nm (-0.55 ± 0.3 mV), which is also observed under TEM to be uniformly sized. The electrostatic potential was determined to be nearly neutral by DLS, which is expected with the use of monomers **1** and **2**. As non-degradable controls, p53-containing nanocapsules crosslinked with the *N,N'*-methylene bisacrylamide was also prepared. The physical properties of the non-degradable p53 nanocapsules (ND p53 NC) were identical to that of the S-S p53 NCs.

To examine the encapsulation effectiveness and redox-responsible release of the p53 nanocapsules, we performed time-dependent ELISA analysis of the p53 NCs both the presence and absence of the reducing agent DTT (Figure 31d). Encapsulated p53 is

physically shielded by the polymer layer and is thus unable to be recognized by the anti-p53 antibody. As expected in the absence of DTT, no native p53 in the solution can be detected within the one hour assay period, indicating the robustness of the polymer layer in both shielding and retaining the p53 cargo. In contrast, the S-S p53 NCs released p53 when 2 mM DTT was added to the nanocapsules, indicating effective degradation of the crosslinker and diffusion of p53 into the solution. The ND p53 NCs control did not release detectable p53 in the presence of 2 mM DTT, further confirming the redox-responsiveness of the S-S p53 NCs.

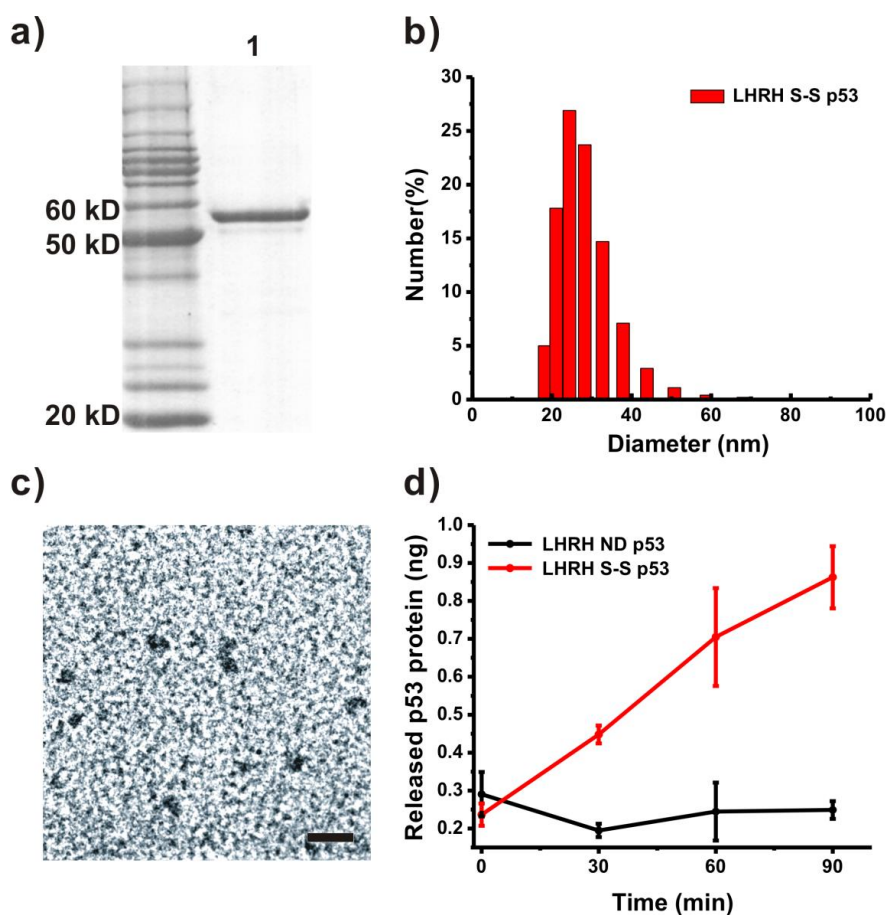


Figure 31. Protein p53 and LHRH p53 NC characterization. a) SDS page of refolded p53 protein (lane 1). b) The hydrodynamic size distribution of the LHRH S-S p53. c) TEM image of LHRH S-S p53. The scale bar represents 50 nm. d) ELISA assay measuring p53 released from LHRH S-S p53 and LHRH ND p53 after treatment with 2 mM DTT over 90 min at 37 °C.

4.3.4. Internalization and Release of p53 in cancer cells

To target the internalization of S-S p53 NCs to cancer cells, we first conjugated the recombinant p53 to rhodamine dye to form Rho-p53. Following encapsulation with **1**, **2** and **3** to form rhodamine-labeled NCs, the LHRH peptide **6** was conjugated to the surface using the bifunctional linker **7**. When added to MDA-MB-231 cell lines, rhodamine fluorescence can be seen inside the cells with short incubation period. When analyzed with confocal microscopy, we observed accumulation of Rho-p53 in the nucleus of the targeted cells, which is the expected localization for the transcription factor (Figure 32b). In contrast, no nucleus overlap between DAPI and rhodamine fluorescence can be observed when the Rho-p53 was encapsulated in nondegradable linker and delivered. This is consistent with the inability of Rho-p53 to escape the polymer shell in the absence of the redox-responsive crosslinker **3**. In this case, all the rhodamine signals remained in the cytoplasm (Figure 32a).

To further quantify the nuclear localization of delivered p53, we performed time course ELISA analysis of p53 concentration in nuclear and cytoplasmic fractions of MDA-MB-231 cells treated with 100 ng/ μ L of S-S p53 NC or ND p53 NC functionalized with LHRH peptide (Figure 32c). The standard curve relating ELISA signal and p53 levels was established using purified recombinant p53. Untreated cells displayed a low level of p53 (mutant in MDA-MB-231) that is less than 0.5 ng per 2.5 μ g of nuclear extract. As shown in Figure 32c, S-S p53 NC treated samples showed a clear accumulation of p53 in the nuclei at time points tested. Close to 7 ng of p53 per 2.5 μ g of nuclear extract was observed after four hours. As expected from Rho-p53 localization studies above, significantly higher amounts of p53 can be detected in S-S samples comparing to ND samples. While the ND p53 NC-treated sample showed ~2 ng of nuclei p53 after one hour treatment, no increase was observed after prolonged incubation time. The effect of S-S p53 NC dosage on intracellular

p53 concentration was also measured using ELISA. Increasing amount of delivered p53 (from 15 to 120 ng/L) led to increases in both cytosolic and nuclear concentration of p53 after one hour (Figure 32d). Therefore, we have shown that LHRH-functionalized, redox-responsive nanocapsules can effectively deliver recombinant p53 into cancer cells. The delivered and released p53 can dramatically increase the concentration of p53 in both cytosol and nuclear. The accumulation in nuclei of cancer cells is especially important, as this is the desired site of action for p53 for cancer cell fate reversal.

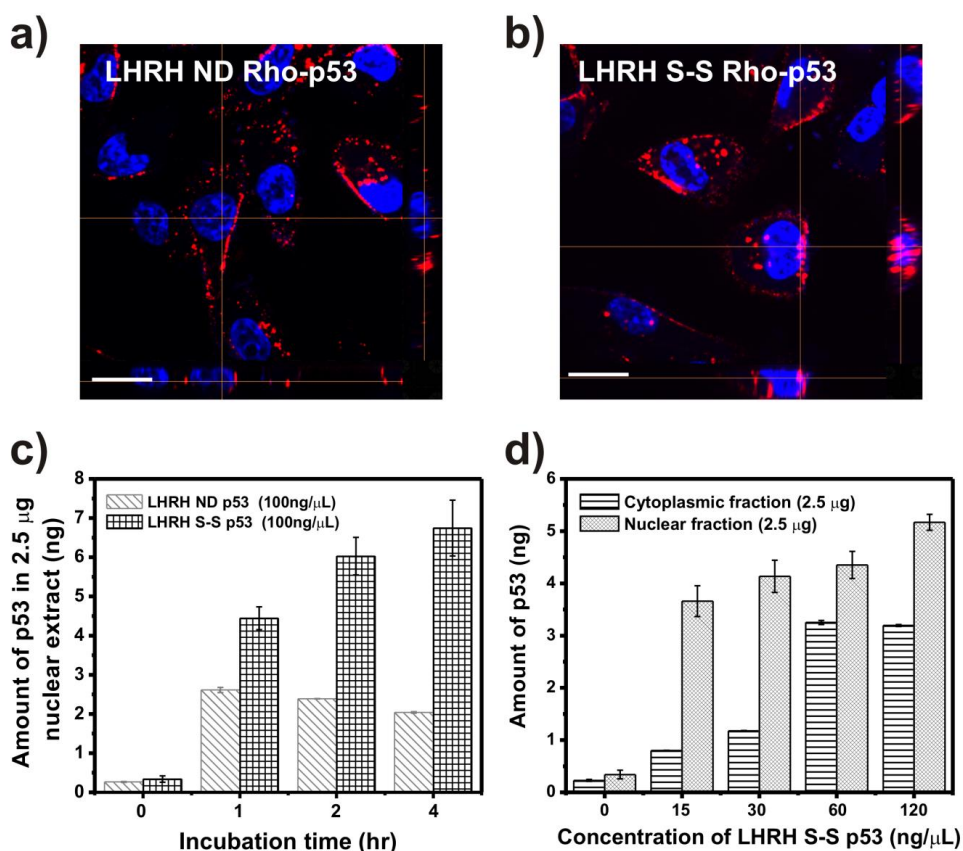


Figure 32. Internalization and location of p53 delivered. Confocal images of MDA-MB-231 cells incubated with 200nM a) LHRH ND Rho-p53 ; b) LHRH S-S Rho-p53; The scale bar represents 20 nm c) ELISA detection of p53 in the nuclear fraction from MDA-MB-231 cells treated with 100 ng/μL LHRH ND p53 or LHRH S-S p53 for various period of time; d) ELISA detection of p53 in the cytoplasmic and nuclear fraction from MDA-MB-231 cells treated with various concentration of LHRH S-S p53 for one hour.

4.3.5. Cytotoxicity of p53 Nanocapsules

To examine the effect of delivered p53 on cell viability, we performed cytotoxicity studies using the LHRH-functionalized nanocapsules. Two different p53 versions were used in this study, the wild type and the “super” p53. The super p53 is the gain of function point mutant S121F that has been shown to display more potent apoptotic activity. The mutation alters the specificity of p53 binding targets, and in particular, attenuates the activation of MDM2 transcription associated with normal p53 overexpression. The decreased MDM2 feedback control therefore increases apoptosis induction. The 121F mutant kills tumor cells irrespective of p53 status but not wild-type mouse embryo fibroblasts¹⁸³. S-S S121F NCs were prepared in the same manner as S-S p53 NC and conjugated to LHRH peptides using click chemistry. Physical characterizations were performed to verify that the NCs were nearly identical in property. Both p53 NCs were then added to different cancer cell lines and the cytotoxicity was measured using MTS assay after 48 hours. As shown in Figure 33, both LHRH targeted NCs showed high selectivity towards the MDA-MB-231 that overexpresses the LHRH receptor. Nearly no toxicity was observed towards either SK-OV-3 or HFF at 800 nM, the highest concentration assayed. The S121F containing NCs showed potent cytotoxicity, with IC₅₀ at ~ 100 nM. In contrast, IC₅₀ for the wild type p53 NCs exceeded ~300 nM. We confirmed observed cell death after delivery of S121F is indeed via apoptosis by using TUNEL assay (Figure 34). Several negative controls were performed to ensure the observed toxicity is due to the combination of targeted delivery of p53, including i) S121F NCs not conjugated to LHRH; ii) S-S eGFP NCs conjugated to LHRH; and iii) S-S eGFP NCs not conjugated to LHRH. In all these controls, the cells remain unaffected by the addition of nanocapsules (Figure 35). These results therefore unequivocally confirm the targeted and functional delivery of p53 can be achieved using the encapsulation and

conjugation strategies.

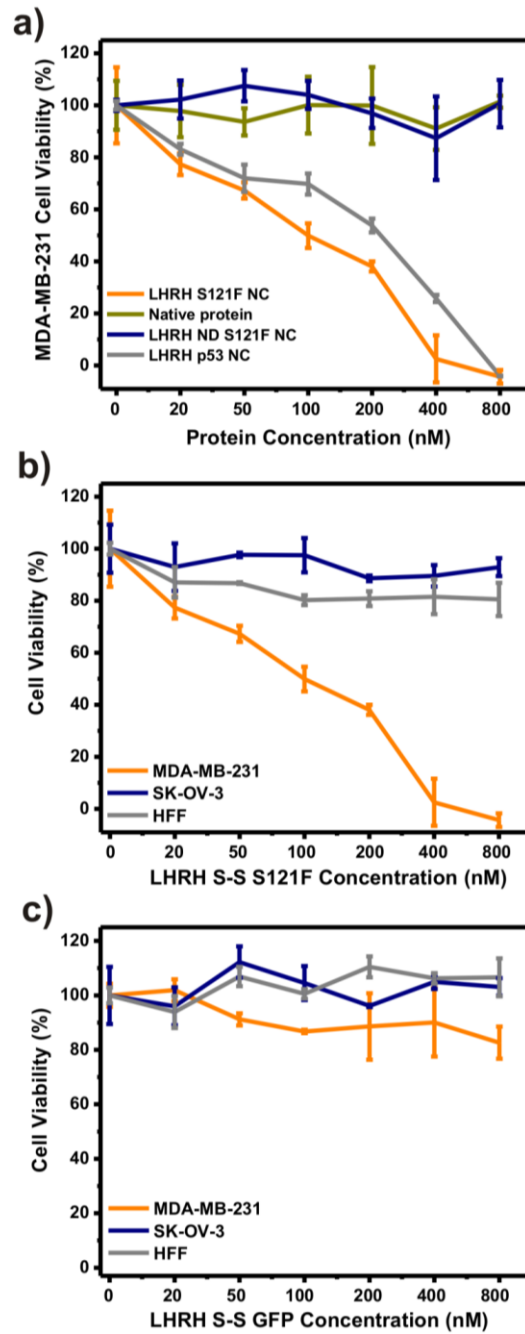


Figure 33. Cytotoxicity associated with protein and LHRH NC treatment. (a) MDA-MB-231 cell viability treated with LHRH S121F NC, native protein, LHRH ND S121F NC, and LHRH p53 NC; (b) MDA-MB-231, SK-OV-3 and HFF cell viability treated with LHRH S121F NC; (c) MDA-MB-231, SK-OV-3 and HFF cell viability treated with LHRH GFP NC.

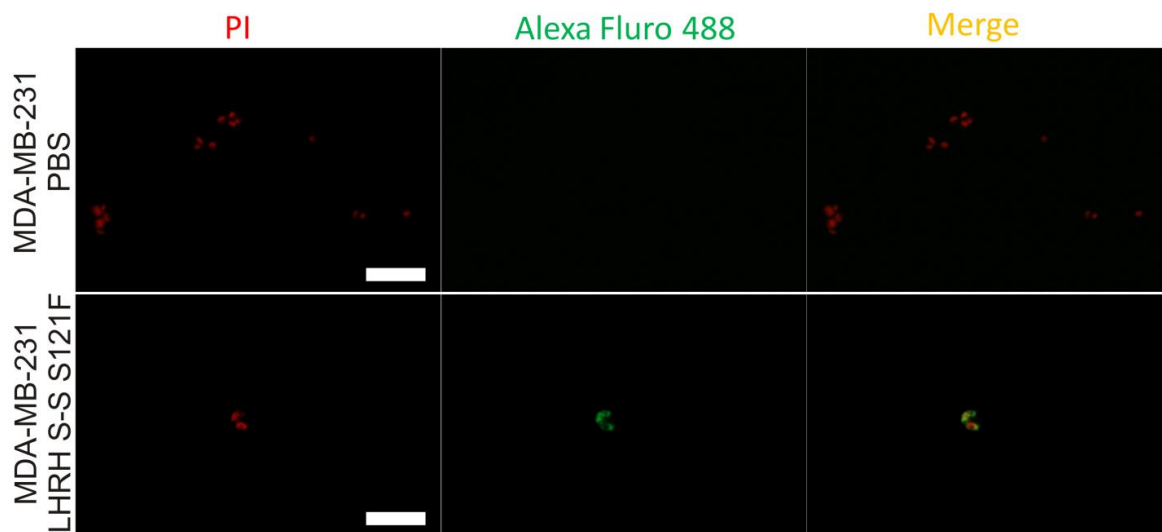


Figure 34. TUNEL assay of MDA-MB-231 cells. MDA-MB-231 cells were treated for 24 hours with PBS as control and 800 nM LHRH S-S S121F. Apoptotic fragmentation of the nucleosome detected by APO-BrdUTM TUNEL. Red fluorescence represents the PI-stained total DNA, and green Alexa Fluor 488 fluorescence represents apoptotic DNA fragmentation. The merged pictures combine the PI-stained nuclei and the Alexa Fluor 488-stained nick end label. The scale bars represent 50 μ m.

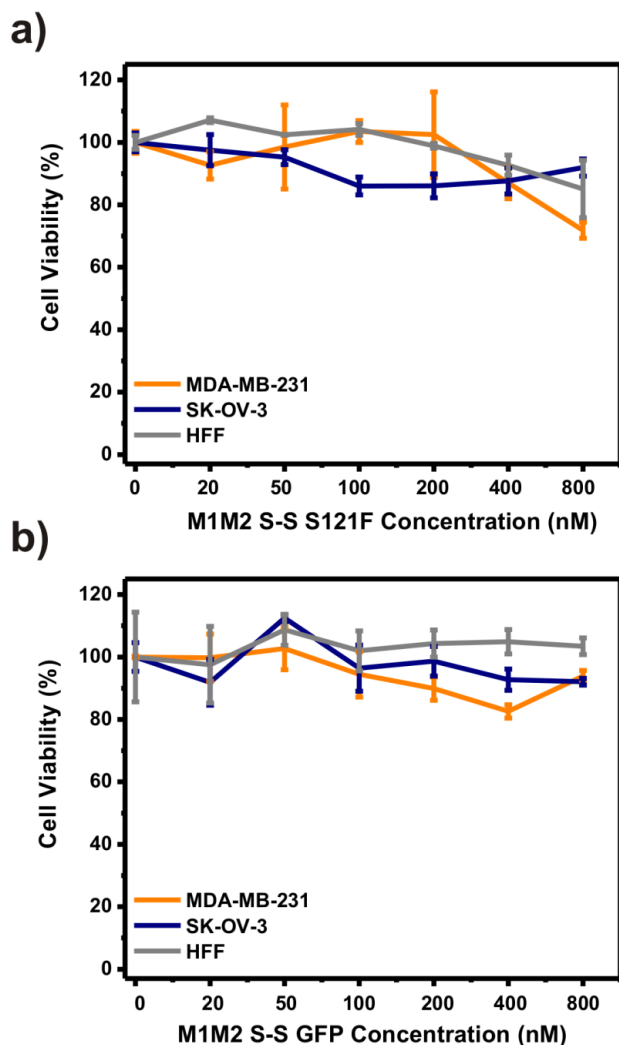


Figure 35. Cytotoxicity of non-targeted nanocapsules. Cell viability curves for a) MDA-MB-231, SK-OV-3 and HFF cells treated with various concentrations of M1M2 S-S S121F; b) MDA-MB-231, SK-OV-3 and HFF cells treated with various concentrations of M1M2 S-S GFP.

4.4 Conclusions

We developed a new polymerization strategy for the synthesis of protein nanocapsules that display azido functional groups on the surfaces. By using a cyclooctyne and NHS containing bifunctional linkers, different targeting ligands such as the LHRH peptide and HER2 ScFv

can be attached to the surface of the protein nanocapsules. Using eGFP as cargo, we demonstrated the specific internalization of the nanocapsules through receptor mediated endocytosis. Finally, we demonstrate this approach can achieve the functional delivery of the genome guardian P53 to trigger apoptosis in targeted cancer cell lines.

Chapter 5 Summary

Direct delivery of proteins to the cytosol of cells holds tremendous potential in therapeutic and diagnostic applications. The development of stimuli-responsive, nano-scale therapeutics that selectively target and attack tumors is a major research focus in cancer nanotechnology. Specific induction of cell death in tumors is considered one of the most desired and effective anticancer therapies. Effective strategies to activate the apoptotic pathway, or other death mechanisms, are currently being intensely pursued. A potent chemotherapy option is directly arming the cancer cells with executioner proteins or apoptotic-inducing proteins that are not targeted by anti-apoptotic maneuvers found in many tumors. In this dissertation, we described a new method to treat cancer by using a native-protein delivery approach, which is a platform to deliver proteins in native forms into cells. The key design feature of our strategy is to first encapsulate protein molecules in a thin layer of water soluble, degradable polymer to form nanometer-sized nanocapsules. The nanocapsule shell facilitates uptake of the protein content into cells, through either positive charge or targeting ligand, and protects the protein both during *in vivo* circulation and endocytosis. To endow the nanocapsules biodegradability once entered the target cells, the polymer shell is crosslinked with redox-sensitive crosslinkers that can be reduced upon encountering the reducing environment of the cytoplasm. Using the nanocapsule as a vehicle, we showed that proteins such as active caspase 3, tumor selective killer apoptin, and tumor suppressor p53 can be delivered and can induce apoptosis in a variety of human cancer cell lines and inhibited tumor growth *in vivo*.

References

- [1] G. Walsh, *Nat Biotechnol* **2010**, 28, 917-924.
- [2] B. Leader, Q. J. Baca, D. E. Golan, *Nature reviews* **2008**, 7, 21-39.
- [3] D. Peer, J. M. Karp, S. Hong, O. C. Farokhzad, R. Margalit, R. Langer, *Nat Nanotechnol* **2007**, 2, 751-760.
- [4] D. W. Pack, A. S. Hoffman, S. Pun, P. S. Stayton, *Nature reviews* **2005**, 4, 581-593.
- [5] R. A. Petros, J. M. DeSimone, *Nature reviews* **2010**, 9, 615-627.
- [6] K. A. Whitehead, R. Langer, D. G. Anderson, *Nature reviews* **2010**, 8, 129-138.
- [7] L. M. Bareford, P. W. Swaan, *Adv. Drug Deliv. Rev.* **2007**, 59, 748-758.
- [8] R. Sawant, V. Torchilin, *Molecular bioSystems*, 6, 628-640.
- [9] L. N. Patel, J. L. Zaro, W. C. Shen, *Pharm Res* **2007**, 24, 1977-1992.
- [10] I. Green, R. Christison, C. J. Voyce, K. R. Bundell, M. A. Lindsay, *Trends Pharmacol Sci* **2003**, 24, 213-215.
- [11] J. J. Shi, A. R. Votruba, O. C. Farokhzad, R. Langer, *Nano Letters* **2010**, 10, 3223-3230.
- [12] A. H. Faraji, P. Wipf, *Bioorganic & medicinal chemistry* **2009**, 17, 2950-2962.
- [13] J. H. Gao, B. Xu, *Nano Today* **2009**, 4, 37-51.
- [14] K. Y. Lee, S. H. Yuk, *Prog Polym Sci* **2007**, 32, 669-697.
- [15] L. Y. Chou, K. Ming, W. C. Chan, *Chemical Society reviews* **2010**.
- [16] V. Gaberc-Porekar, I. Zore, B. Podobnik, V. Menart, *Current Opinion in Drug Discovery & Development* **2008**, 11, 242-250.
- [17] A. V. Kabanov, S. V. Vinogradov, *Angew Chem Int Edit* **2009**, 48, 5418-5429.
- [18] M. A. Stuart, W. T. Huck, J. Genzer, M. Muller, C. Ober, M. Stamm, G. B. Sukhorukov, I. Szleifer, V. V. Tsukruk, M. Urban, F. Winnik, S. Zauscher, I. Luzinov,

- S. Minko, *Nature materials* **2010**, 9, 101-113.
- [19] R. Solaro, *J Polym Sci: Part A: Polym Chem* **2008**, 46, 1-11.
- [20] R. J. Debs, L. P. Freedman, S. Edmunds, K. L. Gaensler, N. Duzgunes, K. R. Yamamoto, *The Journal of biological chemistry* **1990**, 265, 10189-10192.
- [21] L. Liguori, B. Marques, A. Villegas-Mendez, R. Rothe, J. L. Lenormand, *Journal of Controlled Release* **2008**, 126, 217-227.
- [22] O. Zelphati, Y. Wang, S. Kitada, J. C. Reed, P. L. Felgner, J. Corbeil, *The Journal of biological chemistry* **2001**, 276, 35103-35110.
- [23] D. Dalkara, C. Chandrashekar, G. Zuber, *Journal of Controlled Release* **2006**, 116, 353-359.
- [24] D. Dalkara, G. Zuber, J. P. Behr, *Mol Ther* **2004**, 9, 964-969.
- [25] M. M. Fretz, A. Hogset, G. A. Koning, W. Jiskoot, G. Storm, *Pharm Res* **2007**, 24, 2040-2047.
- [26] K. A. D. Gregersen, Z. B. Hill, J. C. Gadd, B. S. Fujimoto, D. J. Maly, D. T. Chiu, *Acs Nano* **2010**.
- [27] B. Zassler, I. E. Blasig, C. Humpel, *Journal of neuro-oncology* **2005**, 71, 127-134.
- [28] C. O. Weill, S. Biri, A. Adib, P. Erbacher, *Cytotechnology* **2008**, 56, 41-48.
- [29] R. H. Muller, M. Radtke, S. A. Wissing, *Adv Drug Deliver Rev* **2002**, 54, S131-S155.
- [30] A. J. Almeida, S. Runge, R. H. Muller, *Int J Pharm* **1997**, 149, 255-265.
- [31] M. J. Roberts, M. D. Bentley, J. M. Harris, *Adv Drug Deliv Rev* **2002**, 54, 459-476.
- [32] A. M. a. G. P. Francesco M. Veronese, in *PEGylated Protein Drugs: Basic Science and Clinical Applications, Vol. 1* (Ed.: F. M. Veronese), Birkhäuser Basel, **2009**.
- [33] J. Futami, M. Kitazoe, T. Maeda, E. Nukui, M. Sakaguchi, J. Kosaka, M. Miyazaki, M. Kosaka, H. Tada, M. Seno, Y. Sasaki, N. H. Huh, M. Namba, H. Yamada, *J Biosci*

- Bioeng* **2005**, *99*, 95-103.
- [34] H. Murata, J. Futami, M. Kitazoe, T. Yonehara, H. Nakanishi, M. Kosaka, H. Tada, M. Sakaguchi, Y. Yagi, M. Seno, N. Huh, H. Yamada, *J Biochem* **2008**, *144*, 447-455.
- [35] J. Futami, H. Yamada, *Curr Pharm Biotechno* **2008**, *9*, 180-184.
- [36] H. Murata, M. Sakaguchi, J. Futami, M. Kitazoe, T. Maeda, H. Doura, M. Kosaka, H. Tada, M. Seno, N. Huh, H. Yamada, *Biochemistry-Us* **2006**, *45*, 6124-6132.
- [37] M. Kitazoe, H. Murata, J. Futami, T. Maeda, M. Sakaguchi, M. Miyazaki, M. Kosaka, H. Tada, M. Seno, N. Huh, M. Namba, M. Nishikawa, Y. Maeda, H. Yamada, *J Biochem* **2005**, *137*, 693-701.
- [38] H. Murata, J. Futami, M. Kitazoe, M. Kosaka, H. Tada, M. Seno, H. Yamada, *J Biosci Bioeng* **2008**, *105*, 34-38.
- [39] C. A. Lackey, O. W. Press, A. S. Hoffman, P. S. Stayton, *Bioconjugate Chem* **2002**, *13*, 996-1001.
- [40] S. Foster, C. L. Duvall, E. F. Crownover, A. S. Hoffman, P. S. Stayton, *Bioconjugate Chem* **2010**, *21*, 2205-2212.
- [41] S. Jung, S. Huh, Y. P. Cheon, S. Park, *Chemical communications (Cambridge, England)* **2009**, 5003-5005.
- [42] Y. Hu, T. Litwin, A. R. Nagaraja, B. Kwong, J. Katz, N. Watson, D. J. Irvine, *Nano Letters* **2007**, *7*, 3056-3064.
- [43] H. Ayame, N. Morimoto, K. Akiyoshi, *Bioconjugate Chem* **2008**, *19*, 882-890.
- [44] T. Nochi, Y. Yuki, H. Takahashi, S. Sawada, M. Mejima, T. Kohda, N. Harada, I. G. Kong, A. Sato, N. Kataoka, D. Tokuhara, S. Kurokawa, Y. Takahashi, H. Tsukada, S. Kozaki, K. Akiyoshi, H. Kiyono, *Nature materials*, *9*, 572-578.
- [45] E. G. Rosenbaugh, J. W. Roat, L. Gao, R. F. Yang, D. S. Manickam, J. X. Yin, H. D.

- Schultz, T. K. Bronich, E. V. Batrakova, A. V. Kabanov, I. H. Zucker, M. C. Zimmerman, *Biomaterials* **2010**, *31*, 5218-5226.
- [46] A. L. Lee, Y. Wang, W. H. Ye, H. S. Yoon, S. Y. Chan, Y. Y. Yang, *Biomaterials* **2008**, *29*, 1224-1232.
- [47] L. Hasadsri, J. Kreuter, H. Hattori, T. Iwasaki, J. M. George, *The Journal of biological chemistry* **2009**, *284*, 6972-6981.
- [48] N. Murthy, M. C. Xu, S. Schuck, J. Kunisawa, N. Shastri, J. M. J. Frechet, *P Natl Acad Sci USA* **2003**, *100*, 4995-5000.
- [49] J. A. Cohen, T. T. Beaudette, W. W. Tseng, E. M. Bachelder, I. Mende, E. G. Engleman, J. M. Frechet, *Bioconjug Chem* **2009**, *20*, 111-119.
- [50] E. M. Bachelder, T. T. Beaudette, K. E. Broaders, J. Dashe, J. M. Frechet, *Journal of the American Chemical Society* **2008**, *130*, 10494-10495.
- [51] T. T. Beaudette, J. A. Cohen, E. M. Bachelder, K. E. Broaders, J. L. Cohen, E. G. Engleman, J. M. J. Frechet, *Journal of the American Chemical Society* **2009**, *131*, 10360-10361.
- [52] E. M. Bachelder, T. T. Beaudette, K. E. Broaders, S. E. Paramonov, J. Dashe, J. M. Frechet, *Molecular pharmaceutics* **2008**, *5*, 876-884.
- [53] S. M. Standley, I. Mende, S. L. Goh, Y. J. Kwon, T. T. Beaudette, E. G. Engleman, J. M. Frechet, *Bioconjug Chem* **2007**, *18*, 77-83.
- [54] J. L. Cohen, A. Almutairi, J. A. Cohen, M. Bernstein, S. L. Brody, D. P. Schuster, J. M. Frechet, *Bioconjug Chem* **2008**, *19*, 876-881.
- [55] M. Diwan, T. G. Park, *Journal of Controlled Release* **2001**, *73*, 233-244.
- [56] M. Yan, J. Du, Z. Gu, M. Liang, Y. Hu, W. Zhang, S. Priceman, L. Wu, Z. H. Zhou, Z. Liu, T. Segura, Y. Tang, Y. Lu, *Nat Nanotechnol* **2010**, *5*, 48-53.

- [57] J. Du, C. Yu, D. Pan, J. Li, W. Chen, M. Yan, T. Segura, Y. Lu, *Journal of the American Chemical Society* **2010**, *132*, 12780-12781.
- [58] Z. Gu, A. Biswas, K. I. Joo, B. Hu, P. Wang, Y. Tang, *Chemical communications (Cambridge, England)*, *46*, 6467-6469.
- [59] Z. Gu, M. Yan, B. Hu, K. I. Joo, A. Biswas, Y. Huang, Y. Lu, P. Wang, Y. Tang, *Nano Letters* **2009**, *9*, 4533-4538.
- [60] A. Biswas, K. I. Joo, J. Liu, M. X. Zhao, G. P. Fan, P. Wang, Z. Gu, Y. Tang, *Acs Nano* **2011**, *5*, 1385-1394.
- [61] K. Takahashi, S. Yamanaka, *Cell* **2006**, *126*, 663-676.
- [62] H. Y. Zhou, S. L. Wu, J. Y. Joo, S. Y. Zhu, D. W. Han, T. X. Lin, S. Trauger, G. Bien, S. Yao, Y. Zhu, G. Siuzdak, H. R. Scholer, L. X. Duan, S. Ding, *Cell Stem Cell* **2009**, *4*, 581-581.
- [63] Y. Lee, T. Ishii, H. Cabral, H. J. Kim, J. H. Seo, N. Nishiyama, H. Oshima, K. Osada, K. Kataoka, *Angewandte Chemie (International ed)* **2009**, *48*, 5309-5312.
- [64] Y. Lee, T. Ishii, H. Kim, N. Nishiyama, Y. Hayakawa, K. Itaka, K. Kataoka, *Angew Chem Int Ed* **2010**, *49*, 1-5.
- [65] S. Hwa Kim, J. Hoon Jeong, C. O. Joe, T. Gwan Park, *Journal of Controlled Release* **2005**, *103*, 625-634.
- [66] T. Akagi, X. Wang, T. Uto, M. Baba, M. Akashi, *Biomaterials* **2007**, *28*, 3427-3436.
- [67] R. De Rose, A. N. Zelikin, A. P. R. Johnston, A. Sexton, S. F. Chong, C. Cortez, W. Mulholland, F. Caruso, S. J. Kent, *Adv Mater* **2008**, *20*, 4698-+.
- [68] P. Rivera-Gil, S. De Koker, B. G. De Geest, W. J. Parak, *Nano Letters* **2009**, *9*, 4398-4402.
- [69] S. J. She, X. G. Zhang, Z. M. Wu, Z. Wang, C. X. Li, *Biomaterials* **2010**, *31*, 6039-

- 6049.
- [70] N. Saito, Y. Usui, K. Aoki, N. Narita, M. Shimizu, K. Hara, N. Ogiwara, K. Nakamura, N. Ishigaki, H. Kato, S. Taruta, M. Endo, *Chemical Society reviews* **2009**, *38*, 1897-1903.
- [71] N. W. Shi Kam, T. C. Jessop, P. A. Wender, H. Dai, *Journal of the American Chemical Society* **2004**, *126*, 6850-6851.
- [72] N. W. S. Kam, Z. A. Liu, H. J. Dai, *Angew Chem Int Edit* **2006**, *45*, 577-581.
- [73] N. W. S. Kam, H. J. Dai, *Journal of the American Chemical Society* **2005**, *127*, 6021-6026.
- [74] P. Zrazhevskiy, M. Sena, X. Gao, *Chemical Society reviews* **2010**, *39*, 4326-4354.
- [75] Y. E. Koshman, S. B. Waters, L. A. Walker, T. Los, P. de Tombe, P. H. Goldspink, B. Russell, *Journal of molecular and cellular cardiology* **2008**, *45*, 853-856.
- [76] K. Nakase, S. Kobayashi, S. Futaki, *Biopolymers* **2010**, *94*, 763-770.
- [77] I. L. Medintz, T. Pons, J. B. Delehanty, K. Susumu, F. M. Brunel, P. E. Dawson, H. Mattoussi, *Bioconjug Chem* **2008**, *19*, 1785-1795.
- [78] E. Boisselier, D. Astruc, *Chemical Society reviews* **2009**, *38*, 1759-1782.
- [79] P. Ghosh, X. Yang, R. Arvizo, Z. J. Zhu, S. S. Agasti, Z. Mo, V. M. Rotello, *Journal of the American Chemical Society*, *132*, 2642-2645.
- [80] J. L. Vivero-Escoto, I. I. Slowing, B. G. Trewyn, V. S. Y. Lin, *Small* **2010**, *6*, 1952-1967.
- [81] Slowing, II, B. G. Trewyn, V. S. Lin, *Journal of the American Chemical Society* **2007**, *129*, 8845-8849.
- [82] I. Slowing, B. G. Trewyn, V. S. Y. Lin, *Journal of the American Chemical Society* **2006**, *128*, 14792-14793.

- [83] S. S. Bale, S. J. Kwon, D. A. Shah, A. Banerjee, J. S. Dordick, R. S. Kane, *Acs Nano*, **4**, 1493-1500.
- [84] S. Laurent, D. Forge, M. Port, A. Roch, C. Robic, L. V. Elst, R. N. Muller, *Chem Rev* **2008**, *108*, 2064-2110.
- [85] J. H. Gao, H. W. Gu, B. Xu, *Source: ACCOUNTS OF CHEMICAL RESEARCH Volume: 42 Issue: 8 Pages: Published: AUG 2009* **2009**, *42*, 1097-1107.
- [86] M. Chorny, E. Hood, R. J. Levy, V. R. Muzykantov, *Journal of Controlled Release*, **146**, 144-151.
- [87] A. Abbing, U. K. Blaschke, S. Grein, M. Kretschmar, C. M. Stark, M. J. Thies, J. Walter, M. Weigand, D. C. Woith, J. Hess, C. O. Reiser, *The Journal of biological chemistry* **2004**, *279*, 27410-27421.
- [88] J. J. Cronican, D. B. Thompson, K. T. Beier, B. R. McNaughton, C. L. Cepko, D. R. Liu, *ACS chemical biology* **2010**, *5*, 747-752.
- [89] Y. T. Lim, M. Y. Cho, J. M. Lee, S. J. Chung, B. H. Chung, *Biomaterials* **2009**, *30*, 1197-1204.
- [90] K. E. Uhrich, S. M. Cannizzaro, R. S. Langer, K. M. Shakesheff, *Chemical reviews* **1999**, *99*, 3181-3198.
- [91] P. D. Thornton, R. J. Mart, S. J. Webb, R. V. Ulijn, *Soft Matter* **2008**, *4*, 821-827.
- [92] P. P. Adiseshaiyah, J. B. Hall, S. E. McNeil, *Wires Nanomed Nanobi* **2010**, *2*, 99-112.
- [93] T. G. Cotter, *Nat Rev Cancer* **2009**, *9*, 501-507.
- [94] H. Zhou, S. Wu, J. Y. Joo, S. Zhu, D. W. Han, T. Lin, S. Trauger, G. Bien, S. Yao, Y. Zhu, G. Siuzdak, H. R. Scholer, L. Duan, S. Ding, *Cell Stem Cell* **2009**, *4*, 381-384.
- [95] K. G. Ford, B. E. Souberbielle, D. Darling, F. Farzaneh, *Gene Ther* **2001**, *8*, 1-4.
- [96] B. Gupta, T. S. Levchenko, V. P. Torchilin, *Adv Drug Deliver Rev* **2005**, *57*, 637-651.

- [97] T. Hirakura, K. Yasugi, T. Nemoto, M. Sato, T. Shimoboji, Y. Aso, N. Morimoto, K. Akiyoshi, *Journal of Controlled Release* **2010**, *142*, 483-489.
- [98] S. Frokjaer, D. E. Otzen, *Nature reviews* **2005**, *4*, 298-306.
- [99] N. Murthy, J. Campbell, N. Fausto, A. S. Hoffman, P. S. Stayton, *Bioconjugate Chem* **2003**, *14*, 412-419.
- [100] R. Haag, F. Kratz, *Angew Chem Int Edit* **2006**, *45*, 1198-1215.
- [101] S. Salmaso, S. Bersani, A. Semenzato, P. Caliceti, *J Nanosci Nanotechno* **2006**, *6*, 2736-2753.
- [102] Y. J. Lu, J. Yang, E. Sega, *Aaps J* **2006**, *8*, E466-E478.
- [103] Y. Yan, A. P. R. Johnston, S. J. Dodds, M. M. J. Kamphuis, C. Ferguson, R. G. Parton, E. C. Nice, J. K. Heath, F. Caruso, *Acs Nano* **2010**, *4*, 2928-2936.
- [104] J. R. Heath, M. E. Davis, *Annu Rev Med* **2008**, *59*, 251-265.
- [105] M. E. Davis, Z. Chen, D. M. Shin, *Nature reviews* **2008**, *7*, 771-782.
- [106] O. Zelphati, Y. Wang, S. Kitada, J. C. Reed, P. L. Felgner, J. Corbeil, *J Biol Chem* **2001**, *276*, 35103-35110.
- [107] S. Martins, B. Sarmiento, D. C. Ferreira, E. B. Souto, *Int J Nanomed* **2007**, *2*, 595-607.
- [108] W. Mehnert, K. Mader, *Adv Drug Deliver Rev* **2001**, *47*, 165-196.
- [109] F. Q. Hu, Y. Hong, H. Yuan, *Int J Pharm* **2004**, *273*, 29-35.
- [110] Z. Gu, M. Yan, B. Hu, K. I. Joo, A. Biswas, Y. Huang, Y. Lu, P. Wang, Y. Tang, *Nano Lett* **2009**, *9*, 4533-4538.
- [111] P. D. Thornton, R. J. Mart, R. V. Ulijn, *Adv Mater* **2007**, *19*, 1252-+.
- [112] B. Kim, N. A. Peppas, *Biomed Microdevices* **2003**, *5*, 333-341.
- [113] T. Nochi, Y. Yuki, H. Takahashi, S. Sawada, M. Mejima, T. Kohda, N. Harada, I. G. Kong, A. Sato, N. Kataoka, D. Tokuhara, S. Kurokawa, Y. Takahashi, H. Tsukada, S.

- Kozaki, K. Akiyoshi, H. Kiyono, *Nature materials* **2010**, *9*, 572-578.
- [114] S. Shu, X. Zhang, Z. Wu, Z. Wang, C. Li, *Biomaterials* **2010**, *31*, 6039-6049.
- [115] P. Ghosh, X. Yang, R. Arvizo, Z. J. Zhu, S. S. Agasti, Z. Mo, V. M. Rotello, *Journal of the American Chemical Society* **2010**, *132*, 2642-2645.
- [116] S. S. Bale, S. J. Kwon, D. A. Shah, A. Banerjee, J. S. Dordick, R. S. Kane, *Acs Nano* **2010**, *4*, 1493-1500.
- [117] R. A. Shimkunas, E. Robinson, R. Lam, S. Lu, X. Y. Xu, X. Q. Zhang, H. J. Huang, E. Osawa, D. Ho, *Biomaterials* **2009**, *30*, 5720-5728.
- [118] N. W. S. Kam, T. C. Jessop, P. A. Wender, H. J. Dai, *Journal of the American Chemical Society* **2004**, *126*, 6850-6851.
- [119] R. Crinelli, E. Carloni, M. Menotta, E. Giacomini, M. Bianchi, G. Ambrosi, L. Giorgi, M. Magnani, *Acs Nano* **2010**, *4*, 2791-2803.
- [120] N. W. S. Kam, Z. A. Liu, H. J. Dai, *Angew Chem Int Edit* **2006**, *45*, 577-581.
- [121] A. Abbing, U. K. Blaschke, S. Grein, M. Kretschmar, C. M. Stark, M. J. Thies, J. Walter, M. Weigand, D. C. Woith, J. Hess, C. O. Reiser, *J Biol Chem* **2004**, *279*, 27410-27421.
- [122] D. A. Christian, S. Cai, D. M. Bowen, Y. Kim, J. D. Pajerowski, D. E. Discher, *Eur J Pharm Biopharm* **2009**, *71*, 463-474.
- [123] S. Parveen, S. K. Sahoo, *Clin Pharmacokinet* **2006**, *45*, 965-988.
- [124] Z. H. Zhang, W. G. Cao, H. L. Jin, J. F. Lovell, M. Yang, L. L. Ding, J. Chen, I. Corbin, Q. M. Luo, G. Zheng, *Angew Chem Int Edit* **2009**, *48*, 9171-9175.
- [125] A. Biswas, K. Joo, J. Liu, M. Zhao, G. Fan, P. Wang, Z. Gu, Y. Tang, *ACS Nano* **2011**, *5*, 1385-1394.
- [126] A. Meister, S. S. Tate, *Annu Rev Biochem* **1976**, *45*, 559-604.

- [127] S. Bauhuber, C. Hozsa, M. Breunig, A. Gopferich, *Adv Mater* **2009**, *21*, 3286-3306.
- [128] S. Takae, K. Miyata, M. Oba, T. Ishii, N. Nishiyama, K. Itaka, Y. Yamasaki, H. Koyama, K. Kataoka, *Journal of the American Chemical Society* **2008**, *130*, 6001-6009.
- [129] Y. Z. You, D. S. Manickam, Q. H. Zhou, D. Oupicky, *Journal of Controlled Release* **2007**, *122*, 217-225.
- [130] Y. Kakizawa, A. Harada, K. Kataoka, *Biomacromolecules* **2001**, *2*, 491-497.
- [131] Y. Lee, H. Mo, H. Koo, J. Y. Park, M. Y. Cho, G. W. Jin, J. S. Park, *Bioconjug Chem* **2007**, *18*, 13-18.
- [132] R. V. Talanian, C. Quinlan, S. Trautz, M. C. Hackett, J. A. Mankovich, D. Banach, T. Ghayur, K. D. Brady, W. W. Wong, *J Biol Chem* **1997**, *272*, 9677-9682.
- [133] Y. Gavrieli, Y. Sherman, S. A. Ben-Sasson, *J Cell Biol* **1992**, *119*, 493-501.
- [134] D. Peer, J. M. Karp, S. Hong, O. C. Farokhzad, R. Margalit, R. Langer, *Nat Nanotechnol* **2007**, *2*, 751-760.
- [135] A. C. Joerger, A. R. Fersht, *Oncogene* **2007**, *26*, 2226-2242.
- [136] M. H. Noteborn, *European journal of pharmacology* **2009**, *625*, 165-173.
- [137] J. B. Gibbs, *Science* **2000**, *287*, 1969-1973.
- [138] J. H. Atkins, L. J. Gershell, *Nature reviews* **2002**, *1*, 491-492.
- [139] G. I. Evan, K. H. Vousden, *Nature* **2001**, *411*, 342-348.
- [140] J. C. Reed, *Cancer Cell* **2003**, *3*, 17-22.
- [141] T. G. Cotter, *Nat Rev Cancer* **2009**, *9*, 501-507.
- [142] A. Russo, M. Terrasi, V. Agnese, D. Santini, V. Bazan, *Ann Oncol* **2006**, *17*, Vii115-Vii123.
- [143] C. J. Brown, S. Lain, C. S. Verma, A. R. Fersht, D. P. Lane, *Nat Rev Cancer* **2009**, *9*,

862-873.

- [144] M. H. M. Noteborn, *European journal of pharmacology* **2009**, *625*, 165-173.
- [145] C. Backendorf, A. E. Visser, A. G. de Boer, R. Zliuerman, M. Visser, P. Voskamp, Y. H. Zhang, M. Noteborn, *Annu Rev Pharmacol* **2008**, *48*, 143-169.
- [146] M. Los, S. Panigrahi, I. Rashedi, S. Mandal, J. Stetefeld, F. Essmann, K. Schulze-Osthoff, *Bba-Mol Cell Res* **2009**, *1793*, 1335-1342.
- [147] S. M. Zhuang, A. Shvarts, H. Vanormondt, A. G. Jochemsen, A. J. Vandereb, M. H. M. Noteborn, *Cancer Res* **1995**, *55*, 486-489.
- [148] J. G. Teodoro, D. W. Heilman, A. E. Parker, M. R. Green, *Gene Dev* **2004**, *18*, 1952-1957.
- [149] A. A. A. M. DanenVanOorschot, D. F. Fischer, J. M. Grimbergen, B. Klein, S. M. Zhuang, J. H. F. Falkenburg, C. Backendorf, P. H. A. Quax, A. J. VanderEb, M. H. M. Noteborn, *Proceedings of the National Academy of Sciences of the United States of America* **1997**, *94*, 5843-5847.
- [150] S. R. Leliveld, Y. H. Zhang, J. L. Rohn, M. H. M. Noteborn, J. P. Abrahams, *The Journal of biological chemistry* **2003**, *278*, 9042-9051.
- [151] S. R. Leliveld, Y. H. Zhang, J. L. Rohn, M. H. Noteborn, J. P. Abrahams, *J Biol Chem* **2003**, *278*, 9042-9051.
- [152] A. A. A. M. Danen-van Oorschot, Y. H. Zhang, S. R. Leliveld, J. L. Rohn, M. C. M. J. Seelen, M. W. Bolk, A. van Zon, S. J. Erkeland, J. P. Abrahams, D. Mumberg, M. H. M. Noteborn, *The Journal of biological chemistry* **2003**, *278*, 27729-27736.
- [153] J. L. Rohn, Y. H. Zhang, R. I. J. M. Aalbers, N. Otto, J. den Hertog, N. V. Henriquez, C. J. H. van de Velde, P. J. K. Kuppen, D. Mumberg, P. Donner, M. H. M. Noteborn, *The Journal of biological chemistry* **2002**, *277*, 50820-50827.

- [154] A. M. Pietersen, M. M. van der Eb, H. J. Rademaker, D. J. M. van den Wollenberg, M. J. W. E. Rabelink, P. J. K. Kuppen, J. H. van Dierendonck, H. van Ormondt, D. Masman, C. J. H. van de Velde, A. J. van der Eb, R. C. Hoeben, M. H. M. Noteborn, *Gene Therapy* **1999**, *6*, 882-892.
- [155] M. M. van der Eb, A. M. Pietersen, F. M. Speetjens, P. J. K. Kuppen, C. J. H. van de Velde, M. H. M. Noteborn, R. C. Hoeben, *Cancer Gene Ther* **2002**, *9*, 53-61.
- [156] D. J. Peng, J. Sun, Y. Z. Wang, J. Tian, Y. H. Zhang, M. H. M. Noteborn, S. Qu, *Cancer Gene Ther* **2007**, *14*, 66-73.
- [157] M. L. Edelstein, M. R. Abedi, J. Wixon, *J Gene Med* **2007**, *9*, 833-842.
- [158] L. Guelen, H. Paterson, J. Gaken, M. Meyers, F. Farzaneh, M. Tavassoli, *Oncogene* **2004**, *23*, 1153-1165.
- [159] J. Sun, Y. Yan, X. T. Wang, X. W. Liu, D. J. Peng, M. Wang, J. Tian, Y. Q. Zong, Y. H. Zhang, M. H. M. Noteborn, S. Qu, *Int J Cancer* **2009**, *124*, 2973-2981.
- [160] C. L. Murriel, S. F. Dowdy, *Expert Opin Drug Deliv* **2006**, *3*, 739-746.
- [161] Z. Gu, A. Biswas, M. X. Zhao, Y. Tang, *Chemical Society reviews* **2011**, *40*, 3638-3655.
- [162] Z. Gu, M. Yan, B. L. Hu, K. I. Joo, A. Biswas, Y. Huang, Y. F. Lu, P. Wang, Y. Tang, *Nano Letters* **2009**, *9*, 4533-4538.
- [163] M. X. Zhao, A. Biswas, B. L. Hu, K. I. Joo, P. Wang, Z. Gu, Y. Tang, *Biomaterials* **2011**, *32*, 5223-5230.
- [164] M. Burek, S. Maddika, C. J. Burek, P. T. Daniel, K. Schulze-Osthoff, M. Los, *Oncogene* **2006**, *25*, 2213-2222.
- [165] R. U. Janicke, M. L. Sprengart, M. R. Wati, A. G. Porter, *The Journal of biological chemistry* **1998**, *273*, 9357-9360.

- [166] N. Kamaly, Z. Y. Xiao, P. M. Valencia, A. F. Radovic-Moreno, O. C. Farokhzad, *Chemical Society reviews* **2012**, *41*, 2971-3010.
- [167] C. Coles, A. Condie, U. Chetty, C. M. Steel, H. J. Evans, J. Prosser, *Cancer Res* **1992**, *52*, 5291-5298.
- [168] M. Lacroix, R. A. Toillon, G. Leclercq, *Endocr Relat Cancer* **2006**, *13*, 293-325.
- [169] M. V. Blagosklonny, *Int J Cancer* **2002**, *98*, 161-166.
- [170] N. Senzer, J. Nemunaitis, M. Nemunaitis, J. Lamont, M. Gore, H. Gabra, R. Eeles, N. Sodha, F. J. Lynch, L. A. Zumstein, K. B. Menander, R. E. Sobol, S. Chada, *Mol Cancer Ther* **2007**, *6*, 1478-1482.
- [171] N. Issaeva, P. Bozko, M. Enge, M. Protopopova, L. G. G. C. Verhoef, M. Masucci, A. Pramanik, G. Selivanova, *Nat Med* **2004**, *10*, 1321-1328.
- [172] L. T. Vassilev, B. T. Vu, B. Graves, D. Carvajal, F. Podlaski, Z. Filipovic, N. Kong, U. Kammlott, C. Lukacs, C. Klein, N. Fotouhi, E. A. Liu, *Science* **2004**, *303*, 844-848.
- [173] A. Friedler, L. O. Hansson, D. B. Veprintsev, S. M. V. Freund, T. M. Rippin, P. V. Nikolova, M. R. Proctor, S. Rudiger, A. R. Fersht, *P Natl Acad Sci USA* **2002**, *99*, 937-942.
- [174] Z. Gu, A. Biswas, M. X. Zhao, Y. Tang, *Chem Soc Rev* **2011**, *40*, 3638-3655.
- [175] M. X. Zhao, B. L. Hu, Z. Gu, K. I. Joo, P. Wang, Y. Tang, *Nano Today* **2013**, *8*, 11-20.
- [176] Y. Lee, T. Ishii, H. Cabral, H. J. Kim, J. H. Seo, N. Nishiyama, H. Oshima, K. Osada, K. Kataoka, *Angew Chem Int Edit* **2009**, *48*, 5309-5312.
- [177] K. Welsch, M. D. A. Perera, J. W. Aylott, W. C. Chan, *Chem Commun* **2009**, 6601-6603.
- [178] A. Nagy, A. V. Schally, *Biol Reprod* **2005**, *73*, 851-859.
- [179] S. S. Dharap, Y. Wang, P. Chandna, J. J. Khandare, B. Qiu, S. Gunaseelan, P. J. Sinko,

- S. Stein, A. Farmanfarmaian, T. Minko, *P Natl Acad Sci USA* **2005**, *102*, 12962-12967.
- [180] S. S. Dharap, B. Qiu, G. C. Williams, P. Sinko, S. Stein, T. Minko, *J Control Release* **2003**, *91*, 61-73.
- [181] A. L. Okorokov, M. B. Sherman, C. Plisson, V. Grinkevich, K. Sigmundsson, G. Selivanova, J. Milner, E. V. Orlova, *Embo J* **2006**, *25*, 5191-5200.
- [182] H. Tidow, R. Melero, E. Mylonas, S. M. V. Freund, J. G. Grossmann, J. M. Carazo, D. I. Svergun, M. Valle, A. R. Fersht, *P Natl Acad Sci USA* **2007**, *104*, 12324-12329.
- [183] E. Saller, E. Tom, M. Brunori, M. Otter, A. Estreicher, D. H. Mack, R. Iggo, *Embo J* **1999**, *18*, 4424-4437.